Power Systems

Canbing Li
Yijia Cao
Yonghong Kuang
Bin Zhou

Influences of Electric Vehicles on Power System and Key Technologies of Vehicle-to-Grid

Science Press
Beijing

Springer

Power Systems

More information about this series at http://www.springer.com/series/4622

Canbing Li · Yijia Cao · Yonghong Kuang
Bin Zhou

Influences of Electric Vehicles on Power System and Key Technologies of Vehicle-to-Grid

Science Press
Beijing

Springer

Canbing Li
College of Electrical and Information Engineering
Hunan University
Changsha, Hunan
China

Yonghong Kuang
College of Electrical and Information Engineering
Hunan University
Changsha, Hunan
China

Yijia Cao
College of Electrical and Information Engineering
Hunan University
Changsha, Hunan
China

Bin Zhou
College of Electrical and Information Engineering
Hunan University
Changsha, Hunan
China

ISSN 1612-1287 ISSN 1860-4676 (electronic)
Power Systems
ISBN 978-3-662-49362-5 ISBN 978-3-662-49364-9 (eBook)
DOI 10.1007/978-3-662-49364-9

Jointly published with Science Press, Beijing

Library of Congress Control Number: 2016931295

Printed on acid-free paper

This Springer imprint is published by SpringerNature
The registered company is Springer-Verlag GmbH Berlin Heidelberg

Preface

With the rapid development of electric vehicles (EVs) as well as the promotion and application of vehicle-to-grid (V2G) technologies, EVs charging loads, as flexible loads, have the potential to participate in the grid services, including peak shaving and valley filling, frequency regulation (FR), emergency power, energy market participation, and so on. Therefore, great attention has been paid to EVs and V2G.

Focusing on the interactions between EVs and power system, this book aims to bring readers with basic knowledge of electrical engineering promptly to the frontier of the EVs' influence on power system and environment. This book may serve as a reference for scientists, electrical engineers, and postgraduate students majoring in electrical engineering or other related fields.

Outline of the Book

This book discusses electrical vehicles integration into power system on three aspects as follows.

In Chap. 1, the influence of EVs on power system through improving urban microclimate and its consequent effects of energy conservation and emission reduction are revealed.

In Chaps. 2–5, V2G technologies are elaborated. In our opinion, V2G technologies can be classified from different perspectives, as depicted in Fig. 1. In terms of the scale of charging stations, it can be divided into large and small scale; in terms of the response signals, it can be divided into electricity price, frequency and voltage; and in terms of the response mode, it can be divided into manual and automatic response.

In Chaps. 6 and 7, planning of EV charging facilities are discussed. Based on the reverse discharge capacity of EVs, advantages, disadvantages, and adaptive range of several typical schemes of the integration of charging facilities into the grid are

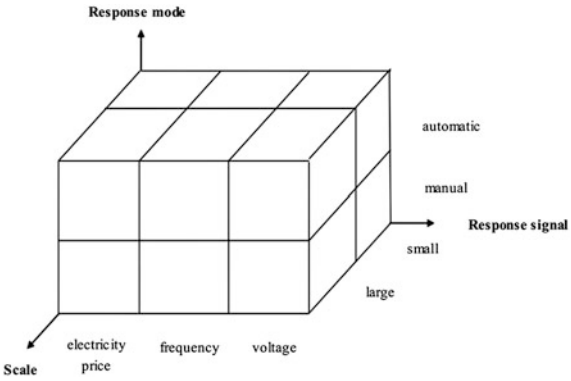

Fig. 1 Structure of V2G

explored, and a method of dividing EV charging facilities planning into different stages based on V2G is proposed.

The contents of each chapter are shown below.

In Chap. 1, the influence of EVs on power system through improving microclimate is elaborated. This chapter studies the interactions between urban microclimate and air-conditioner load in power system and the influence of large-scale EVs' integration into the grid on urban microclimate, and analyzes the indirect influence on power system and its consequent indirect energy-saving effects. This chapter is written by Prof. Canbing Li.

In Chap. 2, the response of EV charging load to time-of-use (TOU) power price is analyzed. Based on the existing research and the state of charge (SOC) curve, an optimized charging model for the regulated market is proposed in this chapter. By using the proposed method, EVs are able to reduce the cost of customers by adjusting charging power and time, thus achieving peak shaving in load demand. This chapter is written by Prof. Yijia Cao.

In Chap. 3, the response of EV charging loads to the grid voltage is analyzed, and a control strategy is proposed. In the proposed strategy, the alternate current (AC) side voltage of electric vehicle charging stations (EVCSs) is selected as the voltage signal and the EV user experience is taken into account. The response priority of EVs is updated real-timely to avoid any EV participating in under-voltage load shedding (UVLS) for a long time. The simulation results show that EVs can help the grid voltage recover to an allowable range and EVs participating in UVLS can be fully charged within the time set by EV users. This chapter is written by Dr. Bin Zhou.

In Chap. 4, a coordinated control strategy for large-scale EVs, battery energy storage stations (BESSs), and traditional FR resources involved in automatic generation control (AGC) is presented. Response priorities and control strategies for the FR resources vary with different operating states. The simulation results show that the proposed method can not only fully utilize the advantages of EVs/BESSs, but also

achieve the coordination among different FR resources, thus improving the frequency stability. This chapter is written by Ms. Yonghong Kuang and Prof. Canbing Li.

In Chap. 5, an asynchronous control method for small-scale dispersed charging EVs to participate in FR is proposed. The results of simulations under different disturbances demonstrate that the gradual participation of EVs in FR can effectively alleviate the frequency deviations and avoid overshoot. This chapter is written by Ms. Yonghong Kuang.

In Chap. 6, three typical schemes of the integration of charging facilities into grid, including electric vehicle charging stations (EVCSs) directly integrated into or adjacent to 110 kV substations, EVCSs integrated into the tie point of looped distribution grid, and the parallel operation of special load with EVCSs, are explored. Furthermore, the advantages, disadvantages, and adaptive range of the above three typical schemes are demonstrated. This chapter is written by Dr. Bin Zhou and Prof. Canbing Li.

In Chap. 7, the EV charging facility planning is explored. Based on V2G, the planning is divided into three stages: demonstration stage, public service stage, and commercial operation stage. Characteristics of each stage are analyzed and the charging demand of each charging method is predicted based on the optimized model of charging methods put forward in this chapter. Results of the case studies reveal the applicability of this planning method. This chapter is written by Dr. Bin Zhou and Prof. Canbing Li.

In surveying this book, readers can obtain information about the interactions between EVs and power systems based on V2G. Although some work on EVs and power systems has been done in this book, there is still plenty of space for development in theory and applications.

Canbing Li
Yijia Cao
Yonghong Kuang
Bin Zhou

Acknowledgments

This book made a summary of our research results achieved in recent years, and many people contributed to this book in various ways. The authors are indebted to their students, Ph.D. Xubin Liu, M.S. Yujiao Chen, M.S. Miao Hu, M.S. Shuyun He, M.S. Rui Yang, and M.S. Xuedong Ren at Hunan University, for their assistance in preparing the materials, pointing out typos, and checking the whole book. Especially, we thank Prof. Jianguo Liu from Michigan State University, Dr. Jin Zhong from the University of Hong Kong, Dr. Jianhui Wang from Argonne National Laboratory, USA, Prof. Chongqing Kang from Tsinghua University, Dr. Peng Zhang from University of Connecticut, and postgraduate students from Hunan University and Zhengzhou University, including Ms. Lina He, Mr. Baling Fang, Mr. Long Zeng, Ms. Guoxuan Xiao, Ms. Mi Zhang, Ms. Haiqing Shi, Ms. Yinghui Geng, Ms. Jinju Zhou, Ms. Yu Liu, Mr. Yi Tan, Mr. Shengwei Tang, Mr. Zhikun Zhang, Mr. Junxiong Li, Mr. Chunyang Wu, Mr. Li Du, and all of the contributors from around the world who have contributed material to this book.

This book is supported by the Key Project of National Natural Science Foundation of China (Grant No. 51137003) and the National Natural Science Foundation of China (Grant No. 51507056). The authors really appreciate the support.

Canbing Li
Yijia Cao
Yonghong Kuang
Bin Zhou

Contents

Abbreviations

ACE	Area control error
ACEC	Air-conditioning energy consumption
AGC	Automatic generation control
BESS	Battery energy storage station
CE	Cumulative effect
CHP	Combined heat and power
CV	Conventional vehicle
EER	Energy efficiency ratio
EMS	Energy management system
EPS	Emergency power supply
EV	Electrical vehicle
EVCP	Electric vehicle charging pile
EVCS	Electric vehicle charging station
FR	Frequency regulation
FSFD	Fixed step fixed delay
HII	Heat island intensity
LFC	Load frequency control
PHEV	Plug-in hybrid electric vehicle
SOC	State of charge
TBC	Tie-line bias control
THE	Temperature and humidity effect
TOU	Time-of-use
UHIE	Urban heat island effect
UPS	Uninterruptible power supply
UVLS	Under-voltage load shedding
V2G	Vehicle to grid
VSVD	Variable step variable delay
WAMS	Wide area monitoring system

Chapter 1
Influences of EVs on Power System by Improving the Microclimate

1.1 Introduction

The influence of EVs on power system is diverse. A lot of literatures have studied the influence of EVs on power system in the following aspects.

First, without the guidance of economic interests and policy, the charging behavior of EV users presents great uncertainty, which results in the randomness of EV charging loads. It increases the difficulty of power system operation and control, and has a bad effect on the reliability of power system [1]. For example, EV users' random charging behaviors may lead to a new peak load when EVs are integrated into the grid during peak-load periods, which will increase the burden on power system, and even result in the instability of power system [2].

Second, with the growth of EVs, EV charging load constitutes a large amount of the overall electric load and will have a significant influence on the operation and planning of power system. The growth of EV charging load requires the balance of power supply. The influence of EVs on generation expansion in different scenarios, including uniform charging scenario, home-based charging scenario, off-peak charging scenario and V2G charging scenario, is studied in [3]. It is discovered that the extra generation expansion is the least in V2G charging scenario. The influence of EVs on the generation side is revealed in [4]. It is discovered that although EVs can provide peaking and peak reserve capacity, they cannot be used as firm peaking capacity because of their uncertain availability. The influence of EVs on the transmission grid is indirect. Large-scale access of EVs to the grid results in the growth of electric load and the time and space uncertainty of EV charging load will have influence on the transmission grid security, economic operation and planning [5]. The influence of EVs on power system mainly focuses on the distribution grid. The influence of EV charging load on the voltage of the typical low voltage distribution grid in the UK is revealed in [6]. It is discovered that the higher the aggregation level of the integration of EVs is, the more likely the voltage statutory limits are to be maintained. The influence of EV charging load on the life of

C. Li et al., *Influences of Electric Vehicles on Power System and Key Technologies of Vehicle-to-Grid*, Power Systems,
DOI 10.1007/978-3-662-49364-9_1

distribution transformers is revealed in [7]. It is discovered that the access of EVs will reduce the life of distribution transformers.

Third, EVs as a large-capacity energy storage device can participate in grid services, including peak shaving and valley filling, FR, emergency power supply (EPS), and increase the grid's capacity in the integration of new and intermittent energy [2, 8–10]. EV owners can buy electricity from the market mainly at valley hours to charge their EVs, and sell it at peak hours by taking advantage of the EV storage capability, achieving peak shaving and valley filling [2]. EVs as an energy storage device can help the conventional FR resources suppress the power system frequency fluctuation. In other words, EVs has the capacity in participating in FR [8]. In [9], the reverse discharge capacity of EVs is explored. It is discovered that EVs can serve as the EPS of important loads, which will reduce the blackout time of important loads. In [10], the influence of EVs on the grid's capacity in the integration of new energy is explored. It is discovered that EVs can support the large-scale integration of new energy into grid based on V2G.

In this chapter, the effect of EVs on power system from a unique perspective is revealed, which is to reduce air-conditioning energy consumption (ACEC) by improving microclimate. The idea in this chapter can be presented as the following figure (see Fig. 1.1).

First, the impact of urban microclimate on ACEC is explored with three effects, including urban heat island effect (UHIE), temperature and humidity effect (THE) and cumulative effect (CE). In previous studies, CE is ignored. Therefore, the impact of microclimate on ACEC is underestimated remarkably. Second, based on the impact of microclimate on ACEC, the interaction between urban microclimate and electric ACEC is revealed. Based on the discovery, ACEC can be reduced significantly by improving microclimate. Third, the influence of EVs on urban microclimate is demonstrated. It is discovered that EVs emit much less heat than conventional vehicles (CVs) within the same mileage, so the replacement of CVs by EVs can reduce heat emission to benefit the local climate and global climate. Finally, the influence of EVs on power system by improving microclimate is revealed. It is discovered that EVs can improve microclimate by mitigating heat emission to dramatically reduce ACEC.

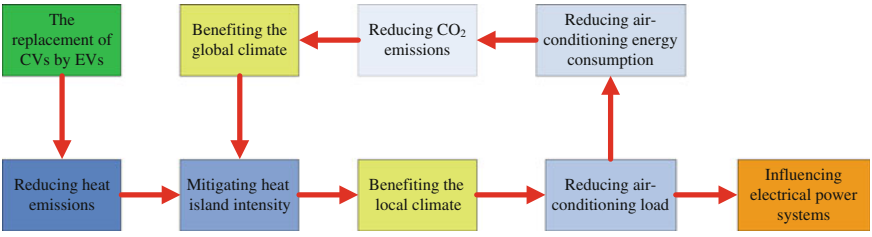

Fig. 1.1 Influences of EVs on power system by improving the microclimate

1.2 The Impact of Urban Microclimate on Electric ACEC

Energy consumption is closely related to climate change [11]. During the process of global warming, the deterioration of urban microclimate becomes more serious [12]. Urban microclimate involves characteristics of the local climate between the near-ground atmosphere and the topsoil in a relatively small space, including temperature, humidity, etc. Microclimate deterioration has caused a tremendous impact on more than 50 % of the world's population [13]. Additionally, with the development of urbanization process, more and more people will be affected [14, 15]. One of the prominent phenomena of urban microclimate deterioration is the stronger heat island intensity (HII). In many cities, UHIE contributes to higher temperatures in urban areas, leading to the increasing of ACEC. The energy consumed by electric air-conditioning is 30–50 % of the total electric energy consumed during summer, and this proportion even exceeds 50 % in some commercially developed cities [16, 17]. Therefore, many literatures focus on air-conditioning energy saving [18, 19]. And building thermal insulation is an effective measure to reduce ACEC [20].

ACEC is closely related with the temperature perceived by human, while the latter is affected by UHIE, THE and CE.

The impact of UHIE on ACEC has been widely studied. Hirano and Fujita studied the impact of UHIE on ACEC in Tokyo [21]. Giridharan et al. reported the impact of UHIE in Hong Kong [22]. Hassid et al. evaluated it in Athens [23], and Kolokotroni et al. analyzed it in London [24]. However, during high temperature season, electric ACEC is determined by the temperature perceived by human, which is different from the measured temperature. This phenomenon has been applied in power load forecasting [25]. But, in most of previous literatures, the relationship between temperature and ACEC was studied with the measured temperature, not the perceived temperature. In some literatures, the influence of relative humidity was recognized [26, 27]. However, the influence of CE has never been mentioned so far. Because of the difference between the measured temperature and the perceived temperature, the previous results might be different from the real situation.

In this section, a method which takes UHIE, THE and CE into consideration is proposed to calculate temperature perceived by human. So, in this way, the influence of urban microclimate on ACEC is assessed in a more accurate way. The way that these three effects influence perceived temperature and change ACEC is explained as follows.

First, UHIE has a direct effect on ACEC. Due to UHIE, urban residents are living in a much hotter environment. The temperature difference between urban and suburban areas could reach as much as 12 °C [28, 29]. Therefore, urban residents consume much energy when using air-conditioners. In the US, 3–8 % of the wasted energy consumption is caused by UHIE [30], resulting in an extra cost of 1 billion dollars on energy consumption each year [31].

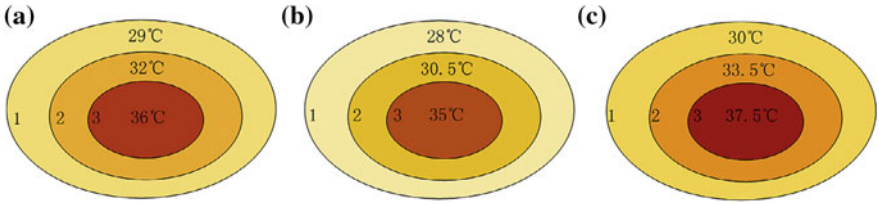

Fig. 1.2 Coupling relationship of UHIE and CE. **a** Temperature in different areas in the first day. **b** Temperature in different areas in the second day. **c** Temperature in different areas in the third day. Reprinted from Refs. [47, 63], Copyright 2013, with permission from Elsevier

Second, the perceived temperature is affected by relative humidity at the high temperature. That is, under the same temperature conditions, if relative humidity is higher, people will feel much hotter. Therefore, ACEC is greater in a day with high humidity than one with low humidity. This phenomenon is called THE. So, THE has a significant influence on ACEC in some cities with high humidity climate.

During successive days of high temperatures, the perceived temperature is higher than measured temperature. The phenomenon is called CE. The successive days of high temperatures contribute to a large increase in electric ACEC. In over 30 cities in China we sampled, CE has a significant impact on electric ACEC. In certain cities, electric ACEC driven by the CE accounted for 10 % of the total electric ACEC. Therefore, it is believed that CE is a common phenomenon.

It should be noted that these effects, especially UHIE and CE, are coupled. The coupling relationship between UHIE and CE is shown in Fig. 1.2, which is a virtual case. In the first day, temperature in urban center (area 3) is higher than other areas because of UHIE, which directly leads to part of the ACEC; in the second day, continual UHIE contributes to successive high-temperature in urban center (area 3) and ACEC increases sharply under the influence of UHIE and CE; in the third day, the same situation comes again.

ACEC has a notable relationship with the perceived temperature. In order to precisely describe the relationship between perceived temperature and measured temperature, it is necessary to take UHIE, CE and THE into consideration together.

1.2.1 Case and Data Selection

Air-conditioners can be classified into electric, gas-fired and automobile air-conditioners. Due to the lack and unavailability of data on gas-fired air-conditioners and automobile air-conditioners, in this chapter, electric ACEC is regarded as an example to analyze the interaction between urban microclimate and ACEC.

The data analyzed are from January to December in 2005 in Beijing. After 2005, the detailed data of power system are defined as confidential data in China. Therefore, data from the year of 2005 as the recent public data is selected. Besides, it is difficult to get separate electricity consumption data of urban area of Beijing.

Since the urban area of Beijing has covered about 74 % of the total area of Beijing and its GDP accounts for 98 % of the Beijing's total GDP [32] and GDP has a strong correlation with power load, electricity consumption data of Beijing are preferred to the electricity consumption data of Beijing urban area.

The total area of Beijing is around 16,400 km^2 and the urban area of Beijing is about 12,187 km^2. In this chapter, the urban area represents both city center and city districts. City district, as a part of the city, is characterized by large population density, concentrated floating population and developed culture, economy and trade. With a total population of approximately 20 million, Beijing (N39°54′20″ and E116° 25′29″) is located in a typical warm temperate zone and has a semi-moist continental monsoon climate featuring a hot and rainy summer. The highest temperature in summer in Beijing is higher than 42 °C. In the summer of 2011, the highest daily energy load in Beijing was approximately 19,100 with 8,000 MW constituted by the air-conditioning load, which was issued by the power utility. The air-conditioning load has exceeded 40 % of the total energy load [33]. Beijing is characterized by a strong UHIE because the suburban temperature is low and the city is surrounded by mountains [34]. Therefore, Beijing is particularly suitable for this study.

1.2.2 Electrical ACEC Data

The electrical load changes constantly and can be categorized into four major categories based on its features: basic normal load, weather-sensitive load, special-event load and random load [35]. The basic normal load changes little over a short term. Furthermore, weather-sensitive load accounts for a larger proportion of the electrical load than special-event load and random load combined. And the weather-sensitive load is primarily associated with the air-conditioning load in the summer. Thus, the load in this chapter refers particularly to the weather-sensitive load (air-conditioning load in the summer).

To study the relationship between electric ACEC and temperature, electric ACEC needs to be separated from the total electric energy consumption. Figure 1.3 displays the curve of entire 2005 daily electric energy consumption of Beijing. And it can be observed that the daily energy consumption in April was the lowest of the year, which was attributed to its comfortable weather and the consequent low weather-sensitive load. After May, the daily energy consumption began to rise and reached a peak in July and August. Afterward, it decreased with the decreasing of temperature. Although weather-sensitive energy consumption was also low in October, the average daily energy consumption was larger compared with that in April due to the growth of the basic normal energy consumption caused by the economic development throughout these 6 months. During the rest of the year, the heat energy consumption increased as the temperature decreased, leading to the rise of average daily energy consumption. In addition, during national holidays, for example, May 1st–7th and October 1st–7th, the average daily energy consumption decreased to its minimum value.

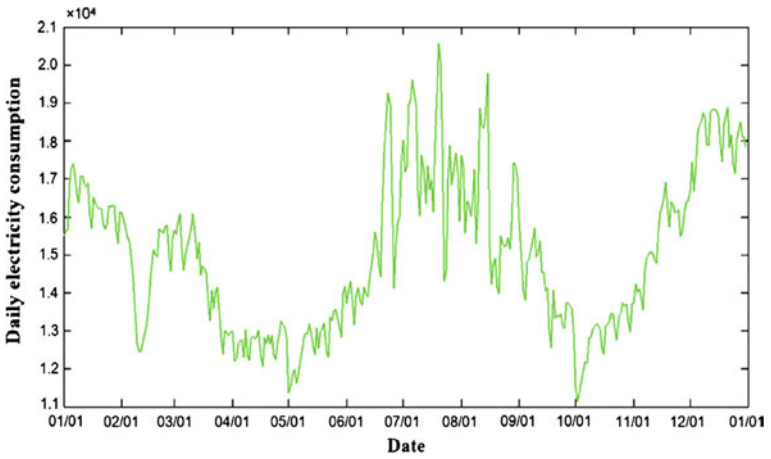

Fig. 1.3 Daily electricity consumption *curve* of Beijing. Reprinted from Refs. [47, 63], Copyright 2013, with permission from Elsevier

The average daily energy consumption in April and October are selected to represent the basic normal energy consumption. A method is used to obtain an approximation of electric ACEC by power utilities. As shown in Fig. 1.3, the average daily energy consumption fluctuates on a weekly basis. Therefore, the basic normal energy consumption from Monday to Sunday is computed and subtracted from the summer daily energy consumption on a weekly basis. The basic normal energy consumption corresponding to the value shown in Table 1.1 was subtracted from the daily energy consumption from May (not including May 1st–7th) to September. The high-order polynomial is most commonly used in fitting the load-temperature relationship [36, 37]. However, the use of a high-order polynomial cannot explain the physical meaning of the relationship. In this study, a logistic curve is chosen to fit the load-temperature relationship during the high temperature season. The daily energy consumption is proportional to the average load, and it can also be described by a logistic curve.

Table 1.1 Consumption of basic normal energy

Week	Consumption of basic normal energy (10 MWh)
Monday	12,787.575
Tuesday	12,871.519
Wednesday	12,802.219
Thursday	12,847.238
Friday	13,018.186
Saturday	12,354.308
Sunday	12,223.548

Reprinted from Refs. [47, 63], Copyright 2013, with permission from Elsevier

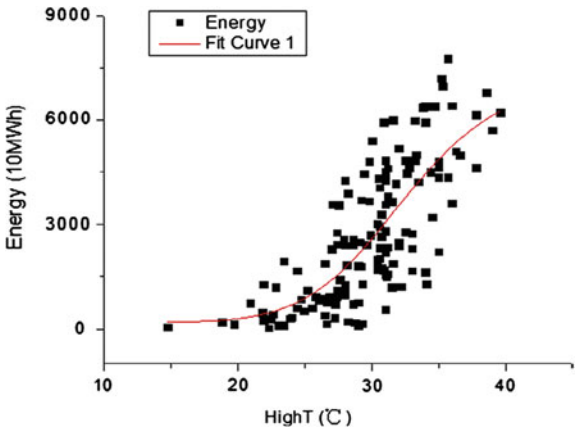

Fig. 1.4 Logistic *curve* used to fit the relationship between the daily average temperature and electric ACEC in Beijing in the summer of 2005. Reprinted from Refs. [47, 63], Copyright 2013, with permission from Elsevier

The fitting curve is shown in Fig. 1.4. The electric ACEC increases as the temperature increases. The data was from May (not including May 1st–7th) to September in 2005 and the coefficient of determination (R^2) was 0.81. The daily energy consumption reflects the energy consumption level of the whole day, and the average daily temperature describes the overall temperature of a day. The relationship between the average daily temperature and electric ACEC is indicated by the following equation:

$$y = (687.93 - 7189.41) \Big/ \left(1 + (x/27.22)^{13.66}\right) + 7189.41 \qquad (1.1)$$

where x represents the average temperature and y represents the electric ACEC.

1.2.3 Effect of UHIE on Perceived Temperature

UHIE refers to the significant increase in temperature in urban areas compared with that in rural areas, and the temperature varies in different urban areas. Due to UHIE, urban residents live in a much hotter environment. The UHIE is attributed to three causes. First, the ground surface properties are different in urban and rural areas, resulting in great differences in the thermal properties of these two areas. Urban areas have less reflection and evapotranspiration but absorb more heat. Heat conduction is more rapid and heat radiation is slower in urban areas compared with suburban areas; therefore, urban areas store more heat. Second, there is more anthropogenic heat in urban areas than in suburban areas. Third, high-level air pollution and aerosol particles in urban areas, to some extent, block the heat within the city. The more developed the urban area is, the more apparent the UHIE will be. Beijing, as the capital of China, exhibits a more apparent phenomenon of UHIE. The intensity of UHIE can be measured in terms of *HII*, which can be calculated by

subtracting the background rural temperature from urban temperature. Generally, the background rural temperature is assumed to be the average temperature of several locations in the surrounding rural areas [38]. The equation is as follows:

$$HII = T_{urb} - T_{sub} \tag{1.2}$$

where *HII* refers to the heat island intensity, T_{urb} refers to the average daily temperature of urban area and T_{sub} refers to the average daily temperature of several locations in the surrounding rural areas. *HII* is calculated by using the data from [38, 39]. The average *HII* was approximately 2.5 °C in the summer of 2005 in Beijing.

1.2.4 *Effect of THE on Perceived Temperature*

THE refers to influences of relative humidity on the perceived temperature. In 1978, George Winterling developed the concept of "humiture" (later was called the heat index by the US National Weather Service) to comprehensively reflect the perceived temperature [40]. The research of Burton shows that relative humidity has a slight influence on the perceived temperature when the air temperature is moderate, but it has a large effect when the air temperature is high or low [41]. Because the focus of our study is on high temperature season, it is necessary to consider the influence of relative humidity.

The formula used to calculate the heat index is shown in (1.3), which considers the influence of relative humidity on temperature. Different scholars have provided different polynomial coefficients for this calculation [42, 43].

$$HI = c_1 + c_2T + c_3R + c_4TR + c_5T^2 + c_6R^2 + c_7T^2R + c_8TR^2 + c_9T^2R^2 \tag{1.3}$$

where *HI*, *T*, and *R* represent the heat index (in degrees Fahrenheit), temperature (in degrees Fahrenheit) and relative humidity (as a percent), respectively. After trying a variety of coefficient values, the following coefficients proposed in [42, 43] were used:

$$c_1 = -42.38, \quad c_2 = 2.049, \quad c_3 = 10.14, \quad c_4 = -0.2248, \quad c_5 = -6.838 \times 10^{-3},$$
$$c_6 = -5.482 \times 10^{-2}, \quad c_7 = 1.228 \times 10^{-3}, \quad c_8 = 8.528 \times 10^{-4}, \quad c_9 = -1.99 \times 10^{-6}.$$

The temperature (*T*) should be higher than 27 °C (80 °*F*), and the relative humidity (*R*) should be higher than 40 %. Using the formula above, a heat index table is obtained, as shown in Table 1.2. In this table, the heat index below the green line is higher than the ambient temperature due to the influence of relative humidity.

Table 1.2 Heat index table

T	R (%)											
°C	40	45	50	55	60	65	70	75	80	85	90	95
43	40.1	40.3	40.6	40.9	41.2	41.5	41.8	42.1	42.4	42.6	42.9	43.2
42	39.4	39.7	40.0	40.2	40.5	40.8	41.1	41.3	41.6	41.9	42.2	42.4
41	38.7	39.0	39.3	39.5	39.8	40.1	40.3	40.6	40.9	41.1	41.4	41.6
40	38.0	38.3	38.5	38.8	39.0	39.3	39.6	39.8	40.1	40.3	40.6	40.8
39	37.3	37.6	37.8	38.0	38.3	38.5	38.8	39.0	39.3	39.5	39.8	40.0
38	36.6	36.8	37.0	37.3	37.5	37.7	38.0	38.2	38.4	38.7	38.9	39.1
37	35.8	36.0	36.3	36.5	36.7	36.9	37.2	37.4	37.6	37.8	38.1	38.3
36	35.0	35.2	35.4	35.7	35.9	36.1	36.3	36.5	36.7	37.0	37.2	37.4
35	34.2	34.4	34.6	34.8	35.0	35.2	35.5	35.7	35.9	36.1	36.3	36.5
34	33.4	33.6	33.8	34.0	34.2	34.4	34.6	34.8	35.0	35.2	35.4	35.6
33	32.5	32.7	32.9	33.1	33.3	33.5	33.7	33.9	34.1	34.3	34.4	34.6
32	31.7	31.8	32.0	32.2	32.4	32.6	32.8	32.9	33.1	33.3	33.5	33.7
31	30.8	30.9	31.1	31.3	31.5	31.6	31.8	32.0	32.2	32.4	32.5	32.7
30	29.8	30.0	30.2	30.4	30.5	30.7	30.9	31.0	31.2	31.4	31.5	31.7
29	28.9	29.1	29.2	29.4	29.6	29.7	29.9	30.1	30.2	30.4	30.5	30.7
28	28.0	28.1	28.3	28.4	28.6	28.7	28.9	29.1	29.2	29.4	29.5	29.7
27	27.0	27.1	27.3	27.4	27.6	27.7	27.9	28.0	28.2	28.3	28.5	28.6

Reprinted from Refs. [47, 63], Copyright 2013, with permission from Elsevier

1.2.5 *Effect of CE on Perceived Temperature*

In the electric power load forecasting, CE indicates that electric ACEC is influenced not only by the temperature of that day, but also by the temperature of the previous day or days.

The following equation could be used to modify the temperature.

$$T_{DayMod} = \left(T_{day1}\lambda_{day1} + T_{day2}\lambda_{day2}\right) / \left(\lambda_{day1} + \lambda_{day2}\right) \tag{1.4}$$

In (1.4), λ represents the weight, which varies with temperature. It should reflect how the temperature influences electric ACEC. The subscript $day1$ means the day whose temperature is modified. The subscript $day2$ means the previous day of $day1$. T_{DayMod} is the modified temperature of $day1$. The method used to calculate λ in this chapter is presented in (1.5). The relationship between temperature and λ is shown in Fig. 1.5. Temperature has a great influence on electric ACEC when it is between 22 and 32 °C, while the influence decreases outside this range. Therefore, the rate of change of λ within this range will increase.

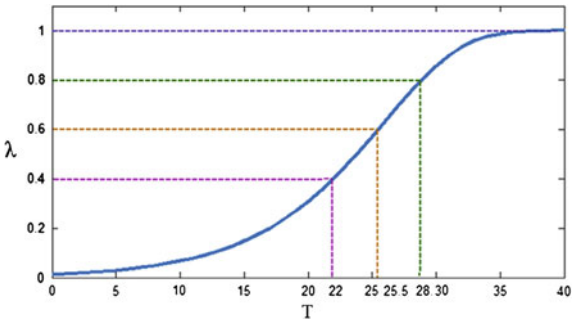

Fig. 1.5 Relationship between temperature and λ. Reprinted from Refs. [47, 63], Copyright 2013, with permission from Elsevier

$$\lambda = 1 - \exp(-\exp((T-26)/6))\sqrt{b^2 - 4ac} \tag{1.5}$$

It is worth noting that the temperature of the previous day in (1.4) should be the modified temperature, because it contains the temperature information of previous days.

The modification method is suitable for common circumstances with the exception of following circumstances:

As human's temperature sensation lags considerably behind weather changes, electric ACEC will grow rapidly after successive high-temperature days. In this situation, the modified temperature based on Eq. (1.4) can not reflect the exponential growth tendency of electric ACEC. Equation (1.6) is adopted instead:

$$T_{DayMod} = \left(\sum_{i \le 3} T_i \times \exp((n+1)/20)\right) \Big/ 3 \tag{1.6}$$

where i is 1, 2, 3, representing the day needed to be modified, a day before it and two days before it, respectively, and n represents the nth day in the sequence of consecutive high temperature days. People have seasonal habits of using air-conditioners. For example, in the early summer, air-conditioners are not in use even when the temperature is over 35 °C, while people will run air-conditioners when the average temperature is over 30 °C in mid-summer. Therefore, it is defined that the third day of m consecutive days ($m \ge 3$) above 35 °C is the beginning of high temperature days in early summer, and in mid-summer, when there are 3 days or more above 30 °C once the average temperature reaches 35 °C, the high temperature days begin.

Rain falls frequently during the summer in Beijing, but showery precipitation has a minimal cooling effect. As showery precipitation is short-lived and the rainfall associated with showery precipitation is low, the heat energy cannot be carried away from the earth's surface in a timely manner. Additionally, barometric pressure changes before or after a thunderstorm make people feel hot, causing an increase in electric ACEC. However, torrential rain is heavy and long-lasting, which cools the air quickly and decreases electric ACEC significantly. By assigning a weighting

factor of 6 to days with torrential rain, the cooling effect exerted on the following days greatly increases.

1.3 Interaction Between Urban Microclimate and Electric ACEC

1.3.1 Comprehensive Effect of Urban Microclimate on Electric ACEC

In Sect. 1.2, the influences of UHIE, THE and CE on ACEC are studied separately. In this section, they are considered in a comprehensive way. In other words, all of the three effects on electric ACEC are taken into consideration together in this subsection. The process of this comprehensive influence is shown in Fig. 1.6. The influence of urban microclimate on electric ACEC can be illustrated on both a temporal scale and a spatial scale. With regard to the temporal scale, the model contains weather information for several days, whereas at the spatial scale, UHIE, THE, CE and other factors that may affect the urban air temperature are integrated.

This type of integrated effect can be illustrated by the temperature T' as follows:

$$T' = h\{g[f(T)]\} \tag{1.7}$$

where T represents the air temperature without UHIE; $f(x)$ represents the influence of UHIE on temperature, $f(x) = x + HII$; $g(x)$ represents the influence of THE on temperature, $g(x) = HI(T, H)$; $h(x)$ represents the influence of the CE on temperature, and $h(x) = T_{DayMod}$.

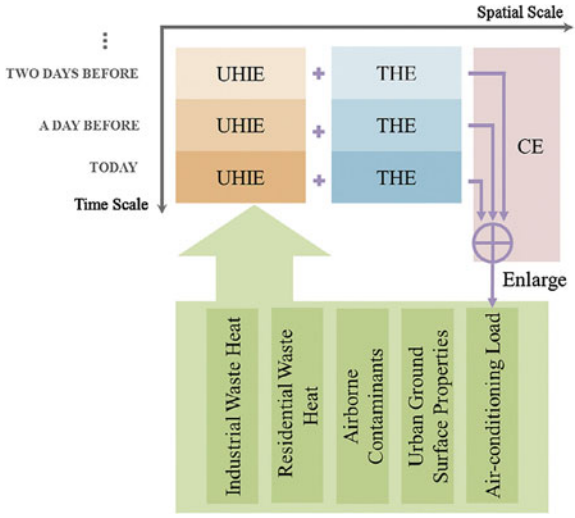

Fig. 1.6 Effect of urban microclimate on electric ACEC. Reprinted from Refs. [47, 63], Copyright 2013, with permission from Elsevier

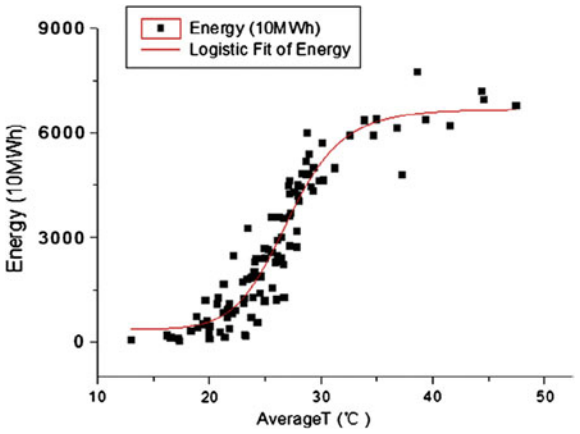

Fig. 1.7 The fitting curve of the relationship between temperature and electric ACEC based on consideration of the effect of urban microclimate. Reprinted from Refs. [47, 63], Copyright 2013, with permission from Elsevier

The high temperature season, namely summer in this chapter, is defined from the Chinese traditional solar term Xiazhi (June 21, 2005) to Chushu (August 23, 2005). During the period, the electric ACEC accounted for 24 % of the total electricity consumption and UHIE, THE and CE all existed. T is replaced by T' from June 21–August 23 and the relationship between the daily average temperature and electric ACEC from May to September (excepting May 1st–7th) is fitted again. A new relationship is obtained in (1.8) and the fitting curve is presented in Fig. 1.7. The coefficient of determination (R^2) increases from 0.81 to 0.90, proving that it is T', not T, which actually reflects human thermal sensation. So, the new mathematical relationship y′ can better reflect the relationship between the temperature and electric ACEC.

$$y' = (370.08 - 6668.21) \Big/ \left(1 + (x/27.1)^{11.09}\right) + 6668.21 \tag{1.8}$$

Electric ACEC should be $y'(T)$ when considering none of the three effects, while electric ACEC should be $y'(T')$ when considering all of the three effects. Thus, the electric ACEC resulting from UHIE, THE and CE is $y'(T') - y'(T)$. The electric ACEC resulting from the CE is $y'(T') - y'\{g[f(T')]\}$. The electric ACEC resulting from THE is $y'\{g[f(T)]\} - y'[f(T)]$. The electric ACEC resulting from UHIE is $y'[f(T)] - y'(T)$.

1.3.2 The Feedback of Electric ACEC on Urban Microclimate

It is known that electric air-conditioners produce waste heat which consists of two parts. The first is the heat converted from electric energy and the heat removed from the indoor air according to the energy efficiency ratio (EER) k. Thus, the total electric

air-conditioning waste heat is $(1 + k)$ times of that derived from energy consumption. According to the preliminary market survey, the EER value of residential and commercial air-conditioners in Beijing is approximately between 2 to 4. Thus, the total waste heat is 3–5 times of that derived from energy consumption. 4 times is chosen in this study.

The increased temperature caused by the waste heat can be calculated based on the following equation:

$$\Delta t = Q/mc \tag{1.9}$$

where Δt, Q, m and c are the temperature variation, heat variation, mass of air and specific heat capacity of air, respectively.

At 30 °C and standard atmospheric pressure, the dry air density is 1.165 kg/m^3, and the specific heat is 1.013 kJ/(kg × °C). The volume of air influenced by the waste heat can be calculated as the area of Beijing times its height. The statistics of [44] show that buildings with more than 10 floors (about 30 m if each floor is 3 m high) accounted for 41.4 % of the total buildings in Beijing in 2003. The master planning for Beijing city states that the height of Beijing's buildings is generally not more than 60 m [45]. So, the buildings which are higher than 60 m are ignored. That is, the buildings between 30–60 m high account for 41.4 % of the total buildings. Besides, Ref. [44] also shows that buildings with 1–3 floors, buildings with 4–6 floors and buildings with 7–9 floors account for 41.4, 35.9, 5.4 % of the total buildings, respectively. According to the data above, the average height of buildings in Beijing is estimated as the following equation: 2 × 3 × 17.3 % + 5 × 3 × 35.9 % + 8 × 3 × 5.4 % + 45 × 41.4 % = 26.3 m. Therefore, the mass of air in Beijing can be calculated as 1.165 kg/m^3 × 12,187 km^2 × 26.3 m = 3.734 × 10^{11} kg.

Besides, the electricity consumed by electric air-conditioners produces air pollutants during the generation process [46], and one ton of standard coal releases 8.5 kg of SO_2 and 7.4 kg of NO_x.

1.4 Discussion About Interaction Between Urban Microclimate and Electric ACEC

Urban microclimate characterized with UHIE, THE and CE has significant effects on ACEC. On the other hand, ACEC influences urban microclimate by strengthening UHIE. Therefore, the interaction between urban microclimate and ACEC is a saturated and positive feedback with a time lag [47].

As shown in Fig. 1.8, UHIE, THE and CE give rise to the increase in the electric ACEC during the summer. The characteristics of electric ACEC include: first, it produces large amounts of waste heat; second, it increases the emissions of CO_2, SO_2 and NO_x [48]; and third, the electric air-conditioning load contributes significantly to the peak load. Thus, the increased air-conditioning load may lead to an

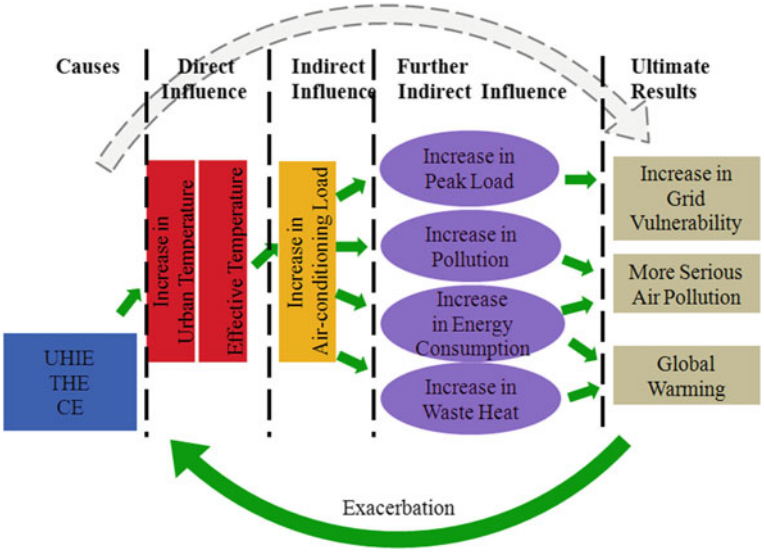

Fig. 1.8 Interaction between urban microclimate and electric ACEC. Reprinted from Refs. [47, 63], Copyright 2013, with permission from Elsevier

increase in the peak load, air pollution, waste heat and fuel consumption, and the increased peak load could further increase the vulnerability of power grid. The increase in fuel consumption could arouse an increase in air pollution and carbon emission. Additionally, the increase in fuel consumption and waste heat contributes to the global warming [49, 50]. These effects will in turn exacerbate UHIE, THE and CE, leading to a vicious cycle.

This study shows that, in Beijing from 2005, electric ACEC resulting from the comprehensive influence of those effects accounted for 11.28 % of summer's total electricity consumption and this percentage reached a peak of 20.4 %. The electric ACEC resulting from the comprehensive influence of UHIE, THE and CE accounted for 47 % of the summer's total electric ACEC and that the highest daily ratio could reach 85 %. It is much higher than the result in [30]. The electric ACEC resulting from CE, THE and UHIE were 287,455 MWh, 217,980 MWh and 815,299 MWh, respectively. The impact of urban microclimate on electric ACEC is shown in Fig. 1.9. The ratios of electric ACEC resulting from CE, THE and UHIE to the total air-conditioning consumption were 10.18, 7.72 and 28.88 %, respectively. The percentages on the right represent the ratios of electric ACEC resulting from each effect to the total air-conditioning consumption, and the percentages on the red arrows represent the increase in the amplitude of air-conditioning consumption resulting from each effect.

This study also indicates that electric air-conditioners discharged 3×10^9–5×10^9 kJ of waste heat, which largely increased the temperature during the summer of 2005 in Beijing. For example, on July 3, 2005, the rising temperature

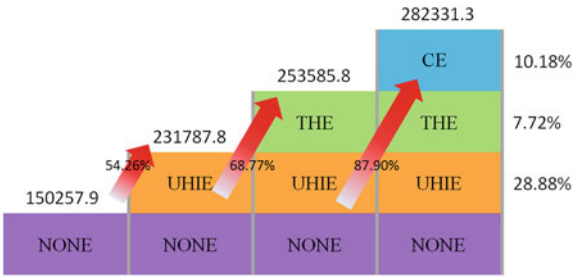

Fig. 1.9 The influence of urban microclimate on electric ACEC. Reprinted from Refs. [47, 63], Copyright 2013, with permission from Elsevier

due to electric air-conditioning waste heat was approximately 1.94 °C, nearly half of which was caused by the deterioration of urban microclimate. Moreover, the carbon emissions generated from air-conditioners reached 2.5 Mt in the summer of 2005 in Beijing.

All data used in this analysis are data in 2005, and it is conservatively estimated that ACEC may have increased by more than 100 % during the period. Thus, the current ACEC and deterioration of urban microclimate caused by the interaction is much greater than that in 2005.

If the average daily temperature of urban district decreased by 1 °C in the summer, considering the influence of UHIE, THE and CE, the energy consumption would decrease by 12.8 % during this period, along with carbon and waste heat decreasing by 0.3 Mt and 3.9×10^{12}–6.5×10^{12} kJ, respectively. On July 3, 2005, the decrease in the electric air-conditioning waste heat emission reduced the ambient temperature by 0.43 °C.

The implementation of measures to control certain links in this vicious cycle could contribute to the saving of energy and the mitigation of global warming [51, 52]. During this process, only UHIE can be artificially mitigated, while THE and CE are regarded as the effects of people's sensation of the weather which are considered uncontrollable. Effective measures to mitigate UHIE can contribute to a more comfortable living environment for citizens and energy consumption reduction. ACEC estimated in this chapter is much larger than that reported in previous literatures because of two reasons. The first is the influence of CE, which has never been mentioned before, and comprehensive influences of CE, UHIE and THE on temperature. The second is the positive feedback of ACEC on urban microclimate, which is always ignored in previous literatures.

It can be achieved to decrease urban temperature in two ways: mitigating UHIE directly or reducing the waste heat. Corresponding measures can be implemented to realize energy saving of a single air-conditioner, such as issuing a policy for the rational use of air-conditioners, achieving more efficient city planning and improving city traffic management [53, 54]. A monitoring system for energy saving of air-conditioners in urban areas to reduce ACEC and waste heat would be

established. By monitoring urban microclimate and the use of air-conditioners, the operation of air-conditioners can be adjusted according to the monitoring results in a timely manner.

1.5 The Influence of EVs on Urban Microclimate

As of December 2013, there were 405,000 highway-capable plug-in electric passenger cars and utility vans worldwide [55]. There is an increasingly hot debate on whether the replacement of CVs by EVs should be delayed or accelerated among researchers, enterprises, and governments [56], since EVs require higher cost and cause more pollution than CVs in the manufacturing process [57, 58].

Urban UHIE is influential in metropolitan areas [59]. For example, the surface temperatures in some urban areas of Beijing, China, on July 5, 2010, were nearly 50 °C [60, 61]. UHIE, which contributes to the extremely high temperatures in urban areas, is the main cause of this phenomenon.

UHIE would cause huge ACEC [13, 24, 62]. The positive feedback of ACEC on UHIE was proposed and evaluated in [63–65]. Heat emitted by vehicles and air-conditioners in buildings is the main source of anthropogenic heat emissions in urban areas and one of the main causes of UHIE [66]. As shown in Sect. 1.3.2, the strength of UHIE is measured in terms of HII and HII is calculated as the urban temperature minus the rural temperature, which depends on heat emissions, aerosol pollution, underlying ground surface, and ventilation, etc.

The replacement of CVs by EVs has important implications for UHIE. There is no doubt that CVs will be replaced by EVs in the long run due to fossil energy scarcity. However, there is an increasingly hot debate on whether the replacement of CVs by EVs should be delayed or accelerated [56]. Here two hidden benefits of EVs for addressing climate change to support the acceleration of the replacement are revealed. EVs emit much less heat than CVs within the same mileage, so the replacement of CVs by EVs can reduce heat emission to benefit local climate and reduce energy consumption to benefit global climate, as shown in Fig. 1.10.

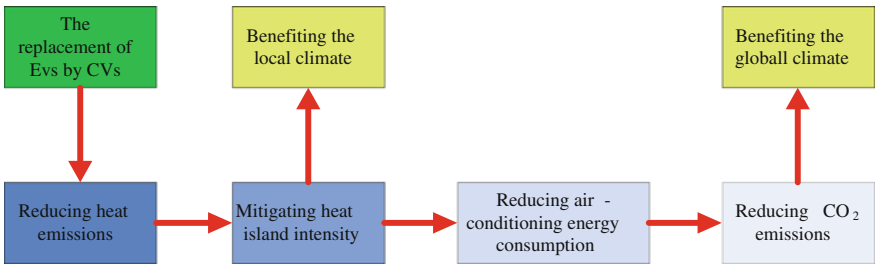

Fig. 1.10 Two hidden benefits of EVs for climate change. Reprinted by permission from Macmillan Publishers Ltd: Ref. [67], Copyright 2015

1.6 Case Study on Influences of EVs on Urban Microclimate

Heat emission ratio of EVs to CVs. Energy consumed by vehicles is all converted to heat directly or indirectly and eventually emitted to the air. Engines of CVs convert fuel energy into thermal and mechanical energy. Then the mechanical energy is converted to heat by overcoming mechanical friction (bearings, hubs, driveshafts, etc.), wind resistance and tire rolling resistance. Energy consumed by EVs is also converted to heat eventually [67].

In Beijing, the average fuel economy of light-duty vehicles was estimated to be 20.6 miles per gallon in 2012 [64]. The heat emitted by gasoline combustion per gallon is 130 million joules [68]. Therefore, the average heat emitted by CVs per mile would be 6.31 million joules, as shown in (1.10).

$$P_1 = \frac{1}{E_1} \times Q_1 = \frac{1}{20.6} \times (130 \times 10^6) = 6.31 \times 10^6 \,(\mathrm{J}) \tag{1.10}$$

where P_1 is the heat emission per mile by a CV, E_1 is the fuel economy, and Q_1 refers to the energy contained in a gallon of gasoline.

The electricity consumed by one EV per mile in China ranges from 18 to 25 kWh/100 km for different models [69]. Accordingly, taking the average, it is estimated as 0.346 kWh/mile. 1 kWh is equal to 3.6 million joules. The heat emitted by one EV per mile would be:

$$P_2 = E_2 \times Q_2 = 0.346 \times (3.6 \times 10^6) = 1.25 \times 10^6 \,(\mathrm{J}) \tag{1.11}$$

where P_2 is heat emission per mile by the EV, E_2 is the electricity per mile consumed by the EV, and Q_2 is the energy contained in a kilowatt-hour.

According to these assumptions and Eqs. (1.10) and (1.11), heat emitted by EVs per mile is estimated to be 19.8 % of that emitted by CVs, as shown in (1.12).

$$r = \frac{P_2}{P_1} = \frac{1.25}{6.31} \times 100\,\% = 19.8\,\% \tag{1.12}$$

where r is the ratio of heat emitted by EVs to that emitted by CVs.

Reduction of heat emission. In 2012, there were 5.2 million vehicles in Beijing [70]; the average daily driving distance was 30 miles [70]. The daily heat emitted by CVs was

$$H_1 = N_1 \times L \times P_1 = (5.2 \times 10^6) \times 30 \times (6.31 \times 10^6) = 9.85 \times 10^{14} \,(\mathrm{J}) \tag{1.13}$$

where H_1 is the daily heat emitted by CVs in the summer of 2012; N_1 is the number of vehicles in Beijing in 2012, and L is the average daily driving distance.

In the summer of 2012, the average load of air-conditioners in buildings was 5 million kW [71]. Therefore, the daily heat emitted by air-conditioners in buildings was

$$H_2 = P_2 \times N_2 \times Q_2 = (5 \times 10^6) \times 24 \times (3.6 \times 10^6) = 4.32 \times 10^{14}\,(\mathrm{J}) \quad (1.14)$$

where H_2 is the daily heat emitted by air-conditioners, P_2 is the average load of air-conditioners, and N_2 is the number of working hours per day. If CVs were replaced by EVs, the daily reduction of heat emission would be

$$H_3 = H_1 \times (1 - r) = (9.85 \times 10^{14}) \times (1 - 19.8\,\%) = 7.90 \times 10^{14}\,(\mathrm{J}) \quad (1.15)$$

where H_3 is the reduction of heat emission if CVs were replaced by EVs; r is defined in (1.12).

HII mitigation. The average HII was 2.77 °C during the summer of 2005 in Beijing [39] and 2.90 °C in 2009 [72]. The data in 2012 are not available from official statistics or academic papers. According to the growth rate of HII from 2005 to 2009, HII is estimated to be 3.0 °C in 2012.

Heat emission, mainly caused by vehicles and air-conditioners in buildings, contributes to about half of the HII in Beijing [73]. The decreased heat emission resulting from vehicle replacement is 1.83 times the emission of air-conditioners in buildings, according to Eqs. (1.13)–(1.15). Therefore, the replacement of CVs by EVs would have reduced HII by 0.97 °C in 2012 in Beijing, as shown in (1.16).

$$\Delta\mathrm{HII} = \mathrm{HII} \times k_1 \times \frac{H_3}{H_2 + H_3} = 3.0 \times 0.5 \times \frac{7.90}{4.32 + 7.90} = 0.97\,(^\circ\mathrm{C}) \quad (1.16)$$

where ΔHII is the decrease in HII resulting from the replacement of CVs by EVs, and k_1 is the contribution of heat emission to HII in Beijing.

Reduction of CO_2. In 2012 in China, 740 g CO_2 was emitted when one kWh of electricity was supplied to consumers [74]. Therefore, when 14.89 million kWh of electricity is saved, CO_2 emission could be reduced by 11,019 tonnes.

1.7 Reduction of ACEC

If HII were to decrease by 1 °C, the energy consumed by air-conditioners in buildings would decrease by 12.8 % during the summer in Beijing [63]. ACEC has occupied an increasing proportion of total energy consumption in recent years [69], which ensures the validity of our estimation. The reduction of HII resulting from vehicle replacement is near 1 °C; therefore it is assumed that the relationship between the reduction of HII and the energy saving of air-conditioners is linear. If CVs were replaced by EVs, the energy consumed by air-conditioners in buildings would decrease by 12.41 % during the summer in Beijing, as shown in (1.17).

$$k_2 = \Delta \mathrm{HII} \times 12.8\,\% = 12.41\,\% \tag{1.17}$$

where k_2 is the percentage of the decreased energy consumed by air-conditioners in buildings.

The amount of daily energy that could be saved is equal to 14.89 million kWh of electricity, reaching 27.59 % of the total electricity consumed by EVs, as shown in (1.18) and (1.19).

$$\Delta P_3 = P_3 \times N_2 \times k_2 = (5 \times 10^6) \times 24 \times 12.41\,\% = 14.89 \times 10^6\,(\mathrm{kWh}) \tag{1.18}$$

$$k_3 = \frac{\Delta P_3}{E_2 \times L \times N_1} = \frac{14.89 \times 10^6}{0.346 \times 30 \times (5.2 \times 10^6)} \times 100\,\% = 27.59\,\% \tag{1.19}$$

where ΔP_3 is the decreased energy consumed by air-conditioners in buildings if CVs were replaced by EVs, and k_3 is the ratio of ΔP_3 to energy consumed by EVs. With the decrease in ACEC, less heat would be emitted, which will also further contribute to mitigating UHIE and boosting energy saving.

According to the analysis and estimation above, the replacement of CVs by EVs can substantially alleviate UHIE in the summer in metropolitan areas, which can improve the local climate and significantly reduce ACEC and greenhouse gas emissions, thus contributing to addressing global climate change.

1.8 Conclusions

In Beijing in 2012, the average heat emission by a CV and an EV per mile were estimated to be 6.31 million joules and 1.25 million joules, respectively. Average heat emitted by an EV per mile was about 19.8 % of the heat emitted by a CV per mile.

In the summer of 2012, the daily heat emitted by CVs was 9.85×10^{14} joules and the daily heat emitted by air-conditioners was 4.32×10^{14} joules. If CVs were replaced by EVs, the reduction of daily heat emitted by vehicles would be 7.90×10^{14} joules.

The average HII was estimated at 3.0 °C in the summer of 2012 in Beijing. Heat emission, which is mainly caused by vehicles and air-conditioners in buildings, contributed about half of the HII in Beijing [73]. The decreased heat emission resulting from vehicle replacement is 1.83 times the emission of air-conditioners in buildings. Therefore, the replacement of CVs by EVs would have reduced HII by 0.97 °C in the summer of 2012 in Beijing (Fig. 1.11). Because of the reduction of HII, the energy consumed by air-conditioners in buildings would have decreased by 12.41 %. The amount of daily energy that could be saved is equal to 14.89 million kWh of electricity, which could reduce CO_2 emissions by 11,019 tonnes per day (Fig. 1.11). The results are described in Fig. 1.11.

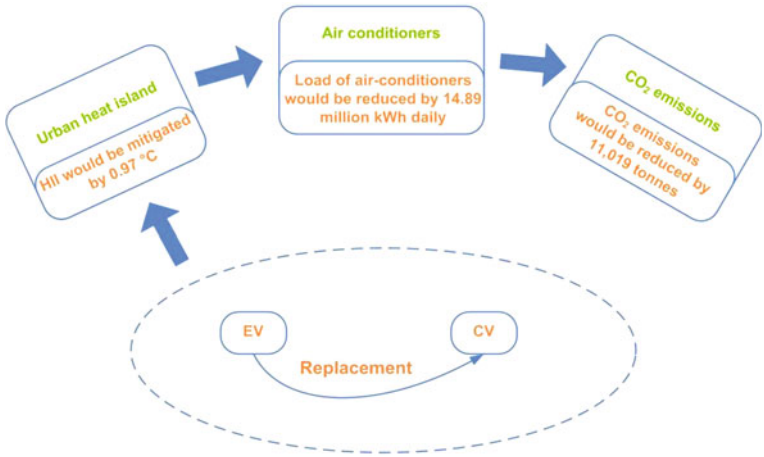

Fig. 1.11 Overview of the benefits of replacing CVs with EVs. Reprinted by permission from Macmillan Publishers Ltd: Ref. [67], Copyright 2015

The data in this chapter are mainly from earlier studies and the statistics of authorities, including Beijing government and the State Grid Beijing Electric Power Company. In this chapter, some data from other cities other than Beijing and of other years as a result of unavailability of data of 2012 Beijing were used; therefore, the estimated values of the benefits of replacing CVs by EVs are lower than they actually would be. Therefore, conclusion can be made that EVs can improve the microclimate by mitigating heat emission to dramatically reduce ACEC, consequently influencing the power system.

References

1. Xiao H, Huimei Y, Chen W, et al. A survey of influence of electrics vehicle charging on power grid. IEEE 9th Conference on 2014; 2014. p. 121–126.
2. Lopes JAP, Soares FJ, Almeida PMR. Integration of electric vehicles in the electric power system. Proc IEEE. 2011;99(1):168–83.
3. Yu X. Impacts assessment of PHEV charge profiles on generation expansion using national energy modeling system. Proceedings of Power and Energy Society General Meeting-Conversion and Delivery of Electrical Energy in the 21st Century. IEEE 2008; p. 1–5.
4. Denholm P, Short W. An Evaluation of Utility System Impacts and Benefits of Optimally Dispatched. National Renewable Energy Laboratory, Tech. Rep. 2006; NREL/TP-620-40293.
5. McCarthy D, Wolfs P. The HV system impacts of large scale electric vehicle deployments in a metropolitan area. Proceedings of 20th Australasian. IEEE 2010; p. 1–6.
6. Papadopoulos P, Cipcigan LM, Jenkins N, et al. Distribution networks with electric vehicles. Proceedings of the 44th International. IEEE 2009; p. 1–5.
7. Kelly L, Rowe A, Wild P. Analyzing the impacts of plug-in electric vehicles on distribution networks in British Columbia. Proceedings of Electrical Power & Energy Conference (EPEC). IEEE 2009; p. 1–6.

8. Zhong J, He LN, Li CB, et al. Coordinated control for large-scale EV charging facilities and energy storage devices participating in frequency regulation. Appl Energy. 2014;123:253–62.
9. Cao Y, Tan Y, Li C, et al. Typical schemes of electric vehicle charging infrastructure connected to grid. Autom Electr Power Syst. 2011;35(14):48–52 (In Chinese).
10. Kempton W, Tomić J. Vehicle-to-grid power implementation: From stabilizing the grid to supporting large-scale renewable energy. J Power Sour. 2005;144(1):280–94.
11. Chua KJ, Chou SK, Yang WM, Yan J. Achieving better energy-efficient air-conditioning—a review of technologies and strategies. Appl Energy. 2013;104:87–104.
12. Root TL, Price JT, Hall KR, et al. Fingerprints of global warming on wild animals and plants. Nature. 2003;421:57–60.
13. Grimm NB, Faeh SH, Golubiewski NE, et al. Global change and the ecology of cities. Science. 2008;319:755–60.
14. Dye C. Health and urban living. Science. 2008;319:766–9.
15. Lederbogen F, Kirsch P, Haddad L, et al. City living and urban upbringing affect neural social stress processing in humans. Nature. 2011;474:498–501.
16. Li CB, Shang J, Zhu S, et al. An analysis of energy consumption caused by air temperature affected accumulative effect of the air conditioning load. Autom Electr Power Syst. 2010;34 (20):30–3.
17. Lam Tony NT, Wan Kevin KW, Wong SL, et al. Impact of climate change on commercial sector air conditioning energy consumption in subtropical Hong Kong. Appl Energy. 2010; 87(7):2321–7.
18. Chua KJ, Chou SK, Yang WM, Yan J. Achieving better energy-efficient air conditioning—a review of technologies and strategies. Appl Energy. 2013;104:87–104.
19. Ascione F, Bianco N, de' Rossi F, Turni G, Peter Vanoli Giuseppe. Green roofs in European climates. Are effective solutions for the energy savings in air-conditioning?. Appl Energy 2013; 104: 845–59.
20. Aktacir MA, Buyukalaca O, Yilmaz T. A case study for influence of building thermal insulation on cooling load and air-conditioning system in the hot and humid regions. Appl Energy. 2010;87(2):599–607.
21. Hirano Y, Fujita T. Evaluation of the impact of the urban heat island on residential and energy consumption in Tokyo. Energy. 2012;37(1):371–83.
22. Giridharan R, Ganesan S, Lau SSY. Daytime urban heat island effect in high-rise and high-density residential developments in Hong Kong. Energy Build. 2004;36(6):525–34.
23. Hassid S, Santamouris M, Papanikolaou N, et al. The effect of the Athens heat island on air conditioning load. Energy Build. 2000;32:131–41.
24. Kolokotroni M, Giannitsaris I, Watkins R. The effect of the London urban heat island on building summer cooling demand and night ventilation strategies. Sol Energy. 2006; 80(4):383–92.
25. Contaxi E, Delkis C, Kavatza S, Vournas C. The effect of humidity in a weather sensitive peak load forecasting model. Proceedings of Power Systems Conference and Exposition. IEEE 2006; p. 1528–1534.
26. Amell AA, Cadavid FJ. Influence of the relative humidity on the air cooling thermal load in gas turbine power plant. Appl Therm Eng. 2002;22:1529–33.
27. Ihara T, Genchi Y, Sato T, et al. City-block-scale sensitivity of electricity consumption to air temperature and air humidity in business districts of Tokyo, Japan. Energy. 2008;33 (11):1634–45.
28. Fang Y, Shen S, Han Y, et al. A study of seasonal urban heat environment in Beijing based on TM image. Clim Environ Res. 2011;16(4):487–93.
29. Patz JA, Lendrum DC, Holloway T, et al. Impact of regional climate change on human health. Nature. 2005;438:310–7.
30. Zhou L, Dickinson RE, Tian Y, et al. Evidence for a significant urbanization effect on climate in China. PNAS. 2004;101(26):9540–4.

31. Rosenfeld A, Romm JJ, Akbari H, et al. Policies to reduce heat islands magnitudes of benefits and incentives to achieve them. Proceedings of the 1996 ACEEE summer study on energy efficiency in buildings 1996; 9:177.
32. China city statistical yearbook 2011. http://tongji.cnki.net/kns55/Navi/Home\Page.aspx?id=N2012020070&name=YZGCA&floor=1.
33. Beijing-China [Internet]. Beijing: The operational support plan for summer peak in 2011 summer. Beijing. http://zhengwu.beijing.gov.cn/gzdt/gggs/t1190167htm.
34. Liu W, Ji C, Zhong J, Jiang X, Zheng Z. Temporal characteristics of the Beijing urban heat island. Theoret Appl Climatol. 2007;87:213–21.
35. Yu E, Liu G, Zhou J. Energy management system. Beijing: Science Press; 1998.
36. Fan JY, McDonald JD. A real-time implementation of short-term load forecasting for distribution energy systems. IEEE Trans Power Syst. 1994;9(2):988–94.
37. Hagan MT, Behr SM. The time series approach to short-term load forecasting. IEEE Trans Power Syst. 1987;2(3):785–91.
38. Oke TR. The energetic basis of the urban heat island. Quarterly Journal of the Royal Meteorological. Society 1982; 108: 1–24.
39. Xinhuanet [Internet] Heat island effect in Beijing: the intensity will be 10 percent lower. http://news.xinhuanet.com/newscenter/2005-08/23/content_3392449.htm.
40. News4Jax [Internet] George Winterling: a lifelong passion for weather. http://www.news4jax.com/news/George-Winterling-A-Lifelong-Passion-For-Weather/-/475880/2047548/-/ot55e0z/-/index.html.
41. Burton AC, Snyder RA, Leach WG. Damp cold versus dry cold specific effects of humidity on heat exchange of unclothed man. J Appl Physiol. 1955;8(3):269–78.
42. Rothfusz LP. The heat index 'equation' (or, more than you ever wanted to know about heat index). NWS Technical Attachment SR90-23. NWS Southern Region Headquarters, Fort Worth, TX.
43. Chu W, Chen Y, Xu Z, et al. Multiregion short-term load forecasting in consideration of HI and load/weather diversity. IEEE Trans Ind Appl. 2011;47(1):222–37.
44. Hu SD. Analysis on high-rise building development in Beijing in recent years. Architctural Technol. 2005;36(6):408–11 (In Chinese).
45. Beijing-China [Internet] The master planning for Beijing city (1991–2010). http://www.bjpc.gov.cn/fzgh_1/csztgh/200710/t195451_8.htm.
46. Akimoto H. Global air quality and pollution. Science. 2003;302:1716–9.
47. Li C, Zhou J, Cao Y, et al. Interaction between urban microclimate and electric air-conditioning energy consumption during high temperature season. Appl Energy. 2014;117:149–56.
48. Zhu D, Tao S, Wang R, et al. Temporal and spatial trends of residential energy consumption and air pollutant emissions in China. Appl Energy. 2013;106:17–24.
49. Meinshausen M, Meinshausen N, Hare W, et al. Greenhouse-gas emission targets for limiting global warming to 2 & #xB0;C. Nature. 2009;458:1158–62.
50. Parker DE. Climate: large-scale warming is not urban. Nature 2004; 290–290.
51. Schiermeier Q, Tollefson J, Scully T, Witze A, Morton O. Energy alternatives: electricity without carbon. Nature. 2008;454:816–23.
52. Kramer GJ, Haigh M. No quick switch to low-carbon energy. Nature. 2009;9(462):568.
53. Bell LE. Cooling, heating, generating energy, and recovering waste heat with thermoelectric systems. Science. 2008;321:1457–61.
54. Sachs JD, Reid WV. Investments toward sustainable development. Science. 2006;312(5776):1002.
55. Zentrum für Sonnenenergieund Wasserstoff-Forschung Baden-Württemberg(ZSW), Weltweit über 400.000 Elektroautos unterwegs. News (2014). http://www.zsw-bw.de/infoportal/presseinformationen/presse-detail/weltweitueber-400000-elektroautos-unterwegs.html.
56. Quill E. Unclogging urban arteries. Science. 2008;319(5864):750–1.
57. Zehner O. Unclean at any speed. IEEE Spectr. 2013;50(7):40–5.

58. Michalek JJ, Chester M, Jaramillo P, et al. Valuation of plug-in vehicle life-cycle air emissions and oil displacement benefits. Proc Natl Acad Sci. 2011;108(40):16554–8.
59. Sanderson, K. Why it's hot in the city. Nature News. (2009). http://www.nature.com/news/2009/091224/full/news.2009.1164.html.
60. China's Energy Information Network, Beijing is in high temperature recently. News (2010). http://epb.nengyuan.net/2010/0706/15047_6.html. (In Chinese).
61. Mu Y. 7000 traffic policemen stick to their post in the high temperature of 40.3uC. Sina news (2010). http://auto.sina.com.cn/service/2010-07-06/1112621362.shtml. (In Chinese).
62. Hashem A. Energy saving potentials and air quality benefits of urban heat island mitigation. Proceedings of the first international conference on passive and low energy cooling for the built environment. Athens: Ernest Orlando Lawrence Berkeley National Laboratory, Berkeley, CA Press, 2005.
63. Li C, Zhou J, Cao Y, et al. Interaction between urban microclimate and electric air-conditioning energy consumption during high temperature season. Appl Energy. 2014;117:149–56.
64. Yang J, Liu Y, Qin P, et al. A review of Beijing's vehicle lottery: short-term effects on vehicle growth, congestion, and fuel consumption. Energy Policy. 2014;1:1–30.
65. Hashem A. Reducing Urban Heat Island: Compendium of Strategies, Urban Heat Island Basics. Technical report. (2013). http://www.epa.gov/heatislands/resources/pdf/BasicsCompendium.pdf.
66. Huo H, Zhang Q, Wang MQ, et al. Environmental implication of electric vehicles in China. Environ Sci Technol. 2010;44(13):4856–61.
67. Li C, Cao Y, Zhang M, et al. Hidden Benefits of Electric Vehicles for Addressing Climate Change. Scientific reports 2015; 5.
68. Alson J. Light-Duty Automotive Technology, Carbon Dioxide Emissions, and Fuel Economy Trends: 1975 through 2013. Technical report. (2014). http://www.epa.gov/heatislands/resources/pdf/BasicsCompendium.pdf.
69. Hou C, Wang H, Ouyang M. Survey of daily vehicle travel distance and impact factors in Beijing. Proceedings of 7th IFAC Symposium on Advances in Automotive Control. Tokyo: International Federation of Automatic Control Press, 2013.
70. Beijing Municipal Bureau of Statistics, Beijing Statistical Yearbook 2012. Technical report. (2012). http://www.bjstats.gov.cn/nj/main/2012-tjnj/index.htm. (In Chinese).
71. Lei B. The high temperature increases the proportion of air conditioning load and the power grid companies response positively. News (2012). http://www.indaa.com.cn/dwxw2011/dwyw/201208/t20120827_1117010.html. (In Chinese).
72. Di S, Wu W, Liu H, Yang S, et al. The correlation ship between urban greenness and heat island effect with RS technology: A case study within 5th Ring Road in Beijing. J Geo-Inf Sci. 2012;4:481–9 (In Chinese).
73. Li Y, Zhao X. An empirical study of the impact of human activity on long-term temperature change in China: A perspective from energy consumption. J Geophys Res: Atmos. 2012;17:1–12.
74. Birol F. World Energy Outlook Special Report 2013: Redrawing the Energy-Climate Map. Technical report. (2013). http://www.iea.org/publications/freepublications/publication/WEO_Special_Report_2013_Redrawing_the_Energy_Climate_Map.pdf. Accessed 21 Sep 2014.

Chapter 2
The Response of EV Charging Loads to TOU Price

2.1 Introduction

One of the bottlenecks that restrict the rapid growth of EVs is the lack of the EV charging facilities [1–5]. The model of fuel cell charger is established and a corresponding control strategy is proposed in [3]. A new concept of mobile charger and its optimal scheduling methods are presented in [4]. With incremental development in EV charging facilities, EV loads are expected to increase phenomenally in the near future, which will bring negative impacts on the stability of power grids [6]. EV loads are seldom taken into account in current practice of power system planning, which results in risks in system operations and management [7].

There are three main ways to enable EV-friendly access to power grid: (1) V2G; (2) the use of energy management equipments (such as energy management concentrator and distributed energy management boxes); (3) the mechanism of electricity pricing. The power electronic converter technology that enables V2G is discussed in [8–10]. Energy management equipments can be used to maintain the balance between demand and supply, thus giving a boost to the utilization of EVs. Local and global smart charging control strategies based on home energy control box are discussed in [11], and it is discovered that smart charging control strategy can reduce peak load and level the load curve. The plug-in hybrid electric vehicle (PHEV) management equipments are adopted to manage PHEVs in cities in [12]. The PHEV management equipments are able to determine the number of PHEVs connected to the grid according to power flow calculation. Based on Micro-Simulation, the capacity of PHEVs connected to power grid by introducing intelligent charging policy implemented in central and distributed locations is optimized. Autostromboxes and the Demand Side Management System are used to manage the charging load in [13]. A global optimization technique is presented to reduce the error between reference curve and the summarized load curve of all charging events. The electricity pricing mechanism serves as the stimulation and guide for power demand and consumption mode of customers. Customers will

C. Li et al., *Influences of Electric Vehicles on Power System and Key Technologies of Vehicle-to-Grid*, Power Systems,
DOI 10.1007/978-3-662-49364-9_2

respond to variable electricity prices, decide whether they prefer charging or discharging EVs, and actively adjust charging rate and time. Countries with mature electricity market environment have focused their research on this area. For instance, an EV charging model based on real-time price information is introduced in [14], while Ref. [15] optimizes the charging process by using the method of quadratic programming and considering the relationship between electricity price and load demand. The objective is to minimize charging cost and maximize discharging profit. Linear programming model is used to make response to the real-time price in [16].

Situations are totally different in countries where electricity market is fully regulated. China's electricity market may be a typical example of regulated market, where electricity prices are decided by the government and, once enacted, remain unchanged for a relatively long time. At present, the electricity pricing mechanism in China mainly includes the catalog price, the stepwise power tariff and the TOU price. Unlike the catalog price and the stepwise power tariff, TOU price is not the same in different periods of one day, making it an important method for demand side management [17]. It is estimated that by 2050 the number of EVs in China will reach 200 million, and the total charging load will be up to 330 million kW [18]. With such a considerable capability, the EVs in China will play a significant role in balancing power supply and demand. Thereby, research on intelligent response to TOU price is of significance in market-regulated countries. Based on the existing research and the SOC curve, this chapter proposes an optimized charging model for a regulated market. By using the proposed method, EVs are able to adjust charging power and time and reduce the cost of customers, thus achieving peak shaving and valley filling in load demand.

2.2 Optimized Charging Model in Response to TOU Price

In regulated electricity markets, TOU price is set by the government in advance, and the prices remain unchanged for a long time. The user can set the expected ending time of charging when EVs are connected to the grid through the charger. To protect the battery from being damaged in charging process, the maximum charging power can also be set artificially. The charger with embedded TOU price module can intelligently formulate optimized charging scheme in consideration of the SOC curve and the maximum charging power set by the user, the aim of which is to minimize the cost and realize peak shaving and valley filling.

Objective Function. Take the cost that EV users need to pay to charge once as objective function

$$\min C = \int_{t_0}^{t_0+T} M(t)P(t)dt \tag{2.1}$$

In (2.1), t_0 is the starting time of charging, T is the duration of charging, $t_0 + T$ is the ending time of charging. $M(t)$ and $P(t)$ represent the unit price and charging power in time t respectively.

Constraints. The initial SOC of various EV batteries are different as driving modes and charging habits of different EV users are not the same. The energy demand of EV users with initial SOC considered is stated as below

$$\int_{t_0}^{t_0+T} P(t)dt = (1 - S_{inl})Q_r \tag{2.2}$$

In (2.2), S_{inl} represents the initial SOC of EV battery and Q_r is the rated capacity of EV battery.

According to Mass Theory [19], in order to reduce the life loss of EV battery, the charging current should not exceed the acceptable charging current of EV battery $I = I_0 e^{-\alpha t}$ (I_0 is the maximum charging current at the starting time, α is ratio of acceptance). Theoretically I_0 is determined by initial SOC and internal resistance of EV battery [20]. The highest acceptable voltage of EV battery should not exceed a certain limited value as well.

From the power expression $P = VI$, the charging power of EV battery should not exceed a certain limited value. The charging power is constrained by (2.3)

$$0 \le P \le P_{battery}(t) \tag{2.3}$$

In (2.3), $P_{battery}(t)$ represents the maximum acceptable charging power of EV battery in time t, which is the function of SOC and temperature of battery. Temperature effect on $P_{battery}(t)$ can be ignored when some measures are taken to keep the temperature of battery constant. Then the maximum acceptable charging power can be expressed as below

$$P_{battery}(t) = f(S) \tag{2.4}$$

In (2.4), S is the current SOC of EV battery. The quantitative relationship between $P_{battery}(t)$ and S can be described by SOC curve which is shown in Fig. 2.1 [21].

Besides the constraint $P_{battery}$, which is the maximum acceptable charging power of EV battery, the maximum charging power is also restricted by: (1) the maximum power P_{user} set by EV users; (2) the maximum power $P_{charger}$ EV charger can output. Therefore, the actual maximum power in charging process is

$$P_{\max} = \min\{P_{user}, P_{charger}, P_{battery}\} \tag{2.5}$$

Usually, both the maximum power P_{user} set by EV users and the maximum power $P_{charger}$ EV charger can output are greater than the maximum acceptable charging power $P_{battery}$ of EV battery. So the actual maximum charging power $P_{\max}$ is limited by $P_{battery}$ in most cases. Equations (2.2)–(2.5) consist of all constraints of optimized model presented above.

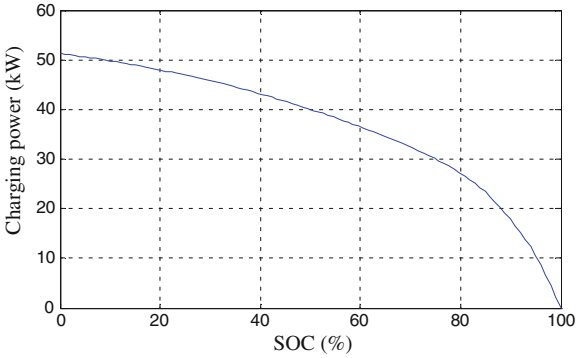

Fig. 2.1 The SOC curve. © (2012) IEEE. Reprinted, with permission, from Ref. [22]

2.3 Algorithm

As a continuous mathematical model, the above optimized model is discretized for the convenience of calculation. The total charging time T is divided into N periods, and the length of each period is Δt. The discretized optimized model can be expressed as:

$$\min C = \sum_{i=1}^{N} M(t_i)P(t_i)\Delta t \tag{2.6}$$

The constraint of maximum charging power limited by SOC is nonlinear, so a heuristic algorithm is designed [22].

(1) Charge the EV battery with the maximum power $P_{\max}$ from the starting time ($t = t_1$) until the battery SOC = 1 or $t = t_N$ (user-specified end time). If the battery is not filled until $t = t_N$, stop the optimization. Otherwise, go to step (2).
(2) An initial feasible solution $P_0 = [p_1, p_2, \ldots, p_n]$ (p represents the charging power) is obtained after step (1). Sorting the N periods based on TOU price is required. Symbols i and j are ascending sorted sequences, which means $M(t_i + 1) > M(t_i)$ and $M(t_j + 1) > M(t_j)$, $i = 1, 2, \ldots, N$, $j = 1, 2, \ldots, N$.
(3) Set charge energy q as optimal step. The charge energy q transferred from high-price period to low-price period is defined as optimal step. The charge power e transferred from high-price period to low-price period can be expressed as $e = q/\Delta t$. In order to improve the precision of the simulation, q should take a small value such as 10^{-6}.
(4) Assign $i = N$.
(5) Assign $j = 1$.
(6) Judge whether the energy left in period t_i is available for transference. When $P(t_i) > e$, go to step (7); otherwise, go to step (11).

(7) Judge the sequence of period t_i and period t_j. If $t_i < t_j$, go to step (8), which means it will not break the SOC constraint when transferring energy q from period t_i to period t_j directly. The reason is as follows: Assume $Q(t_n)$ and $Q(t'_n)$ indicate the energy stored in battery before and after the transference respectively. When n < j, there exists $Q(t'_n) = Q(t_n)(n < i)$ or $Q(t'_n) = Q(t_n) - q\ (n \geq i)$; when $n = j$, there exists $Q(t'_n) = Q(t_n)$. It can be seen clearly that the SOC of EV battery in each period will not increase. As the charging power doesn't exceed the limit before the transference, the charging power cannot exceed the limit after the transference either. If $t_i > t_j$, go to step (9).

(8) Transfer the energy from the high-price period to the low-price period. It can be expressed with mathematical equations as: $P(t_i) = P(t_i) - e$; $P(t_j) = P(t_j) + e$. After this, the procedure goes to step (6).

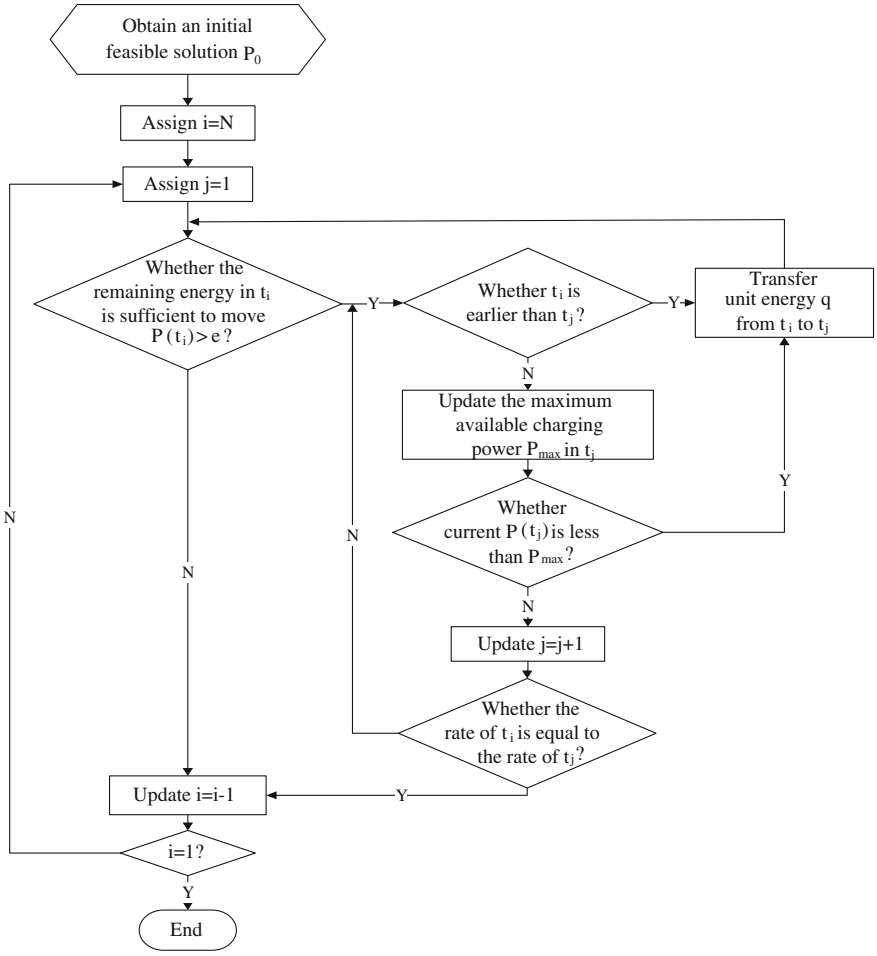

Fig. 2.2 The flowchart of optimization charge. © (2012) IEEE. Reprinted, with permission, from Ref. [22]

(9) Judge whether $P(t_j)$ is sufficient to achieve the maximum charging power $P_{\max}$. If $P(t_j) < P_{\max}$, go to step (8); otherwise, go to step (10).
(10) Set $j = j + 1$ and judge whether the price of period t_j is equal to the price of period t_i. If $M(t_i) = M(t_j)$, go to step (11); Otherwise, go to step (7).
(11) Set $i = i - 1$ and judge whether i is equal to 1. When $i = 1$, it means there is no more energy that can be transferred from the high-price period to the low-price period, then stop the optimization. Otherwise, go to step (5).

The flowchart of the above optimization program is shown in Fig. 2.2.

2.4 Case Study

In order to verify the effectiveness of the optimized charging model presented in this chapter, a typical charging pattern for comparison is adopted. It is a common charging pattern of "plug and charge", the charging profile of which is consistent with the charging characteristics of battery. Nevertheless, the charging profile may not follow the charging characteristics of battery in the optimized charging pattern, as it is determined by optimized charging algorithm which has been stated in previous section of this chapter. The charging cost and energy demand in different time are compared separately in two cases: single EV and multi-EV. In multi-EV case, the diversity of initial SOC and the starting charging time of different EVs should be considered. A probability model is introduced to describe the diversity, which will be discussed later. For single EV case, the randomness of initial SOC and the starting time of charging are neglected and assigned with specified value so as to get determined results, which is beneficial for us to understand the optimized charging model. In the following section, settings and results of simulation will be presented.

2.4.1 Settings of Simulation

Typical charging characteristics of lithium-ion battery. The charging curve of the lithium-ion battery equipped in Nissan Altra EV is shown in Fig. 2.3 [23]. In completely discharging situations, the demand for energy is 29.07 kWh. In this study, the charging curve in Fig. 2.3 of typical charging pattern is employed.

The starting time of charging. It has much randomness at the starting time of charging. And a distribution model of the starting time is established to describe this randomness. Assume that the distribution of the starting time obeys a Gaussian distribution, that is

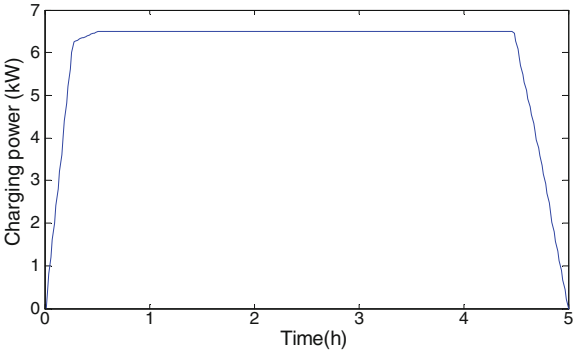

Fig. 2.3 The charging curve of the lithium-ion battery equipped in Nissan Altra EV. © (2012) IEEE. Reprinted, with permission, from Ref. [22]

$$f(t, \mu, \sigma) = \frac{1}{\sqrt{2\pi\sigma^2}} e^{-(t-\mu)^2/(2\sigma^2)} \tag{2.7}$$

Most EV users start charging after returning home from work at 18:00 and the starting time for charging of more than ninety percent of EV users is between 13:00 and 23:00. Therefore, in this case, it takes μ as 18 and takes σ as 5 [16]. The probability distribution of the starting time is shown in Fig. 2.4.

The initial SOC. The initial SOC of EV battery also presents some certain randomness. Using probability distribution model, it is described as

$$f(\mathrm{s}, \mu, \sigma) = \frac{1}{\sqrt{2\pi\sigma^2}} e^{-(\mathrm{s}-\mu)^2/(2\sigma^2)} \tag{2.8}$$

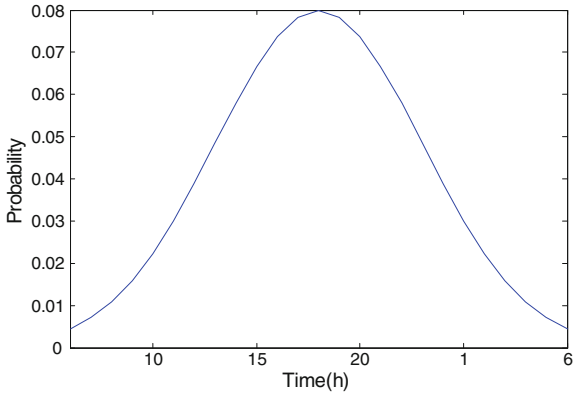

Fig. 2.4 The distribution curve of the starting time of charging. © (2012) IEEE. Reprinted, with permission, from Ref. [22]

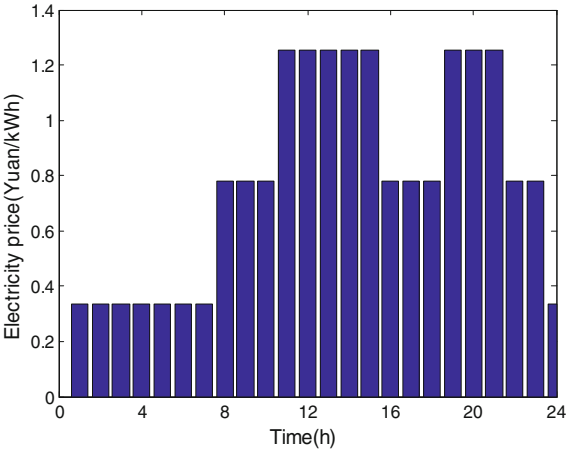

Fig. 2.5 The histogram of TOU price. © (2012) IEEE. Reprinted, with permission, from Ref. [22]

s represents the initial SOC of EV battery and it is commonly between 0.2 and 0.8. It takes μ as 0.5 and takes σ as 0.3. μ is the average value of SOC and σ is the standard deviation.

TOU price. According to the actual TOU price implemented in Beijing, the period of valley load is defined as 23:00–07:00, totally 8 h; the period of peak load is defined as 10:00–15:00 and 18:00–21:00, totally 8 h. The remaining time is the period of flat load. Adopting the actual price of electricity in the city, the prices of peak, flat and valley load period are 1.253, 0.781 and 0.335 Yuan/kWh. The histogram of TOU price is shown in Fig. 2.5.

2.4.2 The Results and Analysis of Simulation

(1) The case of charging for single EV
In order to verify the effectiveness of the optimized charging model and for the convenience to observe the optimization process, the case of charging for single EV is implemented. Taking 20:00 as the starting time of charging and 12 h as the total charging time, the energy demand of typical charging pattern and optimized charging pattern in different time is shown in Fig. 2.6. As it can be seen, the optimized charging pattern can avoid peak demands and choose intelligently to charge in the time of valley demands, which can reduce charging costs.

(2) The case of charging for multi-EV
The starting time of charging and initial SOC should be considered in the case of charging for multi-EV. Therefore, the Gaussian distribution function is implemented to describe the differences. According to data of 2010, the number of automobiles in Beijing reached 4.69 million [24]. Assume the penetration of EVs (defined as the ratio of the number of EVs and the total

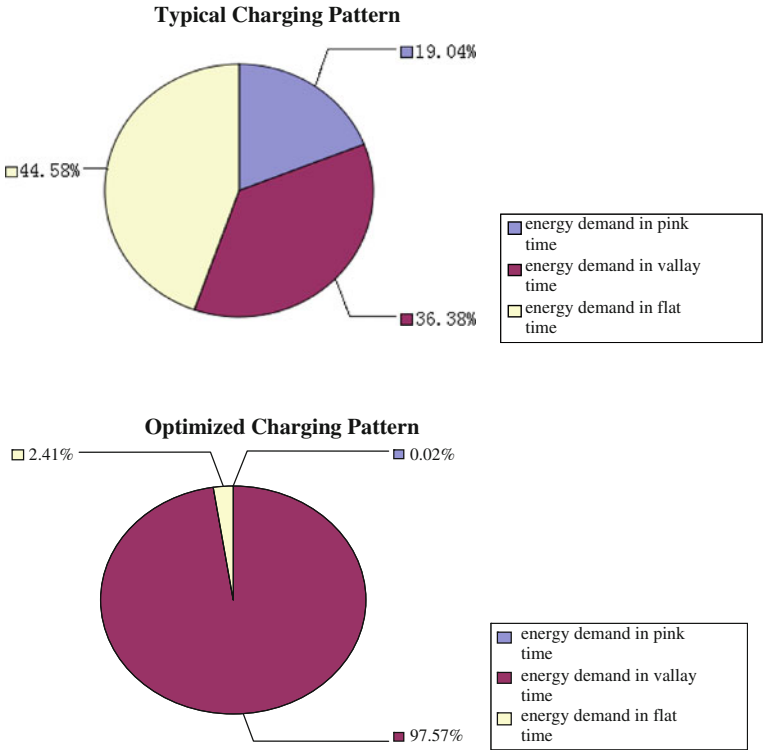

Fig. 2.6 The comparison of different charging patterns for single EV. © (2012) IEEE. Reprinted, with permission, from Ref. [22]

number of automobiles [11]) is 5 % and the number of EVs is about 234,500. In the process of computation, the average charging time of EV is about six hours. Figure 2.7 shows the energy demand of different charging patterns in Multi-EV charging case. As it can be seen, the optimized charging pattern in Multi-EV charging case can shift a mass of peak load to valley load, which is similar with that of single charging case.

Table 2.1 lists the charging cost of different charging patterns in different cases. It is clearly seen that the optimized charging pattern can bring a significant reduction in the charging cost of EV users. And it is evident that the performance of single EV case shown in the table is better than that of multi-EV case. The reason may be attributed to the available optimal space. In single EV case, the time span of charging covers more low-price periods, which means the optimal space and it is relatively large. So, through the optimization, almost all of the charging will be concentrated in low-price periods resulting in a better performance. From another perspective, it is implied that the charging cost will be less if EV users can consciously arrange appropriate plug-in time.

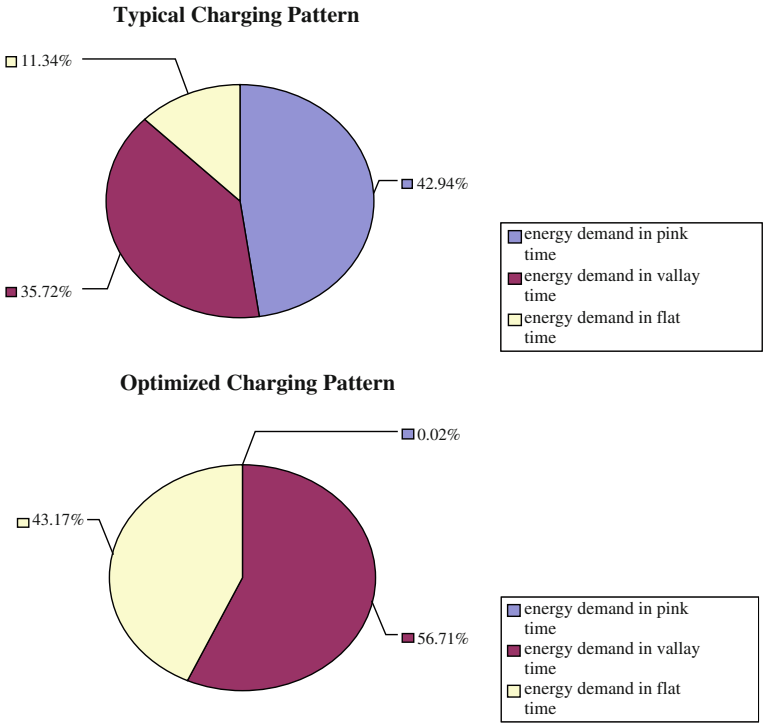

Fig. 2.7 The comparison of different charging patterns for multi-EV. © (2012) IEEE. Reprinted, with permission, from Ref. [22]

Table 2.1 The charging cost of different charging patterns in different cases

	Typical charging pattern	Optimized charging pattern	Reduction in cost (%)
The charging cost of single EV (Yuan)	20.673	10.02	51.52
The charging cost of multi-EV (104 × Yuan)	2179.4	1314.9	39.67

© (2012) IEEE. Reprinted, with permission, from Ref. [22]

2.5 Conclusions

In this chapter an intelligent charging method for EV charging facilities is proposed in response to TOU price. The purpose is to alleviate the stress in power grid under peak demand and to meet requirements for the demand response in regulated markets.

A comparative analysis of typical charging pattern and optimized charging pattern for charging performance in different cases is also presented. Simulation

results of both single EV and multi-EV have validated the effectiveness of the proposed approach. This chapter can serve as a useful reference for research on charging strategies in an open electricity market.

References

1. Etezadi-Amoli M, Choma K, Stefani J. Rapid-charge electric-vehicle stations. IEEE Trans Power Del. 2010;25(3):1883–7.
2. Takagi M, Iwafune Y, Yamamoto H, et al. Energy storage of PV using batteries of battery switch stations. Proceedings of IEEE International Symposium Industrial Electronics (ISIE) 2010;3413–3419.
3. Jiang Z, Dougal R. Control strategies for active power sharing in a fuel-cell-powered battery-charging station. IEEE Trans Ind Appl. 2004;40(3):917–24.
4. Li Z, Sahinoglu Z, Tao Z, et al. Electric vehicles network with nomadic portable charging stations. Proceedings of IEEE 72nd Vehicular Technology Conference Fall (VTC 2010-Fall) 2010;1–5.
5. Zhu X, Chen W, Luo J. Design and exploitation of supervisory control system for commercial electric vehicle charging station based on virtual DPU technology. Proceedings of 2010 Power System Technology 2010;1–5.
6. Salihi JT. Energy requirements for electric cars and their impact on electric generation and distribution systems. IEEE Trans Ind Appl 1973;IA-9(5):516–531.
7. Kabisch S, Schmitt A, Winter M, et al. Interconnections and communications of electric vehicles and smart grids. Proceedings of IEEE Smart Grid Communications Conference 2010;61–166.
8. Zhou X, Wang G, Lukic S et al. Multifunction bi-directional battery charger for plug-in hybrid electric vehicle application. Proceedings of IEEE Energy Conversation Congress Exposition 2009;3930–3936.
9. Pillai JR, Bak-Jensen B. Vehicle-to-grid for islanded power system operation in Bornholm. Proceedings of IEEE Power Energy Society General Meeting 2010;1–8.
10. Kisacikoglu MC, Ozpineci B, Tolbert L M. Examination of a PHEV bidirectional charger system for V2G reactive power compensation. Proceedings of 25th Annual IEEE Application Power Electronics Conference Exposition (APEC) 2010;458–465.
11. Mets K, Verschueren T, Haerick W, et al. Optimizing smart energy control strategies for plug-in hybrid electric vehicle charging. Proceedings of IEEE/IFIP Network Operation and Management Symposium Workshops (NOMS) 2010;293–299.
12. Rashid A, Waraichs D. Plug-in hybrid electric vehicles and smart grid: Investigations based on a micro-simulation. ETH, Eidgenössische Technische Hochschule Zürich, IVT, Institut für Verkehrsplanung und Transport systeme 2009;1–23.
13. Westermann D, Agsten M, Schlegel S. Empirical BEV model for power flow analysis and demand side management purposes. Modern Electric Power System 2010, Wroclaw, Poland. http://www.meps10.pwr.wroc.pl/submission/data/papers/12.6.pdf.
14. Markel T, Kuss M, Denholm P. Communication and control of electric drive vehicles supporting renewable. Proceedings of IEEE Vehicle Power Propulsion Conference 2009;27–34.
15. Shrestha GB, Chew BC. Study on the optimization of charge discharge cycle of electric vehicle batteries in the context of Singapore. Proceedings of AUPEC Conference 2007;1–7.
16. Qian K, Zhou C, Allan M, et al. Modeling of load demand due to EV battery charging in distribution systems. IEEE Trans Power Syst 2010;1–9.
17. Wang B, Li Y, Gao C. Demand side management outlook under smart grid infrastructure. Autom Electric Power Syst. 2009;33(20):17–22.

18. Xiao L, Lin L. Construction of unified new-energy based power grid and promotion of China's smart grid. Adv Technol Electr Eng Energy. 2009;28(4):54–9.
19. Yang Y, Lin Z, Qin D, et al. Control strategy and simulation study on NiMH battery quick charging for regenerative braking of HEV. J Chongqing Univ. 2007;30(3):1–5.
20. Meissner E, Richter G. Battery monitoring and electrical energy management precondition for future vehicle electric power systems. Power Sources. 2003;116(1–2):79–98.
21. Nelson RF. Power requirements for batteries in hybrid electric vehicles. Power Source. 2000;91(1):2–26.
22. Cao YJ, Tang SW, Li CB, et al. An optimized EV charging model considering TOU price and SOC curve. IEEE Trans Smart Grid. 2012;3(1):388–93.
23. Madrid C, Argueta J, Smith J. Performance characterization-1999 Nissan Altra-EV with lithium-ion battery. Southern California EDISON; 1999.
24. Qi Q, Yang Z. Vehicle population in Beijing over 4.69 million and drivers over 6.2 million. 2010. http://auto.qq.com/a/20101201/000110.htm.

Chapter 3
The Response of EV Charging Load to the Grid Voltage

3.1 Introduction

Modern power system is a complicated, nonlinear and dynamic system with large scale. Improving power system stability has always been a hot topic. The problem of power system stability can be classified from different perspectives. In view of the causes of instability, it can generally be divided into angle stability and voltage stability [1, 2]. Although angle instability is more common, the attention has also been paid to voltage instability as a result of a number of large-scale power failure incidents, such as the voltage collapse of Tokyo Grid in Japan on July 23, 1987, Quebec Grid in Canada on March 13, 1989, and Western Systems Coordinating Council in America on August 10, 1996 [3, 4]. Most of these incidents occurred in a short time and were hard to be detected during the formation of voltage instability, making it difficult for operators to take emergency measures timely.

In order to prevent power system from collapsing, methods for maintaining voltage stability have been studied for a long time, one of which is UVLS [5]. Known as an effective measure against voltage instability, the philosophy of UVLS is to shed the selected loads due to a system disturbance to make the voltage recover to acceptable levels and avoid a large-scale voltage collapse of the system [6–8]. At present, UVLS is used in many countries, such as USA, Canada, Spain, China, et al. While for different countries, the UVLS type may have a difference. Currently, UVLS schemes are usually divided into two types: the distributed and the centralized load shedding scheme, which are also basic types [6–9]. The distributed load shedding scheme has relay protection equipments at each load to be shed, thus it is also called local load shedding scheme. When the protector senses that voltage collapse will occur in the area, the load will be shed by the protection. The centralized load shedding scheme measures one or more critical buses in one area and then sends trip signal to different spots in this area to shed load. As voltage instability can be determined through low voltage in the area, the basis of the centralized load shedding scheme is that if voltage of one critical bus is low, then

C. Li et al., *Influences of Electric Vehicles on Power System and Key Technologies of Vehicle-to-Grid*, Power Systems,
DOI 10.1007/978-3-662-49364-9_3

voltage of the whole area is also low. This scheme is dependent on high speed communication and can use many parameters other than voltage. These two methods have different advantages [8]. For example, the reliability is increased by diversification of the distributed system, as failure of one component of the distributed system will not directly affect the operation of other components. It is different from the centralized system, the reliability of which depends on only a few relays, or one relay that can be improved by indicators from any part of the system, besides voltage level, which can be used to predict the approaching of voltage instability.

Besides, the UVLS type can be classified in terms of shed controllers which are named as fixed step fixed delay (FSFD) and variable step variable delay (VSVD) [10]. Closed loop is adopted in FSFD, which means the voltage signal is affected by previous actions and a greater drop in voltage will result in a larger amount of load to be shed and a shorter shedding delay [11]. And controllers of VSVD are set up to automatically adjust their action according to severity situations, then the faster decrease in voltage will lead to a larger amount of load to be shed and a shorter delay [12, 13].

The type and amount of load to be shed as well as time delay are important parameters of UVLS. The selection of loads to be shed is based on the model and operation state of power system. Loads of areas where the voltage tends to be instable will be taken into consideration firstly. In addition, the constant loads, for example, motor loads and industrial loads with their own generators can be shed to maintain the voltage stability [8, 13]. In terms of the amount of loads to be shed, it is determined by system planners who will carry out numerous studies by using P-V curves as well as other analytical methods [7, 8]. The purpose is to retain voltage stability under credible contingencies. And for the time delay of UVLS, the selection of appropriate time delay is limited by load characteristics, power source and rate of voltage change. And the time delay should be short enough to prevent voltage collapse and long enough to avoid undesired tripping for faults or transient voltage dips which may not require load shedding [8].

As the analysis in Chap. 1, fossil fuels are not renewable and the replacement of CVs by EVs can ease the world's energy tension and reduce heat emission, so the rapid development of EVs and the replacement have been an inevitable trend. Electricity consumed by EVs can account for a large proportion of the total electricity consumption when the number of EVs occupies a large proportion of cars ownership. For example, in 2012, there were 5.2 million EVs and the average daily driving distance was 30 miles in Beijing. In view of current technology, the average electricity consumed by an EV was 0.346 kWh per mile in China, so the electricity consumed by EVs would be 53.976 million kWh if CVs were replaced by EVs. Even neglecting the loss of EVCSs during the charging process and the self-discharge of batteries, the annual electricity consumed by EVs would be 19.701 million kWh, which would account for 22.533 % of the total electricity consumption of Beijing in 2012. Therefore, EV charging loads would play an important role in power system if CVs were placed by EVs.

However, with the application of V2G technology, the large-scale integration of EVs into the grid will be an inevitable trend, which causes a great effect on the grid voltage [14]. Therefore, the influence of EVs' integration on grid voltage is studied in many literatures. The influence of EVs on a UK generic low voltage distribution grid under different EV aggregation levels and penetration scenarios is analyzed in [15]. Taking the integration of 24 users at the low voltage segment level into consideration, a power systems computer aided design (PSCAD/EMDTC) model of the urban radial UK generic distribution network is used in this research. The simulation results show that the statutory low-voltage limit is exceeded at the remote end of the network for the minimum load and 50–100 % penetration extreme conditions. Then, the research of Muhammad SK, et al. presents a detailed review of energy management model to maintain transient voltage stability through EVs in V2G model [16], and a transient voltage stability margin index is proposed to test the capability of EVs in contributing storage and supply services to the grid. The results show that EVs can provide the base load for a short term and can act as spinning reserve to enhance the grid stability. And through changing the penetration of EVs, the transient voltage stability of the distribution network, especially micro-grid, can be achieved.

According to the analysis above, the integration of EV has a great influence on the grid voltage, and the negative effect of EVs on the grid can be reduced when EV charging loads are used as the controllable loads, which can improve the grid voltage stability. As the charging voltage level of EVs is generally the lowest voltage level in the power supply system and EV charging loads will account for a large proportion of electric loads in the future, the participation of EVs in UVLS according to the AC-side voltage of EVCSs is of great significance to prevent voltage collapse.

3.2 The Profile of the Proposed Strategy

3.2.1 The Selection of Voltage Signal

In the proposed strategy, EVs' charging power will be adjusted according to the AC side voltage deviation of EVCSs. And the reasons for adopting local voltage signal of EVCS are as follows:

First, there is no need to use communication facilities, thus EV charging load can participate in the system voltage regulation with lower cost. On the contrary, if the medium or high node voltage is adopted as benchmark signal, communication facilities will be needed between transformer stations and EVCSs, the cost of which is rather high. Besides, once the communication failure or delay occurs, the results of voltage regulation with the participation of EV charging loads will be severely affected.

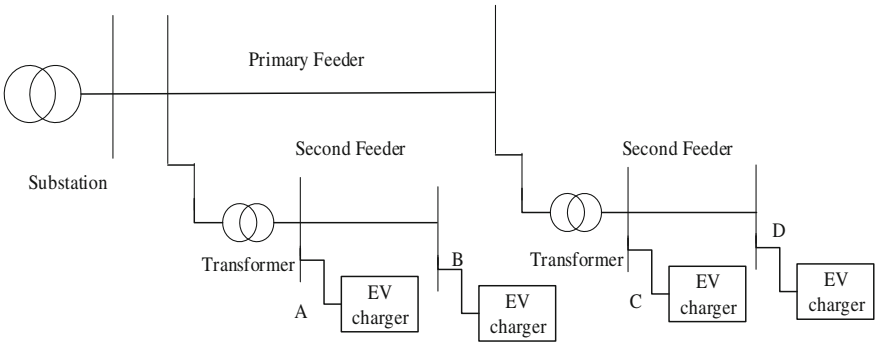

Fig. 3.1 A distributed network with several EV chargers

Second, as electrical distances from different EVCSs to the substation are not the same, the voltage losses are different, too. Thus, the AC side voltage of EVCSs is different. According to different voltage of EVCSs, EV charging load will participate in voltage regulation in turn when there is a great voltage deviation at the transformer substation. As there is no synchronous adjustment of EVCSs, the voltage overshoot can be avoided. As shown in Fig. 3.1, there are four EVCSs in the distributed network: A, B, C and D. Obviously, the electrical distances from which to the 110 kV substation are different. Suppose that the voltage level, the amount of EV charging load and other parameters are the same, then the relationship among AC side voltages of EVCSs is $U_A > U_B > U_C > U_D$. Charger D has the largest voltage deviation according to Thevenin theorem when there is a system voltage drop due to the large increase of loads. Then EV charging load of D will first participate in voltage regulation. If the voltage deviation is still large after the adjustment of EVs' charging power, the EVs at charger C will make a response to the voltage regulation. That is to say, EV charging loads will participate in voltage regulation by the order D > B > C > A. So, without synchronous adjustment of EVCSs, the voltage overshoot can be avoided.

3.2.2 UVLS with the Participation of EV Charging Load

The strategy of voltage regulation with the participation of EV charging load is to reduce the charging power when the voltage drops to a certain value. It can improve the voltage stability of power system, but affect the EV user experience inevitably. Thus, the initial SOC and charging time set by EV users need to be taken into consideration to reduce the influence on user experience while changing the charging power. With user experience, SOC and charging habits of different EV users taken into consideration, the strategy that EVs participate in UVLS is proposed in the chapter, steps of which are as follows:

1. Calculate the power to be shed P_{shed}.

V_s and V_s' are voltages before and after load shedding respectively, and V_s' is the minimum voltage required to maintain stable operation of power system in the chapter. The system characteristics are assessed by using a $P-V$ curve, $P = f(V)$, which can be obtained by continuous power flow with the power factor of loads holding constant. P_s and P_s' are the power of load drawn from $P = f(V)$ at the given voltage V_s and V_s', respectively. The amount of load to be shed is as follows:

$$P_{shed} = P_s - P_s' \tag{3.1}$$

2. The current number of EVs integrated into the grid is N (EV_1, EV_2, …, EV_i, …, EV_n), where EV_i is the ith EV. d is defined as the difference of charging time:

$$d_i = t_{user\_i} - t_{\text{battery}\_i} \tag{3.2}$$

where t_{user_i} is the charging time set by EV user; $t_{battery\_i}$ is the charging time needed for SOC of EV_i to reach the maximum, which can be calculated according to the initial SOC, charging power and the characteristic of EV battery, as can be seen in (2.2).

3. The EVs that can participate in UVLS are selected, priorities of which are calculated in this step.

With the user experience taken into consideration, the selection of EVs and the rank of their priorities are updated by re-reading the EVs' information by time interval T. The selection rule is as follows:

$$\Delta_d = d - T > t_{const} \tag{3.3}$$

where t_{const} is a time constant and $t_{const} \geq 0$ in general, which means the adjustment of EVs' charging power has no influence on the final SOC of EV battery and the strategy has little effect on the EV user experience. However, t_{const} will be a negative value when the voltage drops to the critical point and may develop into a voltage collapse.

The priorities of EVs are ranked according to Δ_d. And the larger the Δ_d is, the higher the priority of EV is.

4. Adjust EV charging power.

According to the selection and rank of priorities in step (3), EVs that can participate in UVLS are ranked as EV_1, EV_2, …, EV_j, …, EV_m, where EV_j is the jth EV. Then the number of EVs involved in the voltage response and the charging power to be shed ΔP is calculated by Eqs. (3.3) and (3.4).

$$\begin{cases} \sum_{j=1}^{k-1} \Delta P_j < P_{\text{shed}} \\ \sum_{j=1}^{k} \Delta P_j >= P_{\text{shed}} \end{cases} \tag{3.4}$$

where k is the number of EVs involved in the voltage response, $k \leq m$.

$$\Delta P_j = \begin{cases} 0, & 0.9V_s \leq V_s' \leq V_s \\ 0.1P_{b\_j}, & 0.8V_s \leq V_s' < 0.9V_s \\ 0.3P_{b\_j}, & 0.7V_s \leq V_s' < 0.8V_s \\ 0.5P_{b\_j}, & V_s' < 0.7V_s \end{cases} \tag{3.5}$$

The adjustment of EV charging power is as below:

$$P'_{b\_j} = P_{b\_j} - \Delta P_j \tag{3.6}$$

where P_{b_j} and P'_{b_j} are EV charging power before and after the adjustment respectively, P_{b_j} is equal to the maximum charging power of EV_j.

5. If the AC side voltage of EVCSs recovers to allowable range, then end the process; otherwise, return to step (1).

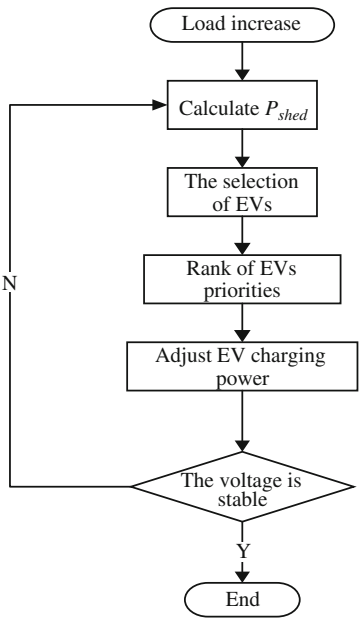

Fig. 3.2 The flowchart of UVLS with EVs' participation

In the proposed strategy, the priorities of EVs are ranked and updated with time by setting time interval T. That is to say, the EVs that participate in voltage response may not meet the selection rule next time (3.3), which makes them exit the regulation. Thus, the EV user experience is guaranteed as much as possible. The flowchart of the above strategy is shown in Fig. 3.2.

3.3 Case Study

3.3.1 Parameters and Model of Simulation

1. The charging start time of EVs

As the analysis of Chap. 2, it has much randomness of the charging behavior of EVs without economic interests and policy guidance. The charging start time used in this chapter is selected randomly according to the Gaussian distribution model established in Chap. 2, as shown in (2.7).

2. The charging characteristics of lithium-ion battery

The lithium-ion battery adopted in the Chap. 2 is used in this chapter, charging characteristics of which are shown as Fig. 2.3. Incompletely discharging situations, the demand for energy is 29.07 kWh.

3. The initial value of SOC

The initial value of EVs' SOC is random, and it can be obtained according to Eq. (2.8).

4. The charging time of EVs

The required charging time $t_{battery}$, after which the SOC of EV battery will reach its maximum, is calculated based on the charging start time t_{start}, battery characteristics and the initial value of SOC. And t_{user} is the charging time set up by users, which can be calculated according to Eq. (3.7).

$$t_{user} = t_{uend} - t_{start} \tag{3.7}$$

In (3.7), t_{uend} refers to the charging stop time set by the users, and it is selected randomly according to Eq. (2.7) and meets the requirement: $t_{uend} > t_{start}$.

5. The system of simulation

The IEEE 14-bus distribution system is selected in this chapter, as is shown in Fig. 3.3. The node 6, node 10 and node 12 are chosen to be integrated by EV loads, names of which are A, B and C in the chapter.

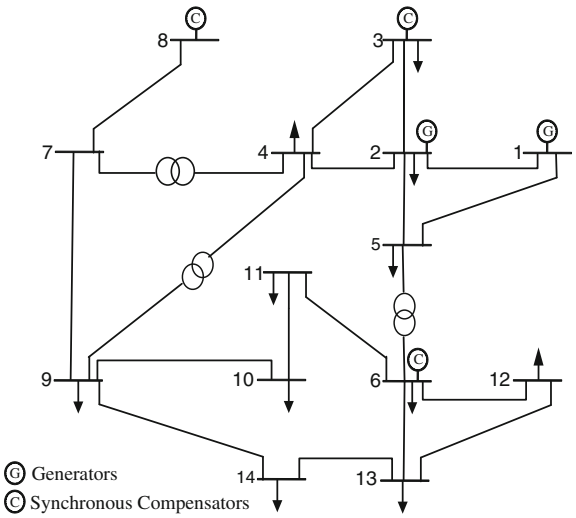

Fig. 3.3 IEEE 14-bus test system © [2011] IEEE. Reprinted, with permission, from Ref. [Voltage stability improvement using "Sen" transformer]

3.3.2 Results of the Simulation

1. The influence of EVs' integration on the system voltage

Different node voltage curves at different penetration of EV charging loads are shown in Fig. 3.4. EV charging loads are integrated into the system under different penetration. At the penetration of 20, 40 and 60 %, the voltages of node A are 1.007, 0.9609 and 0.9141 respectively (without exceptional note, all the voltage

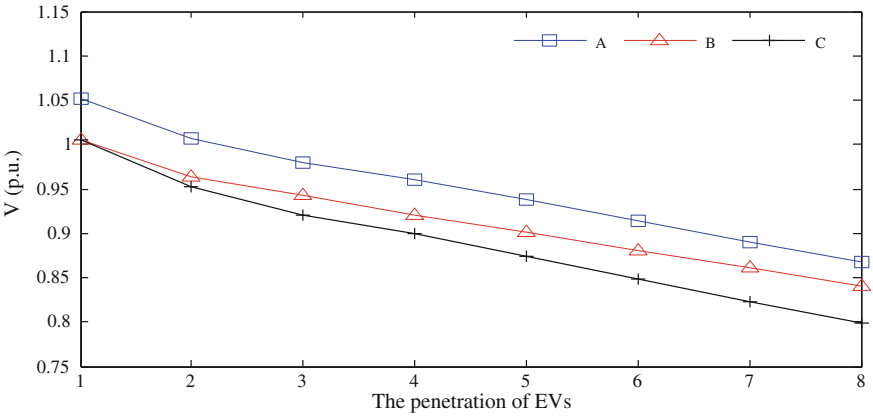

Fig. 3.4 Influences of EVs on each node voltage under different penetration

involved in this section are displayed by p.u.). As shown in Fig. 3.4, the integration of EVs makes the node voltage drop; moreover, the increase of penetration results in a greater voltage drop and fluctuation. When the penetration is 60 %, the fluctuation time of node A voltage is 7.1604 s. In addition, different charging node voltages present different extents of dropping at the same penetration.

2. UVLS with EVs' participation

The main cause of voltage drop or collapse is a sudden great increase of system loads in the power system. In China, the allowable range of voltage deviation of 10 kV level is 7 % with reference to the system rated voltage. The impact of a sudden large increase of system loads on node voltage is shown in Fig. 3.5. As can be seen, when t is within [20, 120], EVs are integrated into EVCSs randomly and irregularly (the charging start time is generated by a random function); when t = 120 s, the penetration of EV is 20 %; and when t = 130 s, there is a sudden increase of loads, leading to a sharp decline of node voltage and the lowest node voltage reaching 0.9397. The system rated voltage is 1.05, so the maximum voltage deviation is 10.505 % and the voltage fluctuation time is 13.125 s. Based on the strategy proposed in Sect. 3.2.2, the node voltage curve is shown in Fig. 3.6 when EVs participate in UVLS, where the penetration, EVs charging start time and other settings are the same with the above simulation. The AC side voltage of EVCSs decreases after system loads increase suddenly, and then EVs which meet the response condition participate in UVLS. These EVs' priorities are ranked and then listed in Table 3.1. As shown in Fig. 3.6, the lowest transient voltage is 0.9882, and the maximum voltage deviation is 5.89 % (less than 7 %), which meets the allowable range of 10 kV voltage level. In other words, the system voltage recovers to the allowable range under the UVLS with merely EV charging load participating in. In addition, UVLS helps the maximum difference of voltage fluctuations reduce to 0.0481 from 0.0591 and the voltage fluctuation time reduces to 8.75 s from 13.125 s.

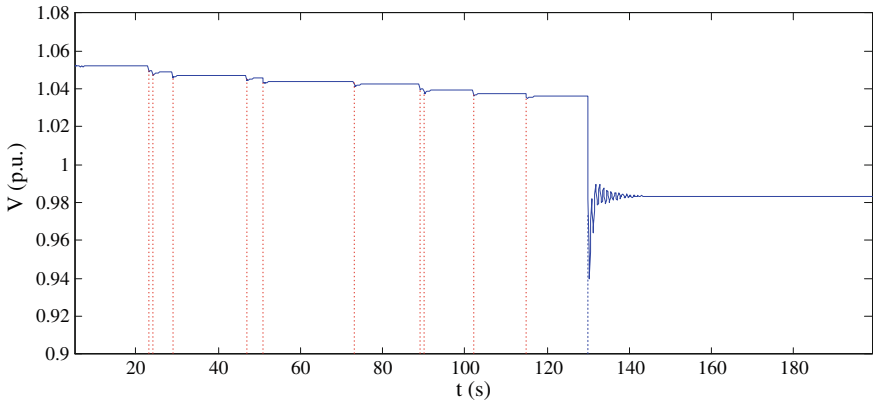

Fig. 3.5 The node voltage curve at a sudden load increase

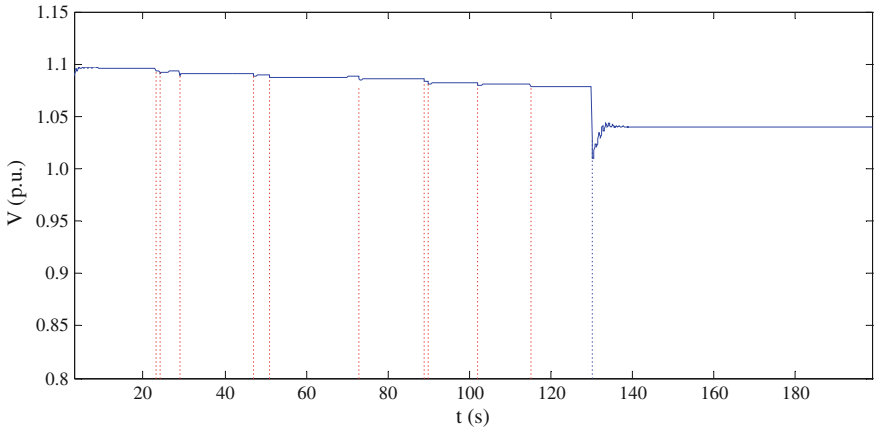

Fig. 3.6 The node voltage curve with EVs' participation in UVLS

As can be seen in Table 3.1, priorities of EV_8, EV_9 and EV_{10} are zero since the load increases, which means the SOC of EV battery cannot reach maximum within the charging time set by EV users. Therefore, EV_8, EV_9 and EV_{10} do not make a response to the voltage regulation. On the contrary, EV_3, EV_5 and EV_6 have been participating in UVLS until the end of simulation. With the rank and update of priorities, other EVs ever participated in the regulation exit when the priority drops to zero. Thus, the priorities of EVs are ranked and updated with time, through which the final SOC will not be affected and the EV user experience can be guaranteed.

The simulation result shows that:

1. The penetration of the EV charging load will influence the node voltage and the increasing penetration of EVs will lead to a greater voltage drop.
2. A sudden increase of system load will result in voltage drop and fluctuation. In the absence of load shedding measures, there is a large voltage deviation, long fluctuation time and great fluctuation amplitude.

Table 3.1 The ranked priorities of EVs

EVs	t + T	t + 2T	t + 3T	t + 4T	t + 5T	t + 6T	t + 7T	t + 8T
1	4	4	3	3	3	2	1	0
2	2	2	1	1	1	0	0	0
3	6	6	5	5	5	4	3	2
4	3	3	2	2	2	1	0	0
5	6	6	5	5	5	4	3	2
6	5	5	4	4	4	3	2	1
7	1	1	0	0	0	0	0	0
8	0	0	0	0	0	0	0	0
9	0	0	0	0	0	0	0	0
10	0	0	0	0	0	0	0	0

3. When the system load increases suddenly, AC side voltage of EVCSs will drop. UVLS with EVs' participation makes the voltage recover to the allowable range. In addition, the fluctuation time is shorter and the fluctuation amplitude is reduced. All these will help operators and planners get more time to deal with accidents.
4. The priorities of EVs are ranked and updated with time, through which a single EV can avoid participating in voltage regulation for a long time and EV user experience is guaranteed.

3.4 Conclusions

With the growing number of EVs and the wide application of V2G technology, EV charging load has a greater influence on power system. A strategy of UVLS with EVs' participation is proposed in this chapter. Steps of the strategy are as follows. Firstly, the power needed to be shed is calculated according to the AC side voltage deviation extent of EVCSs. Secondly, the EV charging time redundancy of EVs is calculated according to the required charging time of EVs and the time set up by users; moreover, the larger the time redundancy is, the higher the priority of EV participating in UVLS is. Thirdly, the EV charging power is adjusted according to the priority of EVs and amount of load to be shed. In this proposed scheme, AC side voltage of EVCSs instead of the node voltage is selected as the voltage detection signal. One of its advantages is that there is no need for complicated communication facilities. In addition, since the electrical distance from EVCSs to the substation is different, the AC side voltage deviation of EVCS is also different, so EV charging load participate in the voltage response in turn to avoid overshoot. Taking the users experience into account, the priority of EVs participating in UVLS is updated with time, thus avoiding that a single EV participate in UVLS for a long time.

Simulation results show that when the system load increases suddenly, AC side voltage of EVCSs will drop. The proposed strategy of UVLS can not only help the voltage recover to the allowable range but also reduce fluctuation time and amplitude significantly. The stability of the system voltage is improved, and more time will be reserved for operators and planners to deal with accidents. Additionally, as the priorities of EVs participating in UVLS are updated real-timely, EV user experience can be guaranteed. Thus, EV charging load can be used not only as user loads, but also as controllable loads to improve the voltage stability of the distribution network.

References

1. Vournas CD, Sauer PW, Pai MA. Relationships between voltage and angel stability of power systems. Electr Power Energy Syst. 1996;18(8):493–500.
2. Ouassima A, Francis AO, Louis A, et al. Application of a multivariable feedback linearization scheme for rotor angle stability and voltage regulation of power systems. IEEE Trans Power Syst. 1999;14(2):620–8.
3. Klaric M, Kuzle I, Tesnjak S, et al. Under voltage load shedding using global voltage collapse index. Power Syst Conf Exposition. 2004;1:453–9.
4. Taylor CW. Improving grid behavior. IEEE Spectr. 1999;36(6):40–5.
5. Wiszniewski A. New criteria of voltage stability margin for the purpose of load shedding. IEEE Trans Power Deliv. 2007;22(3):1367–71.
6. Taylor CW. Concepts of under voltage load shedding for voltage stability. IEEE Trans Power Deliv. 1992;7(2):480–8.
7. Mozina C. Under voltage load shedding. Proceedings of 60th Annual Conference for Protective Relay Engineers 2007; 16–34.
8. Begovic M. Summary of "system protection and voltage stability". IEEE Trans Power Deliv. 1995;10(2):631–8.
9. Jingjing Z. Research on under-voltage load-shedding to prevent voltage collapse of electric power system. Proceedings of Power and Energy Engineering Conference, APPEEC 2009, Asia-Pacific 2009; 1–4.
10. Nizam M, Mohamed A, Hussain A. An adaptive under voltage load shedding against voltage collapse based power transfer stability index. J Electr Eng Technol. 2007;2(4):420–7.
11. Moors C, Lefebvre D, Van Custem T. Load shedding controllers against voltage instability: a comparison of design. Proc IEEE Porto Power Tech. 2001;2(2):2–6.
12. Lefebvre D, Bernard S, Van CT. Under voltage load shedding scheme for hydro-quebec system. Proc Power Eng Soc Gen Meet. 2004;4:13–7.
13. Van CT, Vournas CD. Emergency voltage stability controls: an overview. Proceedings of Power Engineering Society General Meeting, 2007. IEEE 2007; 1–10.
14. Zhong J, He L, Li C, et al. Coordinated control for large-scale EV charging facilities and energy storage devices participating in frequency regulation. Appl Energy. 2014;123:253–62.
15. Papadopoulos P, Cipcigan LM, Jenkins N, et al. Distribution networks with electric vehicles. Proceedings of the 44th International 2009; 1–5.
16. Khalid MS. Impact of energy management of electric vehicles on transient voltage stability of microgrid. International Electric Vehicle Symposium and Exhibition 2015; 1–11.

Chapter 4
The Response of Large-Scale EV Charging Loads to Frequency

4.1 Introduction

Power system stability is a requirement for the security and economic operation of power system. Many major blackouts are caused by power system instability, which proves the importance of power system stability [1]. As frequency stability is an important part of power system stability, a lot of attention has been attracted on it [2]. Frequency stability reflects the balance of active power between the power supply side and the demand side. When the balance is broken, frequency deviation is not in the allowable range, which will result in the uneconomic operation of power system, and even cause security questions. In order to keep power system safe, stable and economic, methods for maintaining frequency stability have been studied for a long time. One method is to adjust the active power output of generator equipment; the second is to prepare enough reserve capacity for generator equipment. Load frequency control (LFC) is adopted to maintain frequency stability in modern power system, which is an important and mature means to improve power quality and keep the safe and economic operation at present [3].

The growth of EVs is very fast, which makes EVs have the great potential for participating in FR based on V2G. Frequency stability is ensured by the constantly changing power to balance the power of varying load. EVs in different scales can be aggregated to integrate into the grid, so the way of EVs' integration is very flexible. Therefore, EVs are very suitable to participate in FR.

4.2 Characteristics of EV Charging Loads

As EVs have many characteristics, a lot of researches are focused on the characteristics of EV charging loads, battery charge and discharge characteristics and power harmonics problems [4, 5]. The generic battery model considering dynamic

C. Li et al., *Influences of Electric Vehicles on Power System and Key Technologies of Vehicle-to-Grid*, Power Systems,
DOI 10.1007/978-3-662-49364-9_4

response, the phenomenon of self-discharge and temperature and other factors has been studied in [6–10]. The research of power harmonic focuses on the characteristics of a single charger and modeling is studied in [11–16]. In more sophisticated smart grid systems, EVs will be used as bidirectional energy trader. EV owners buy electricity at a low price during the valley, to meet their own need; and sell electricity at a high price during the peak hours, to act as backup power supplies.

Characteristics of EV charging loads are related to many factors including the scale of development, drivers' behavior, battery characteristics, etc., which are rather random. In [17], vehicles with various levels of battery capacity are taken into account, such as compact cars, mid-size cars and SUV, then the load characteristic under different charging powers has been compared and studied, without mention of the impact on power grid. Considering various charging behaviors, the charging load curves are obtained by Monte Carlo simulation algorithm in [18, 19]. Furthermore, the characteristics of EV charging loads are also related to its charging modes, which have different effects on load modeling.

Based on a review of the existing literature, EV charging loads have the distinctive characteristics as follows:

(1) The scale of EV charging loads is relatively small at present. Therefore, V2G should be fully studied at the beginning of construction, forming a unified standard for EV charging facilities so that most of the EVs can participate in demand response in the future.
(2) EVs are expected to gain a significant share in the total power system loads, thus V2G will have a far-reaching influence on power system operation [17, 18].
(3) The charging of EVs is featured with electromagnetic and chemical processes without mechanical processes. Consequently, the time constant of EV power adjustment is smaller, namely EVs are characterized with rapid response [19].
(4) The charging of EVs is non-rigid on a relatively short time scale (e.g., within minutes), namely EV power adjustment lasting for a short time has little impact on the user and EV itself.
(5) Most EV charging loads exist in the receiving system. Compared with the general grid, the receiving system needs more support for the frequency and voltage regulation. And EVs have favorable characteristic of FR. Thus, EVs can accord well with the requirements of FR.

4.3 The Current Related Research of EVs on FR

4.3.1 EVs' Advantages in FR

On the condition of imbalanced supply and demand, power frequency may vary from 49.95 to 50.05 Hz [20]. EVs as flexible charging load can work as this flexible capacity, thus assisting the process of FR.

In view of the characteristics of the EV charging loads and through comparing with the industrial load, the EV charging loads have the following advantages in FR:

(1) EV charging loads are easier to be switched on and off, since there is no complicated mechanical process.
(2) Quicker response speed.
(3) Bidirectional regulation of energy and information.
(4) Less impact on users.
(5) Higher efficiency of comprehensive energy.

In view of the above features, the research of FR with EV charging load is of significance for power system stability, energy conservation and social benefits.

The participation of EVs in FR mainly focuses on the following aspects at present:

(1) The participation of large-scale centralized and decentralized EVs in FR.
(2) According to whether depending on communication system, the studies can be divided into with and without communication system [21].
(3) The participation of EV charging loads in primary FR and secondary FR [4, 22].
(4) The economic dispatching and benefit under the participation of EV charging loads in FR [23, 24].
(5) The participation of EV charging loads in FR of microgrids [25].

4.3.2 The Current Related Research of FR Based on the Coordination Among EVs, AGC, BESSs

AGC is used to maintain the balance between generation and load in power systems, which is generally achieved by adjusting the power output of multiple traditional AGC generation units to control frequency deviation. However, with the large-scale integration of renewable energy, relying on traditional units alone is difficult to fulfill the balance requirements for the future grid. If EVs and BESSs participate in system FR, AGC would respond to frequency deviations both on generation side and load side simultaneously to assist traditional generation units. The contribution of EVs and BESSs to FR has received great attention in the existing literature, and control strategies have been proposed from various perspectives [26–28]. Kempton and Tomic [18] showed that the participation of EVs in system frequency control will reduce the systems' operating costs. Larsen et al. [29] presented that more regulation would allow for the effective integration of fluctuating renewable energy into the system with the introduction of EVs. Lopes et al. [30] presented a conceptual framework to successfully integrate EVs into the power system (e.g., to provide AGC services). Garcia and Lopes [31] showed that the performance of the AGC operation increases with the presence of EVs. However,

in the above-mentioned literatures, how to introduce large-scale EV charging loads and energy storage devices into the regulation of AGC while considering their response priorities is largely missing. Therefore, a coordinated control method, which takes full advantage of EVs and BESSs in coordination with traditional AGC units for FR, is proposed in this chapter.

4.4 Properties of FR Resources

To achieve the coordinated control of multiple FR resources and at the same time to fully make use of the FR ability of EVs and BESSs, it is necessary to analyze the characteristics of traditional FR resources, BESSs and EVs.

4.4.1 Traditional FR Resources

Traditional FR resources mainly include thermal power units and hydropower units. Compared with hydropower units, thermal power units make a slower response to the AGC signals, which results in a poor control performance of power system AGC [32]. And units with higher AGC reserve capacities are actually a kind of waste. In addition, influenced by the function property, thermal power units have a ramp rate limit of 4–5 % p.u./min and hydropower units have a limit of 3–4 % in general [33]. Traditional units have a certain FR deadzone to avoid the frequent adjustments of output (which may greatly affect the units' lifetime) caused by small frequency fluctuations, and the deadzone set in thermal power units and hydropower units are generally not more than ±2 r/min (±0.034 Hz) and ±3 r/min (±0.05 Hz), respectively [33]. Moreover, the rotation speed measurement resolution of most units is coarse, which will cause larger deviations and influences on the FR effects.

4.4.2 Large-Scale Energy Storage Devices

Large-scale energy storage devices mainly focus on the secondary use of decommissioned EV batteries in the future, and also include the large-scale energy storage devices built specifically for FR and peak regulation. In this chapter, the proposed energy storage devices refer to the large-scale decommissioned EV batteries. Compared with traditional units, power-energy storage devices do not have ramp-rate limitations, and the response rate (in milliseconds) is far quicker than that of the traditional units (in seconds). Besides, power-energy storage devices are of high precision and good performance for FR.

Related studies have shown that an energy storage system is approximately 1.7 times more efficient than the hydropower unit, 2.7 times more than the combustion turbine, and 20 times than the steam turbine and combined-cycle turbine [34]. However, due to the limited storage capacity, the energy storage system cannot charge or discharge in one direction for a long time.

4.4.3 EV/BESS FR Resource

Through reasonable guidance and control, EVs can be used as the system FR resource to provide ancillary services. When the system is disturbed or in failure, to help the frequency recover to normal, V2G can respond to system frequency deviations or area control error (ACE) signals by absorbing energy from the grid or feeding its stored energy back into the grid [35]. V2G has the advantages of bi-directional regulation, rapid response and high precision, which presents a faster response rate and better FR effect than the traditional units [36].

In addition, large numbers of decommissioned EV batteries can be collected and used as large-scale BESSs to assist system FR. Therefore, the common participation of large-scale EVs and BESSs constitutes the EV/BESS FR power resource, and then coordinate with the traditional units to contribute to system FR services. Taking into account the electromagnetic power characteristics of fast response rate, the ramp rate constraint of EVs and BESSs can be ignored.

(1) AGC operation with EVs/BESSs

To assist the stable operation of power system, EVs and BESSs coordinate and cooperate with each other in the conventional AGC system. The dispatching center calculates the ACE and then allocates the regulation demand to the available FR resources through a complex algorithm. EVs and BESSs follow the regulation signals from the control center to change their power accordingly when the system security is threatened.

$$\begin{cases} P_{sum} = P_{GEN} + P_{EV/BESS} \\ P_{EV/BESS} = P_{EV} + P_{BESS} \end{cases} \tag{4.1}$$

where $P_{EV/BESS}$ is the total power of EVs and BESSs that are involved in FR; P_{sum} is the total power required to maintain the ACE within the control standard; P_{GEN} is the total regulating power of traditional units that contributes to FR; P_{EV} and P_{BESS} are the total power of EVs and BESSs that provide FR services, respectively. ACE is the difference between the scheduled and actual power generation within a control area on power grid, taking frequency deviation into account: (1) ACE > 0, decrease generation; (2) ACE < 0, increase generation.

$$\begin{cases} P_{GEN} = \sum_{k=1}^{R} P_{GEN\_k} \\ P_{EV/BESS} = \sum_{g=1}^{M} P_{BESS\_g} \\ P_{EV} = \sum_{h=1}^{N} P_{EV\_h} \\ P_{EV\_h} = \sum_{i=1}^{n} P_{EV\_hi} \end{cases} \tag{4.2}$$

where P_{GEN_k}, P_{BESS_g} and P_{EV_h} are the response power of traditional unit k, large-scale BESS g and EV charging station h, respectively; P_{EV_hi} is the response power of EV i at EV charging station h; R, M, N are the total number of traditional units, EV charging stations and BESSs, respectively; and n is the total number of EVs located at charging station h.

Moreover, what deserves to be noticed is that when EVs participate in FR, influences on EV batteries and users caused by charging/discharging should also be considered. Therefore, the battery constraints and user requirements constraint need to be taken into account fully.

(2) Constraints

EV battery capacity constraint. Considering the driving requirement and the influences on battery lifetime caused by over charge or discharge, EV charging/discharging should satisfy the energy constraint:

$$(SOC_{max} - SOC_{io})Q_{iN} \leq \Delta Q_{it} \leq (SOC_{io} - SOC_{min})Q_{iN} \tag{4.3}$$

where

$$\begin{cases} \Delta Q_{iT} = \Delta T_i \cdot P_i \\ \Delta T_i = T_{i\_end} - T_{i\_begin} \end{cases} \tag{4.4}$$

where Q_{iN} is the battery rated capacity of EV i; Q_{iT} is the battery capacity change of EV i in time interval T_i; SOC_{max} and SOC_{min} are the allowable upper and lower limits of battery SOC; SOC_{io} is the initial SOC of EV i; P_i is the charging/discharging power of EV i, with a positive value referring to EV i charging and negative value referring to EV i discharging; T_{i_begin} and T_{i_end} are the "beginning" and "ending" of EV i charging/discharging time involved in the response, respectively.

Power constraint. When EVs respond to the control signals, their charging/discharging power must be within the allowable range:

$$-P_{i\_max} \le P_i \le P_{i\_max} \tag{4.5}$$

where P_{i_max} is the maximum charging/discharging power limitation of EV i.

EV user requirement constraint. Considering the EV user experience, user can preset the EV available time and minimum required SOC value:

$$T_i \in \left[T_{i\_start},\ T_{i\_stop}\right] \tag{4.6}$$

$$SOC_{i\_end} \ge SOC_{i\_set} \tag{4.7}$$

where T_i is the available time (i.e., controllable time) of EV i, during which EV i can be involved in V2G service; T_{i_start} and T_{i_stop} are the allowable start and stop (charging/discharging) time of EV i, respectively; SOC_{i_end} is the battery SOC value of EV i after it participates in FR; and SOC_{i_set} is the minimum SOC required value (setting value) of EV i.

4.5 Coordinated Control Strategy for EVs/BESSs

This chapter mainly discusses EVs/BESSs in coordination with the traditional FR resources, that is, V2G responding to power system security signals actively within a short time. This requires a proper market framework. Some research has been conducted on market structures for EVs to participate in FR. For example, different FR services provided by EVs in the power market of Germany and Sweden were analyzed in [37]. As we mainly focus on how to design the control strategy for EVs and BESSs to assist frequency stability, the details about a possible market framework for EV participation are not discussed here.

4.5.1 Coordination Principle

The block diagram of coordinated control for large-scale EVs, BESSs and traditional units is shown in Fig. 4.1. System operating states are monitored by the dispatch control center in real-time, which are divided according to the system safety level. In the large-scale interconnected power grid, frequency and tie-line power are important indexes to evaluate the system security. In a power system, generation and load must maintain balance moment by moment. AGC is a system for adjusting the power output of multiple generators at different power plants in response to changes in the load. The balance can be judged by measuring the frequency, if it increases, the generators will reduce their output power; otherwise the generators will increase their output, i.e., FR is controlled via AGC. Tie-line bias control (TBC) is the main control type of AGC, whose advantage is that: in each control area, the power output of the AGC generators is adjusted according to

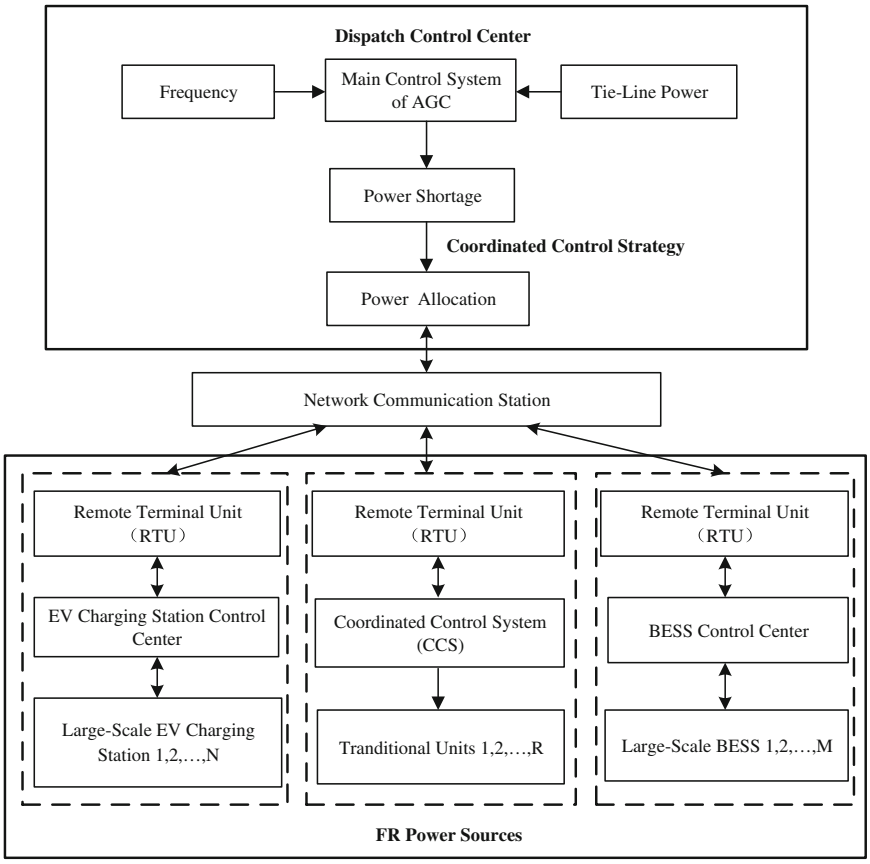

Fig. 4.1 Coordination of EVs, BESSs and traditional units involved in AGC. Reprinted from Ref. [40], Copyright 2014, with permission from Elsevier

its ACE, balancing the load fluctuation automatically. ACE, as the key control signal of AGC, is the synthetic reflection of system frequency and tie-line power. Therefore, EVs and BESSs can charge or discharge according to the ACE signal (instruction) and provide FR services. More precisely, ACE is the key for the participation of EVs and BESSs in regulation service (AGC). The general process is shown in Fig. 4.1.

ACE is small. Considering the influences on EV users, battery performance and lifetime caused by frequent charging and discharging, BESSs and traditional units participate in the response in this case, while EVs will not.

ACE is large. A large disturbance occurs on the system, resulting in a large ACE with a shorter duration (seconds to minutes). Leveraging the EV/BESS advantages of rapid response and large instantaneous power, EVs and BESSs first make response to ensure the balance between supply and demand. Then after a short

while, traditional AGC units respond, and the EVs and BESSs sequentially return to their previous states.

ACE is larger. Serious disturbance occurs on the system, causing the system to enter into an abnormal operating state. Under this situation, ACE is larger and effective measures must be taken quickly to help the system recover to the normal operating state as soon as possible.

Considering the system security, it is noteworthy that when disturbance occurs in a power system, the coordinated principle for EVs/BESSs to participate in FR should be chosen first according to the magnitude of ACE (small or large), then based on the ACE duration (shorter or longer).

4.5.2 Implementation Method for Coordinated FR

The system operating states can be obtained based on a Wide Area Monitoring System (WAMS) and Energy Management System (EMS), which represent the integrated signal of the FR requirements, urgency level and ACE duration. The states are generally divided into five types: normal state, alert state, emergency state, in-extremis state and restorative state, which have been widely used [38, 39]. In the practical operation of power systems, threshold of a system entering into each state is set according to its own characteristics. The operating states are classified based on the system operating parameters, such as frequency, voltage and reserve capability. As this chapter mainly focuses on the frequency stability determined by active power balance, the operating states are corresponding to the ACE. And the general description of the qualitative relationship between the operating states and ACE is: (1) in the normal state, the ACE is small; (2) in the alert state, the ACE is large; (3) in the emergency state, in-extremis state and restorative state, the ACE is larger. Consequently, to achieve the coordinated control of various FR resources, control strategies for FR can be determined respectively according to the different operating states.

The schematic diagram of large-scale EVs and BESSs participating in system regulation services is shown in Fig. 4.2. Power system operating conditions are monitored in real-time by the dispatching center. Dynamic collection and storage of EVs information (e.g., SOC and available time) are performed by the database system of the EV charging station control center, where information of all grid-connected EVs is integrated. Then, each EV charging station sends its own upper and lower limitations of the available (charging/discharging) power capacity as well as the adjustable time to the dispatching center. Similarly, BESS feeds back its upper and lower limitations of the available power to the dispatching center. When the stable operating condition is disrupted and the control signal (ACE) reaches the response threshold, according to the power shortage condition and the EV and BESS feedback information (e.g., available capacity and adjustable time), power allocation and instructions (ACE signals) are sent to EVs, BESSs, and

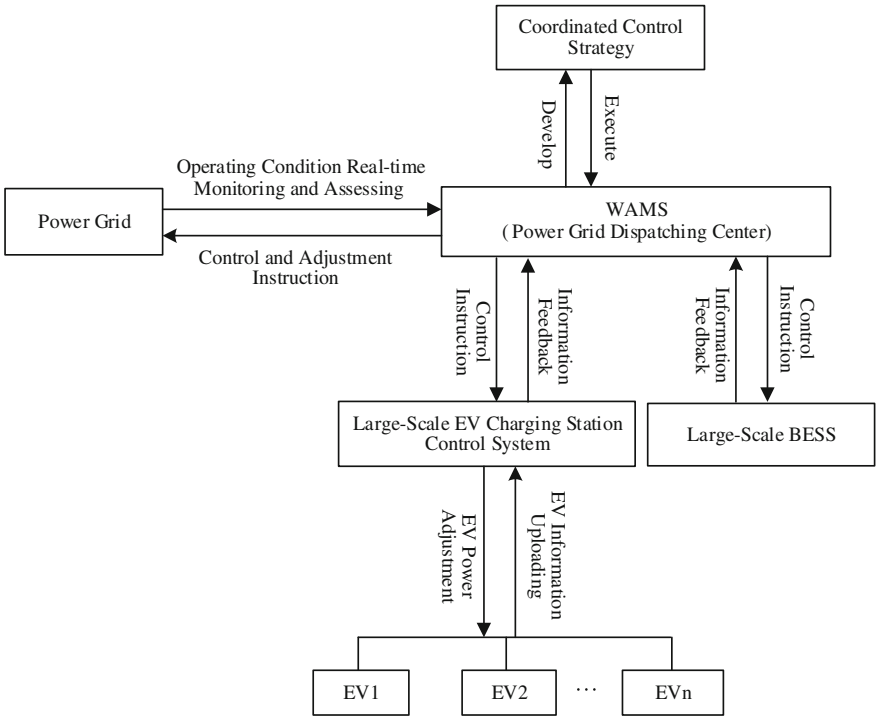

Fig. 4.2 Block diagram of EV/BESS participating in system regulation. Reprinted from Ref. [40], Copyright 2014, with permission from Elsevier

traditional units by the dispatching center. According to the received instruction, the BESS control center adjusts the BESS's charging/discharging power. Similarly, once the EV charging station receives the command, it sets the charging/discharging power command for each charging device of the grid-connected EVs according to their states and information. The general control and decision-making process for EVs and BESSs to participate in FR services is shown in Fig. 4.3.

In different operating states, the requirement for FR is different and thus the control objectives are various. For example, when system is in the normal operating state, the control object is the economic optimization, while it will aim at maximum security when the system is in the abnormal operating state (such as emergency and in-extremis state). As shown in Sect. 4.4, different FR resources have different characteristics in security and economy. Therefore, with the adjustment of the control objective in different operating states, the priority of different FR resources involved in AGC should be adjusted to ensure the coordination of different FR resources [40], which is corresponding to the coordination principle mentioned in Sect. 4.5.1.

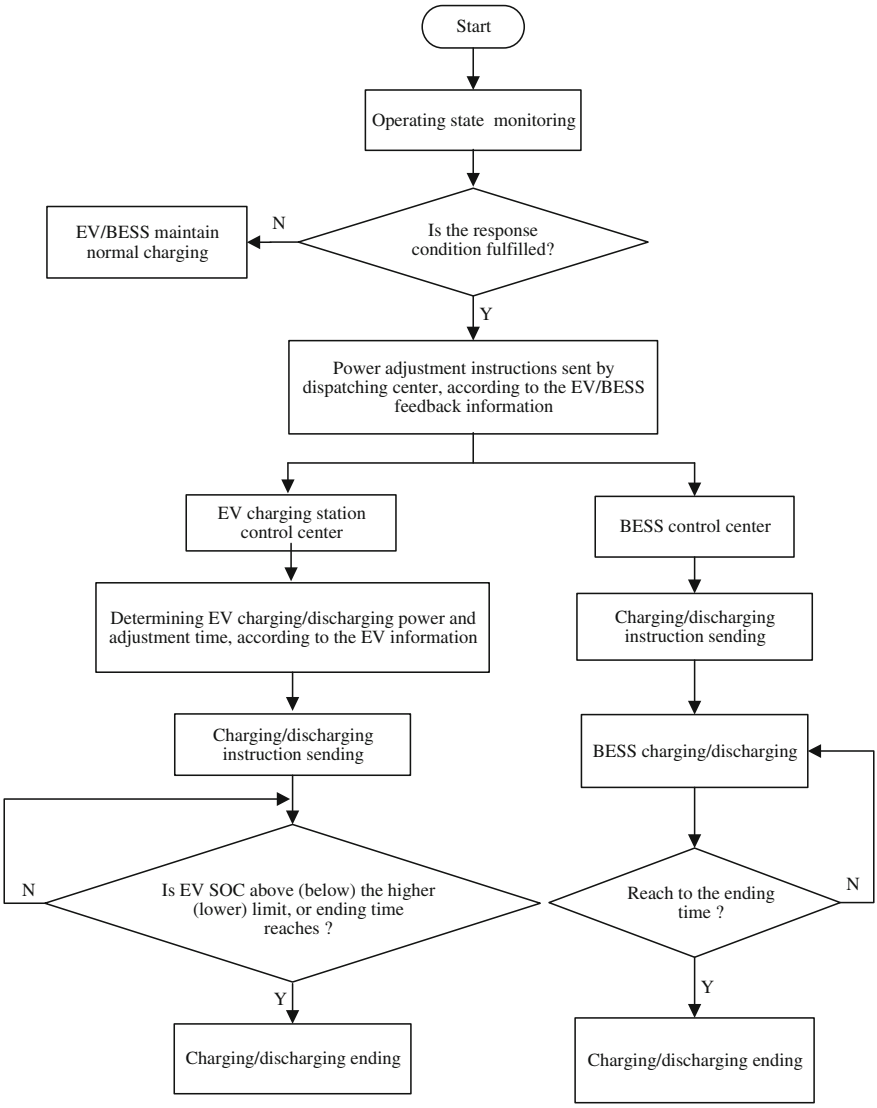

Fig. 4.3 General control scheme of the EV/BESS involved in FR services. Reprinted from Ref. [40], Copyright 2014, with permission from Elsevier

(1) Normal state

Assuming a small disturbance occurs in a power system and results in frequency deviations. In this case, the system is still within the normal operating range (ACE is small), while the ACE has reached the response threshold, as described below:

$$\begin{cases} |\Delta f| \le |\Delta f_{normal}| \\ |ACE| \ge ACE_{set} \end{cases} \tag{4.8}$$

where

$$\begin{cases} \Delta f = f_t - f_N \\ ACE = \Delta P_{tie} + B\Delta f \end{cases} \tag{4.9}$$

where f_t and f_N are the actual frequency and rated frequency, respectively; f and f_{normal} are the measured frequency deviation and the maximum allowable frequency deviation, respectively; ACE_{set} is the maximum allowable absolute value of ACE, namely the minimum AGC response threshold; P_{tie} is the total tie-line power (taking output as positive) exchange deviation between the interconnected system; and B is the power system frequency deviation coefficients.

(2) Alert state

In alert state (ACE is large), the frequency and voltage are both within their allowable range, while the system has already been in the abnormal state. In this situation, a large amount of power is needed to help the system return to normal. At this moment, both EVs and BESSs will participate in the response, while the response threshold for EVs is higher than that for BESSs. Besides, BESSs can also discharge, while EVs cannot. The setting of response threshold is shown below:

$$\begin{cases} ACE_{dz} \le ACE_{aset\_ESS} < ACE_{aset\_EV} \\ ACE_{aset\_ESS} = ACE_{set} + \Delta_a \\ \Delta_a = B\Delta f_a \end{cases} \tag{4.13}$$

where ACE_{aset_ESS} and ACE_{aset_EV} are the response thresholds for BESSs and EVs under the alert state, respectively; Δ_a and Δf_a are the ACE difference and the frequency difference between the critical alert state and critical normal state, respectively.

$$P_{adis-BESS} = \min\left(|ACE + ACE_{aset\_ESS}|, P_{(max)dis-BESS}\right) \tag{4.14}$$

And if $ACE < -ACE_{aset\_EV}$, EVs also participate in the response (decreasing their charging power), and the response power is:

$$P_{ade-EV} = \min\left(|ACE + ACE_{aset\_ESS}| - P_{adis-BESS}, P_{(max)de-EV}\right) \tag{4.15}$$

where $P_{adis\text{-}BESS}$ is the BESSs response power (discharging); $P_{ade\text{-}EV}$ is the EVs response power (decreasing charging power); and $P_{(max)de\text{-}EV}$ is the total EVs maximum allowable power can be decreased.

If $ACE > ACE_{aset\_ESS}$, the BESSs response power is:

$$P_{ach-BESS} = \min\left(ACE - ACE_{aset\_ESS}, P_{(max)ch-BESS}\right) \tag{4.16}$$

And if $ACE > ACE_{aset\_EV}$, EVs also contribute to the response (increasing their charging power), and the response power is:

$$P_{ach-EV} = \min\left(ACE - ACE_{aset\_BESS} - P_{ach-BESS}, P_{(max)ch-EV}\right) \tag{4.17}$$

where $P_{ach\text{-}BESS}$ and $P_{ach\text{-}EV}$ are the BESSs and EVs response power (discharging), respectively; $P_{(max)ch\text{-}BESS}$ and $P_{(max)ch\text{-}EV}$ are the total maximum allowable power of EVs and BESSs can be increased, respectively.

(3) Emergency, in-extremis and restorative state

ACE is larger when the power system is in emergency state, in-extremis or restorative state. Therefore, a larger response power is required to help the system recover to alert or normal state. In this case, EVs and BESSs will participate in response simultaneously, and discharge is allowed for both of them. The setting of the response threshold for EVs and BESSs is shown below:

$$\begin{cases} ACE_{cset\_ESS} = ACE_{cset\_EV} \\ ACE_{cset\_ESS} = ACE_{aset\_ESS} + \Delta_b \\ \Delta_b = B\Delta f_b \end{cases} \tag{4.18}$$

where ACE_{cset_ESS} and ACE_{cset_EV} are the response thresholds for BESSs and EVs under the emergency state, in-extremis state and restorative state, respectively; and Δ_b and Δf_b are the ACE difference and frequency difference between the critical emergency state and critical alert state respectively.

If $ACE < -ACE_{cset\_ESS}$, the EV/BESS response power is:

$$P_{edis-EV/BESS} = \min\left(|ACE + ACE_{cset\_ESS}|, P_{(max)dis-EV/BESS}\right) \tag{4.19}$$

where $P_{edis\text{-}EV/BESS}$ is the EVs and BESSs response power (discharging); and $P_{(max)dis\text{-}EV/BESS}$ is the total EVs and BESSs maximum allowable discharging power.

If $ACE > ACE_{cset\_ESS}$, the EV/BESS response power is:

$$P_{ech-EV/BESS} = \min\left(ACE - ACE_{cset\_ESS}, P_{(max)ch-EV/BESS}\right) \tag{4.20}$$

where $P_{ech\text{-}EV/BESS}$ is the EVs and BESSs response power (charging); and $P_{(max)ch\text{-}EV/BESS}$ is the total EVs and BESSs maximum allowable power can be increased.

In summary, for EVs and BESSs participating in AGC, under the satisfaction of constraints, the more serious the disturbance introduced in the power system is, the larger the ACE signal is, namely the larger the required power adjustment of EVs and BESSs is. Note that EVs and BESSs contributing to the AGC proposed above are suitable for the case that the ACE is with short duration. What deserves to be noticed is that due to the capacity limitation of EVs and BESSs, if the ACE duration is longer, only the traditional units will participate in FR while EVs and BESSs will not.

4.6 Case Study and Results

4.6.1 Simulation Model and Parameters

The simulation model for EVs and BESSs participating in power system AGC is shown in Fig. 4.4, which is carried out using a two-area system model [10]. The

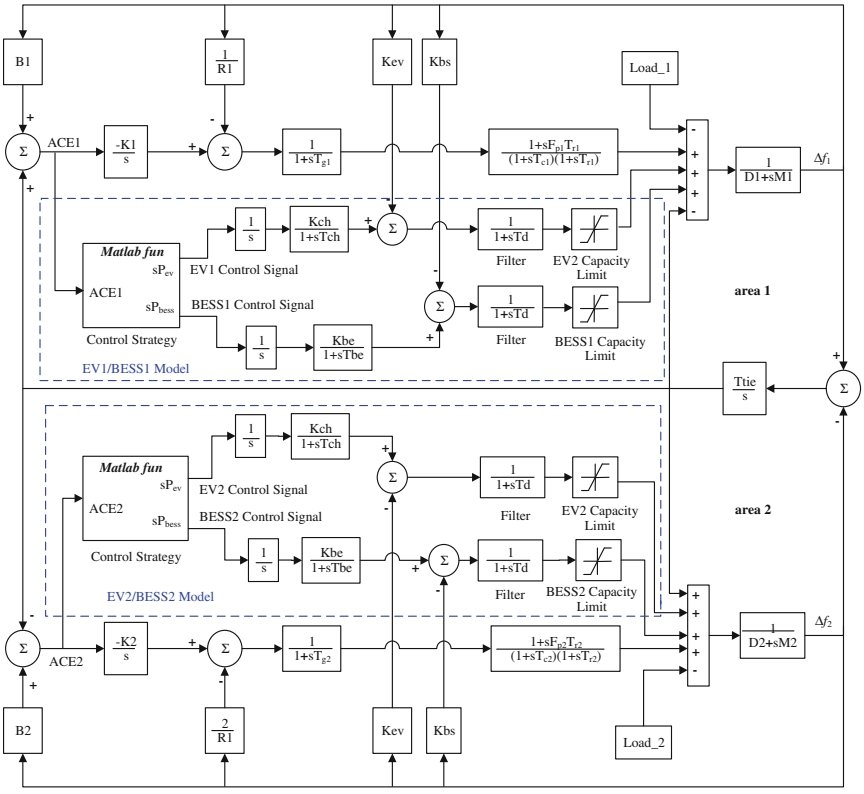

Fig. 4.4 FR of a two-area system model with EVs/BESSs. Reprinted from Ref. [40], Copyright 2014, with permission from Elsevier

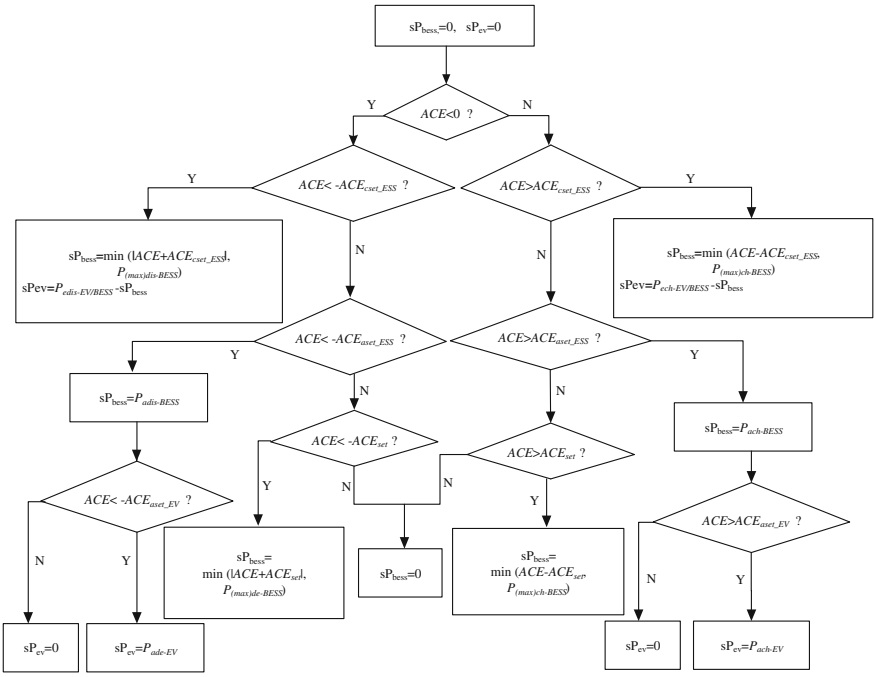

Fig. 4.5 Overview of the Embedded Matlab Function block. Reprinted from Ref. [40], Copyright 2014, with permission from Elsevier

large-scale EVs/BESSs system model is embedded in the simulation system, which is located in the blue dashed box (as shown in Fig. 4.4). In the simulation model, module "Control Strategy" is implemented using the Embedded Matlab Function block as shown in Fig. 4.5. The block is achieved through the user-defined function written according to the coordinated control strategy. The module takes *ACE* as the input signal, sP_{ev} and sP_{bess} (initial values are 0) as the output: power allocation is achieved based on the *ACE* signal, controlling the output power of multiple FR resources. Both the EV charging station and BESS models adopt the first order inertia ratio controllers. EVs and BESSs can either absorb or inject energy, and the saturation block with upper and lower limits (namely capacity limitation) is added in the model.

It is assumed that there are 5 EV charging stations and 3 BESSs in each area (area 1 and area 2). Each EV charging station is assumed to control 100 EVs, and the charging/discharging characteristic coefficient of each EV is taken as 2.5 kW/Hz [33]. In practice, the number of EVs participating in AGC should be forecasted in a short time. However, most research has been conducted on long-term forecasts of EV sales, e.g., one million EVs were forecasted to be on the road by 2015 in the USA [38], and the same number will be achieved by 2020 in Germany [39].

Table 4.1 Parameters of the simulation system model

Parameter	Value	Parameter	Value
System base (MW)	10	D1, D2 (MW/Hz)	1/6
Nominal frequency (Hz)	60	M1, M2 (MW/Hz/s)	2.0
R1, R2 (Hz/MW)	0.3	B1, B2 (MW/Hz)	1/6
T_{g1}, T_{g2} (sec)	0.5	F_{p1}, F_{p2}	30 %
T_{c1}, T_{c2} (sec)	0.8	K1, K2 (MW/Hz/s)	2/15
T_{r1}, T_{r2} (sec)	10	Ttie (MW/Hz)	0.5

Reprinted from Ref. [40], Copyright 2014, with permission from Elsevier

The aggregated operating details of EVs are not readily available. Hence, the SOC_{max} and SOC_{min} are assumed to be 90 and 10 %, respectively. The rated power and charging/discharging characteristic coefficient of each BESS are considered to be 2 MW and 0.4 MW/Hz, respectively. Generally, EV battery capacities range from 15 to 30 kWh. For convenience, each EV is assumed to be equipped with the same battery type (24 kWh) and the maximum V2G power P_{max} is 10 kW. Their initial SOC, namely SOC_{io} is supposed to be 0.3. In addition, previous studies have shown that most EVs are idle over 90 % of the time [41], and at least 90 % of them are parked each time [42]; therefore, this chapter assumes that 90 % of the EVs are available for FR each time. In the simulation model, 5 EV charging stations and 3 BESSs in each area are respectively synthesized into one to deal with. Consequently, the EVs and BESSs frequency characteristic coefficients Kev and Kbs are the comprehensive coefficients of all EVs and BESSs, respectively. Moreover, relevant parameters and response thresholds are shown in Tables 4.1, 4.2, 4.3 and 4.4.

Table 4.2 Parameters of the EV charging station and BESS model

Parameter	Value
EV frequency characteristic coefficient, Kev (MW/Hz)	1.12
BESS frequency characteristic coefficient, Kbs (MW/Hz)	1.2
EV battery gain, Kch	1
BESS battery gain, Kbe	0.8
EV battery filter time constant, Tch (s)	1
BESS battery filter time constant, Tbe (s)	1
1st order delay of DC/AC converter, Td (s)	2

Reprinted from Ref. [40], Copyright 2014, with permission from Elsevier

Table 4.3 Parameters of control strategy

Parameter	Value
f_{normal} (Hz)	0.05
f_a (Hz)	0.05
f_b (Hz)	0.15
ACE_{dz} (p.u.)	0.167 %

Reprinted from Ref. [40], Copyright 2014, with permission from Elsevier

Table 4.4 Response thresholds of the proposed control strategy

Parameter	Value (%)
$_a$ (p.u.)	0.083
$_b$ (p.u.)	0.25
ACE_{set} (p.u.)	0.167
ACE_{aset_EV} (p.u.)	0.32
ACE_{aset_ESS} (p.u.)	0.25
ACE_{cset_EV} (p.u.)	0.5
ACE_{cset_ESS} (p.u.)	0.5

Reprinted from Ref. [40], Copyright 2014, with permission from Elsevier

4.6.2 Simulations of Power System FR

Simulations for EVs and BESSs participating in an interconnected power system AGC under two scenarios are performed. The aim of the simulations is to verify the effectiveness of the control strategy for EVs and BESSs contributing to system FR. Therefore, simulations here are focused on the condition that the disturbances have a short duration.

Scenario 1: Step load disturbance. In this case, at time t = 3 s, 8 MW loads are added (0.8 p.u. step increase) in area 1 (load_1), while 2 MW loads are decreased in area 2 (load_2), resulting in system entering into the emergency state where frequency deviation exceeds 0.25 Hz. Simulation results are shown in Fig. 4.6. In Fig. 4.6a, the system is without the participation of EVs and BESSs. Additionally, simulation results of frequency deviations, without and with considering the coordinated control for EVs and BESSs to participate in system FR under different operating states, are shown as Fig. 4.6b, c, respectively. In other words, coordination under different operating states has not been taken into account in Fig. 4.6b (control strategy does not vary with different operating states), in which the control strategy is adopted according to the normal operating state. In Fig. 4.6c,

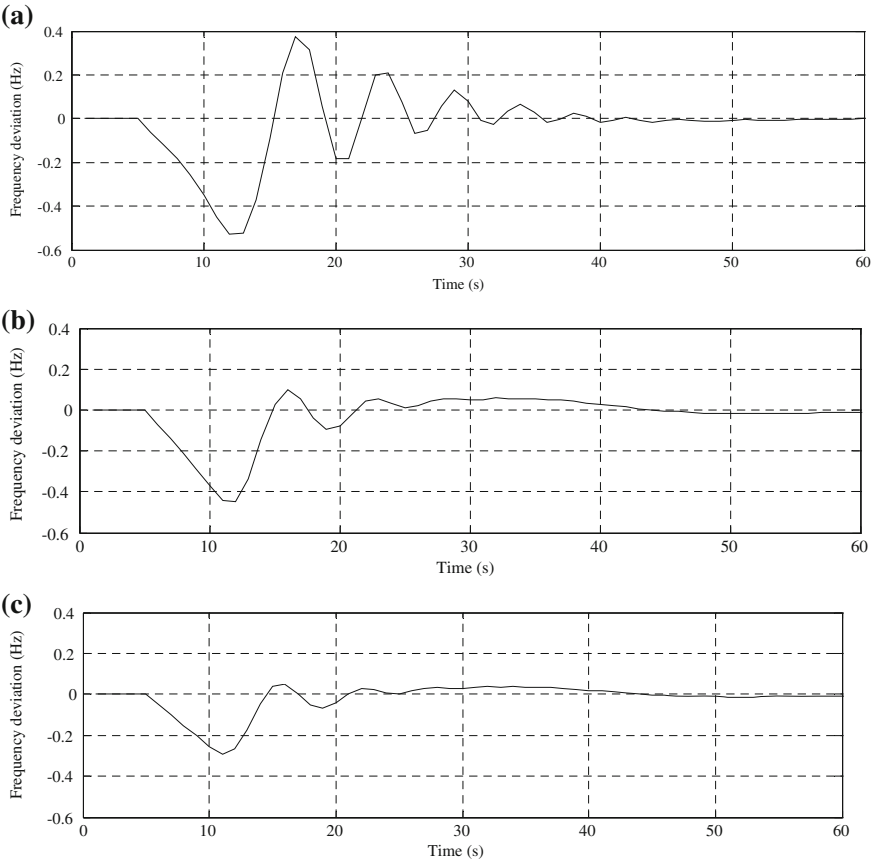

Fig. 4.6 Simulation results of system frequency deviation under a step load increase, without EVs and BESSs (**a**), control strategy does not take in account the coordination (**b**) and adopted the coordinated control strategy (**c**). Reprinted from Ref. [40], Copyright 2014, with permission from Elsevier

the coordinated control strategy under different operating states presented in this chapter is adopted. It clearly shows that without the participation of EVs and BESSs, the maximum frequency deviation falls below −0.529 Hz (Fig. 4.6a). And under the same disturbance, the maximum frequency deviation without and with considering the coordinated control under different operating states are −0.446 Hz (Fig. 4.6b) and −0.290 Hz (Fig. 4.6c) respectively, namely the maximum frequency excursion decreases by 0.239 Hz when taking into account the coordinated control in different operating states. At the same time, the results also show that: through the proposed control strategy, the contribution of EVs and BESSs to AGC

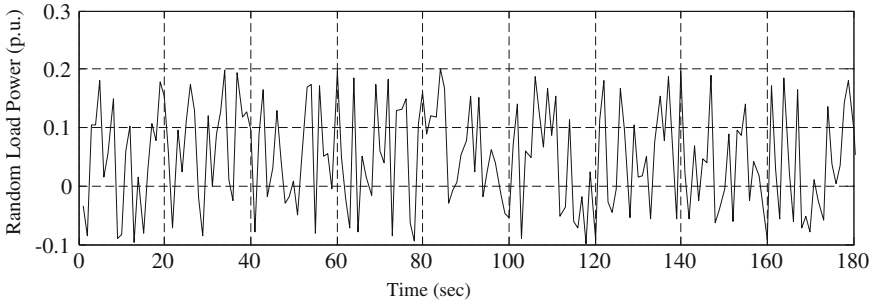

Fig. 4.7 Random fluctuation signals added at load_1. Reprinted from Ref. [40], Copyright 2014, with permission from Elsevier

coordinated with traditional units according to the operating states is beneficial to reduce the overshoot and oscillation, strengthening the stability of the power system.

Scenario 2: Random load fluctuations. In this case, random load fluctuation signals in a time series are assumed to be added at load_1. As shown in Fig. 4.7, random fluctuation signals are time-variant random series within [−0.1, 0.2] p.u. Simulation results of the system frequency deviation, ACE1 and ACE2 are shown in Fig. 4.8. As shown in Fig. 4.8b, the magnitudes of system frequency deviations can be limited within 0.1 Hz under the introduction of EVs and BESSs. However, without the participation of EVs and BESSs, the maximum magnitude is up to 0.23 Hz. In addition, as shown from Fig. 4.8c–f, the magnitude of ACE1 and ACE2 is reduced evidently and can be controlled within a small range (0.05 p.u.) with the inclusion of EVs and BESSs, while the maximum magnitude is 0.1 p.u. without EVs and BESSs. This case can simulate a power system with large-scale integration of renewable energy. From the results, it can also be deduced that the coordination of EVs and BESSs participating in AGC can considerably reduce the amount of response required (power demand) from the AGC units. Simultaneously, it has great potential to contribute to the stable operation of power system and the integration of renewable energy into power grid.

Based on the analysis of the simulation results, it shows that EVs and BESSs participating in system AGC coordinated with traditional units according to the operating states can effectively suppress power system frequency fluctuation and quicken the response rate. Meanwhile, it is beneficial for improving the power system's ability to resist failure and further the integration of large-scale renewable energy. Moreover, the amount of system reserve capacity requirement can be reduced with the introduction of EVs and BESSs.

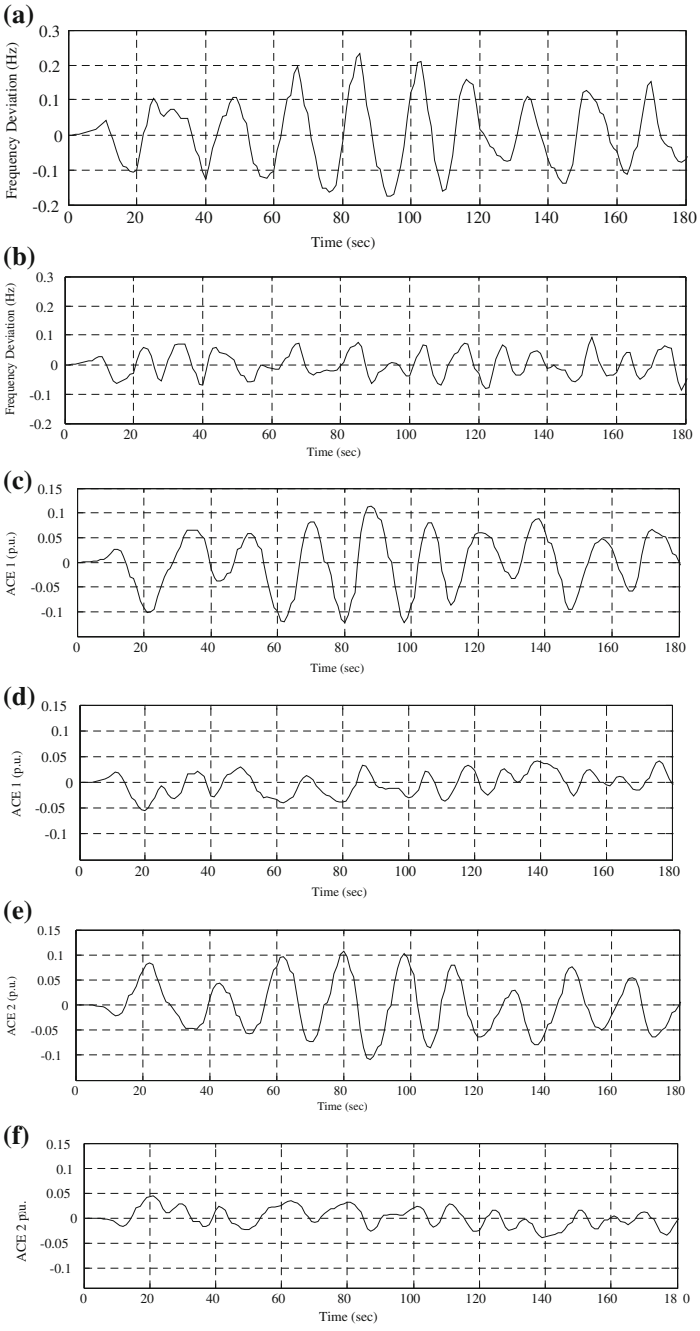

Fig. 4.8 Simulation results under random loads disturbance, system frequency deviation without EV/BESS (**a**), system frequency deviation with EVs/BESSs (**b**), ACE1 without EVs/BESSs (**c**), ACE1 with EVs/BESSs (**d**), ACE2 without EVs/BESSs (**e**) and ACE2 with EVs/BESSs (**f**). Reprinted from Ref. [40], Copyright 2014, with permission from Elsevier

4.7 Conclusions

This chapter studies the coordination of large-scale EVs, BESSs and traditional FR resources involved in system AGC. A control strategy is proposed for EVs and BESSs to provide regulation services coordinated with the traditional AGC units. To achieve the coordination, different response priorities and control strategies are set under different operating states. Considering EVs and BESSs have the characteristics of rapid response and large instantaneous power, EVs and BESSs will provide a fast response when the introduced disturbance is large and with a short duration. However, due to the limited storage capacity of EVs and BESSs, under the case that disturbance is with longer duration, only traditional units will participate in the response continuously. Furthermore, taking the impacts on EV users and batteries lifetime into account, EVs will be not involved in the response if the disturbance is small. Based on the analysis of the simulation results, it shows that EVs and BESSs participating in system AGC, coordinated with traditional units according to the operating states can effectively suppress power system frequency fluctuations and quicken the response rate. Meanwhile, it is beneficial for improving the power system's ability to resist failure and further the integration of large-scale renewable energy. Moreover, the amount of system reserve capacity requirement can also be reduced with the introduction of EVs and BESSs.

References

1. Vassell GS. The northeast blackout of 1965. Public Utilities Fortnightly 1990;126(8).
2. Kundur P, Paserba J, Ajjarapu V, et al. Definition and classification of power system stability IEEE/CIGRE joint task force on stability terms and definitions. IEEE Trans Power Syst. 2004;19(3):1387–401.
3. Talaq J, Al-Basri F. Adaptive fuzzy gain scheduling for load frequency control. IEEE Trans Power Syst. 1999;14(1):145–50.
4. Liu H, Hu Z, Song Y, et al. Decentralized vehicle-to-grid control for primary frequency regulation considering charging demands. IEEE Trans Power Syst. 2013;28(3):1–10.
5. Yang HM, Chung CY, Zhao J. Application of plug-in electric vehicles to frequency regulation based on distributed signal acquisition via limited communication. IEEE Trans Power Syst. 2013;28(2):1017–26.
6. Salameh ZM, Casacca MA, Lynch WA. A mathematical model for lead-scid batteries. IEEE Trans Energy Convers. 1992;7(1):93–8.
7. Durr M, Cruden A, Gair S, et al. Dynamic model of a lead acid battery for use in a domestic fuel cell system. J Power Sources. 2006;161(2):1400–11.
8. Wang XW, Han XQ, Men RJ. Modeling and simulation of lead-acid battery in wind and solar power systems. Shanxi Electric Power. 2009;2:23–6 (In Chinese).
9. Casacca M, Salameh ZM. Determination of lead-acid battery capacity via mathematical modeling techniques. IEEE Trans Energy Convers. 1992;7(3):442–6.
10. The Mathworks, Inc. Matlab R2009b help document: battery-implement generic battery model, TheMathworks, Inc., Natick, MA, USA; 2009.
11. Gómez JC, Morcos MM. Impact of EV battery chargers on the power quality of distribution systems. IEEE Trans Power Delivery. 2003;18(3):975–81.

12. Chan MSW, Chau KT, Chan CC. Modeling of electric vehicle chargers industrial. Proceedings of the 24th Annual Conference of the IEEE. IEEE. 1998;1:433–438.
13. Huang SF. Research on harmonic of electric vehicle chargers. Beijing: Beijing Jiaotong University; 2008 (In Chinese).
14. Li N. Harmonic study of different types of electric vehicle chargers. Beijing: Beijing Jiaotong University; 2010 (In Chinese).
15. Chen XQ, Li P, Hu WT, et al. Analysis of impacts of electric vehicle charger on power grid harmonic. Electric Power. 2008;41(9):31–6 (In Chinese).
16. Lu YX, Zhang M, Pu XW. Harmonic study of electric vehicle chargers. Proc CSU EPSA. 2006;18(3):51–4 (In Chinese).
17. Yilmaz M, Krein PT. Review of benefits and challenges of vehicle-to-grid technology. Proceeding of Energy Conversion Congress and Exposition (ECCE), IEEE. IEEE, 2012. p. 3082–3089.
18. Kempton W, Tomic J. Vehicle-to-grid power implementation: From stabilizing the grid to supporting large-scale renewable energy. Power Sources. 2005;144(1):280–94.
19. Fernandes C, Frías P, Latorre JM. Impact of vehicle-to-grid on power system operation costs: the Spanish case study. Appl Energy. 2012;96:194–202.
20. Dong X, Shi S, Wang B, et al. The offline accident of the large-scale wind generator system and its protection & control scheme 2012.
21. Peng M, Liu L, Jiang C. A review on the economic dispatch and risk management of the large-scale plug-in electric vehicles (PHEVs) penetrated power systems. Renew Sustain Energy Rev. 2012;16(3):1508–15.
22. White CD, Zhang KM. Using vehicle-to-grid technology for frequency regulation and peak-load reduction. J Power Sources. 2011;196(8):3972–80.
23. Kempton W, Tomic J. Vehicle-to-grid power fundamentals: calculating capacity and net revenue. J Power Sources. 2005;144:268–79.
24. Cready E, Lippert J, Pihl J, et al. Technical and economic feasibility of applying used EV batteries in stationary applications. Sandia National Labs., Albuquerque, NM (US); Sandia National Labs., Livermore, CA (US), 2003.
25. Lopes JAP, Polenz SA, Moreira CL. Identification of control and management strategies for LV unbalanced microgrids with plugged-in electric vehicles. Electr Power Syst Res. 2010;80 (8):898–906.
26. Sekyung H, Soohee H, Sezaki K. Development of an optimal vehicle-to-grid aggregator for frequency regulation. IEEE Trans Smart Grid. 2010;1(1):65–72.
27. Pillai JR, Bak-Jensen B. Integration of vehicle-to-grid in the western danish power system. IEEE Trans. on Sustainable Energy. 2011;2(1):12–9.
28. Liang L, Zhong J, Jiao Z. Frequency regulation for a power system with wind power and battery energy storage. Proceedings of IEEE International Conference on Power System Technology. IEEE 2012. p. 1–6.
29. Larsen E, Chandrashekhara DK, Østergård J. Electric vehicles for improved operation of power systems with high wind power penetration. Proceedings of Energy 2030 Conference IEEE. IEEE 2008. p. 1–6.
30. Lopes JAP, Soares FJ, Almeida PMR. Integration of electric vehicles in the electric power system. Proc IEEE. 2011;99(1):168–83.
31. Garcia R, Lopes JAP. Electric vehicle integration into modern power networks. Springer Science & Business Media; 2012.
32. Zhong H, Huan H, Zhi Z, et al. Optimization Design on Boiler-turbine Coordinated Control System with Automatic Generation Control. Proceedings of Power System Technology and IEEE Power India Conference 2008. p. 1–6.
33. Wang R, Liu Z, Song X, et al. Matlab-based simulations of primary frequency control for large thermal generating unit. Power Syst Technol. 2009;33(14):42–6.
34. Energy Storage—a Cheaper, Faster, & Cleaner Alternative to Conventional Frequency Regulation. http://www.ice-energy.com/stuff/contentmgr/files/1/76d44bfc1077e7fad6425102e55c0491/download/cesa_energy_storage_for_frequency_regulation.pdf.

35. Han H. The study on the control strategy of V2G participating peak regulation and frequency regulation of the grid. Beijing Jiaotong University; 2011. (In Chinese).
36. Kempton W, Udo V, Huber K, et al. A test of vehicle-to-grid (V2G) for energy storage and frequency regulation in the PJM system. 2008. http://www.udel.edu/V2G/resources/test-v2g-in-pjm-jan09.pdf.
37. Andersson SL, Elofsson AK, Galus MD, et al. Plug-in hybrid electric vehicles as regulating power providers: case studies of Sweden and Germany. Energy Pol. 2010;38(6):2751–62.
38. Kundur P. Power system stability and control. New York: McGraw-Hill Inc.; 1994.
39. Mili L, Center NV. Taxonomy of the characteristics of power system operating states. In 2nd NSF-VT Resilient and Sustainable Critical Infrastructures (RESIN) Workshop, Tucson, AZ, Jan. 2011. p. 13–15.
40. Zhong J, He L, Li C, et al. Coordinated control for large-scale EV charging facilities and energy storage devices participating in frequency regulation. Appl Energy. 2014;123:253–62.
41. One million electric vehicles by 2015. http://www1.eere.energy.gov/vehiclesandfuels/pdfs/1_million_electric_vehicles_rpt.pdf.
42. Federal Government of Germany. German's federal government national electromobility development plan. 2009.

Chapter 5
The Asynchronous Response of Small-Scale Charging Facilities to Grid Frequency

5.1 Introduction

The increasing penetration of renewable energy sources, such as wind and solar energy, gives rise to new challenges for the operation and dispatch of power systems [1–3]. Demand response is an effective ancillary service for power systems [4–7]. And EV loads can take part in demand response. V2G technology achieves bidirectional power flow between EVs and power systems. Using V2G, the charging EVs can be regarded as not only controllable load, but also distributed energy storage units [8]. FR provided by charging EVs has gained increasing attention [9–12].

EVs participating in the FR can be divided into two types according to participative ways: the centralized mode and the decentralized mode [13–15]. Generally, the centralized mode is applied to the large-scale charging stations where centralized control center and communication network are available. Centralized EV fleets with large storage capacity could exert a greater influence on system frequency and smooth the output power of renewable energy to promote the energy development. Optimization strategies for charging/discharging can be implemented with the help of communication network. By means of communication network, large-scale EVs participate in supplementary FR, and power capacity of the regulation could be dispatched between individual EVs and EV charging stations according to FR capacity and expected V2G power of EVs in [13].

Another mode is decentralized charging EVs participating in FR with aggregator, communication network and central control entity [16–18]. The aggregator collects and delivers control messages and monitoring messages between chargers and central control entities. Various control methods were proposed for decentralized charging EVs to optimize the charging priority, charging time or charging costs [19–21]. In [22], considering the charging demand of each EV, a decentralized V2G control strategy called battery SOC holder was designed to improve the stability of frequency and both scheduled charging and FR could be achieved.

C. Li et al., *Influences of Electric Vehicles on Power System and Key Technologies of Vehicle-to-Grid*, Power Systems,
DOI 10.1007/978-3-662-49364-9_5

In [23], an autonomous distributed V2G control method which considered the convenience of users was proposed, and EVs supplied dispersed spinning reserves for the integration of intermittent renewable energy sources.

With the growing number of EVs, there would be a greater number of dispersed chargers for EVs. It would be costly to establish aggregators and communication network for dispersed chargers. The control methods are necessary and expected for these chargers to participate in FR. And negative impacts, such as over-response resulted by simultaneous response, would be caused without coordination control. For example, charging EVs will reduce charging power when system frequency is low. If the power reduction of charging EVs exceeds the demand of power systems to restore the frequency, the over-response may be caused. Several coordinated control methods for other interruptible load were proposed to solve the problem of the over-response [24–26], which could offer some enlightenment for dispersed charging EVs. In [24], each plug-in electrical vehicle (PEV) adjusted its charging/discharging power in response to a communal virtual price signal, which could improve the system frequency and neutralize the wind power response to the frequency deviation without the central control entity. In [25], a load controller was designed considering both the frequency deviation and the evolution over time of Δf (the $\Delta f - t$ characteristic). Therefore, each controller had different $f - t$ response parameters to determine the moment when the load started to participate in FR. But the controller with shorter duration threshold of frequency deviation responded more frequently than that with longer one and the equality couldn't be ensured for participants. In [26], randomized set of frequency deviation threshold was applied to different appliances to prevent over-activation of the electricity demand as frequency controlled reserve, which could reduce the side effects on power systems. However, the appliances with lower threshold would respond more frequently than that with higher threshold. As can be seen, the equality problem to ensure the equal opportunities for dispersed charging EVs in FR has not been involved so far.

Taking coordination and equality into account, a novel asynchronous control method for dispersed charging EVs to participate in FR is proposed in this chapter.

5.2 Formulation of the Proposed Control Method

To participate in FR, EV chargers change the charging power to participate in FR according to the frequency deviation. So, when system frequency rises over the allowable range, the charging power of EVs can be increased under some constraints of the batteries. Otherwise, EVs can stop charging or reduce their charging power when system frequency decreases below the allowable range. In the emergency conditions, EVs can discharge their energy back into power grid.

In this chapter, each charging EV adopts the same control method with the same parameters, including the measurement cycle T, frequency deviation threshold Δf_{dz} and the proportion of power regulation.

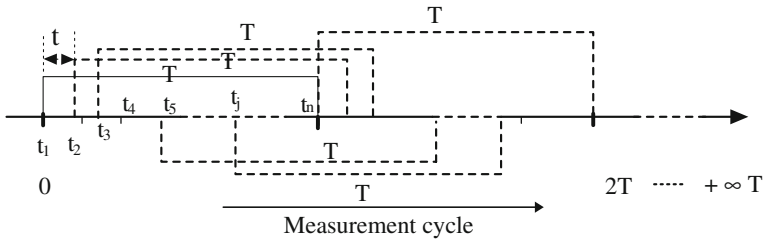

Fig. 5.1 Time distribution of frequency measurement of charging EVs

Compared with the conventional generators, charging EVs respond more rapidly [19]. Consequently, time delay for EVs can be negligible and frequency measurement cycle of EVs should set a small value which is roughly equivalent to time duration of secondary frequency response.

All chargers measure system frequency once each cycle after connecting to the grid, as shown in Fig. 5.1. It is assumed that one of charging EVs detects system frequency at time t_1, then the chargers will measure the frequency at time $t_1 + T$, $t_1 + 2T$, … until the charging is completed or interrupted. The initial time of the frequency measurement is not synchronized for chargers, which depends on the time they are plugged in. Thus, the initial frequency measurement time of each charging EV is independent. It is worth noting that the number of charging EVs participating in FR is changed over time with continuous plug-in and plug-out. When EVs are being charged, they participate in FR coordinately with the same probability by adopting the proposed method. For convenience, only charging EVs are taken into consideration in the book.

The parameter Δf_{dz} refers to the frequency deviation threshold, which is a demarcation point for EVs to participate in FR. In addition, Δf_{dz} is set based on the compromise between system frequency stability and its impact on charging EVs. Response amplitude refers to the variation of output power which is adjusted with the same proportion of power regulation for different types of charging EVs.

5.3 The Demonstration of Coordination

If dispersed charging EVs participate in FR uncoordinated when abnormal frequency deviation happens, over-response may occur. Consequently, the coordinated method without over-response is essential. In this section, it will be proved that the over-response caused by charging EVs can be avoided by adopting the proposed method.

Frequency deviation is caused by the imbalance of active power in the system. It is assumed that the allowable range for frequency deviation is $[-\Delta f_{\mathrm{dz}}, \Delta f_{\mathrm{dz}}]$. Then within the range, charging EVs would not adjust the charging power to participate in FR. Otherwise, charging EVs would adjust the charging power according to

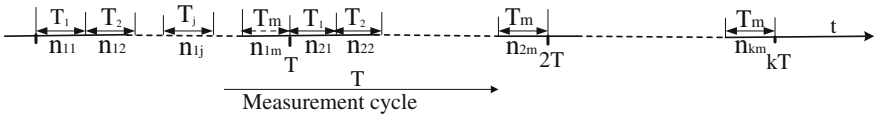

Fig. 5.2 Amounts distribution of the charging EVs based on time-window

frequency deviation. It is assumed that n is the number of charging EVs participating in FR and T is the frequency measurement cycle for charging EVs. Then T is divided into m equal time-windows, as shown in Fig. 5.2, and n_{k1}, n_{k2}, n_{k3}, …, n_{km} is the respective corresponding number of charging EVs in m time-windows in the kth cycle (k referring to the number of frequency measurement cycles). Expectation of charging EVs number in every time-window of k cycles is shown in (5.1).

$$\begin{aligned} EX_1 &= (n_{11} + n_{21} + n_{31} + n_{41} + \cdots + n_{k1}) \times T_1/T \times 1/k \\ EX_2 &= (n_{12} + n_{22} + n_{32} + n_{42} + \cdots + n_{k2}) \times T_2/T \times 1/k \\ EX_3 &= (n_{13} + n_{23} + n_{33} + n_{43} + \cdots + n_{k3}) \times T_3/T \times 1/k \\ &\vdots \\ EX_m &= (n_{1m} + n_{2m} + n_{3m} + n_{4m} + \cdots + n_{km}) \times T_m/T \times 1/k \end{aligned} \tag{5.1}$$

EX_1, EX_2, EX_3, …, EXm represent the expectation of charging EVs number within time-window T_1, T_2, T_3, …, T_m, respectively. Since each charging EV is randomly assigned to a time-window in every cycle for measuring frequency, the probability of entering each time-window is equal. Expectation of charging EVs number to measure the frequency is the same during the same time interval. Thus n/m is the expected number of charging EVs in a time-window, and only one mth of total charging EVs may change their charging power if abnormal frequency deviation is maintained throughout the entire time-window. Therefore, the EVs would not participate in frequency response simultaneously and comply with the rule that expectation of charging EVs number is invariable in unit time whether duration of abnormal frequency is long or short. To further explain the coordination, loads are assumed to increase suddenly at time t_0, which results in a negative frequency deviation (Δf_0) away from the allowable range and power demand ΔP. Then charging EVs that measure system frequency after t_0 will change charging power one by one. The total regulated power of charging EVs (ΔP_{EV}) can be described in (5.2). $\Delta P_{t_{EV_j}}$ is the regulating power of the jth EV at t_j which is shown in Fig. 5.1. And Δf_{EV_j} is the frequency deviation detected by the jth charging EV.

$$\Delta P_{EV} = \sum_{j=0}^{n-1} (\Delta P_{t_{EV_j}} \times g(\Delta f_{EV_j})) \tag{5.2}$$

where g is the piecewise function, as shown in (5.3).

$$g(\Delta f_{EV_j}) = \begin{cases} 1, & \Delta f_{EV_j} \geq f_{dz} \\ 0, & -f_{dz} < \Delta f_{EV_j} < f_{dz} \\ -1 & \Delta f_{EV_j} \leq -f_{dz} \end{cases} \tag{5.3}$$

As shown in (5.2) and (5.3), Δf_0 will decrease gradually with the number of responded charging EVs increasing. As ΔP_{EV} is approximate to ΔP and Δf_0 is within the range of $[-f_{\mathrm{dz}}, f_{\mathrm{dz}}]$, those charging EVs without participating in FR will not respond. Therefore, over-response will not occur and thus negative impacts on power grid could be prevented to some extent. On the other hand, once the frequency deviation exceeds the upper threshold, the dispersed EVs will also be charged and respond to the frequency deviation sequentially, and the over-response can also be prevented by using the proposed method.

5.4 The Demonstration of Equality

In this section, equality means the same opportunities for charging EVs to respond to frequency deviation. The equality of charging EVs participating in FR ensures the implementation of the control method in a fair way and further raises the acceptability of EV owners to this method.

In the control method, each EV is connected to power grid randomly at any point in time and charging EVs are set with the same parameters (response threshold, frequency measure cycle, proportion of power regulation) to participate in FR. From mathematical view, it meets the requirement of rotational symmetry. No charging EV is different from the others. In addition, frequency deviation over allowable range occurs randomly and time duration of abnormal frequency is also random. The initial measurement time and end time of charging EVs is random, too. All of the random variables are independent. As a qualitative analysis, the probability of charging EVs responding to frequency deviation should be equal.

Without loss of generality, it is supposed that l EVs have participated in the FR in a disturbance. Suppose that

$\mathrm{A}_j = \{\mathrm{EV}_j$ participates in FR$\}$ $(j = 1, 2, \ldots, n)$
$\mathrm{B}_{j,i} = \{i$ EVs participate in FR among the first $j - 1$ EVs$\}$ $(j - 1 \geq i)$
$\mathrm{C}_{j,i} = \{i$ EVs participate in FR and other $j - i - 1$ EVs do not participate in FR among the first $j - 1$ EVs$\}$ $j - 1 \geq i)$

where i and j stand for numbers. According to probability theory, the probability of EV_j participation in FR P (A_j) can be inferred as shown in the following formula (5.4).

$$
\begin{aligned}
&P(A_1) = l/n \\
&P(A_2) = P(A_1A_2) + P(\bar{A}_1A_2) = \frac{n-l}{n} \times \frac{l}{n-1} + \frac{l}{n} \times \frac{l-1}{n-1} = \frac{l}{n} \\
&\textit{if} \quad 3 \le j \le l \\
&P(A_j) = \sum_{i=0}^{j-1} P(B_{j,i}A_j) = \sum_{i=0}^{j-1} C_{j-1}^{i} P(C_{j,i}A_j)) \\
&\qquad = \sum_{i=0}^{j-1} C_{j-1}^{i} \frac{(n-l)!}{(n-j+i-l+1)!} \times \frac{l!}{(l-i-1)!} \times \frac{(n-j)!}{n!} = \frac{l}{n} \qquad (5.4) \\
&\textit{if} \quad j > l \\
&P(A_j) = \sum_{i=0}^{l-1} P(B_{j,i}A_j) = \sum_{i=0}^{l-1} C_{j-1}^{i} P(C_{j,i}A_j)) \\
&\qquad = \sum_{i=0}^{l-1} C_{j-1}^{i} \frac{(n-l)!}{(n-j+i-l+1)!} \times \frac{l!}{(l-i-1)!} \times \frac{(n-j)!}{n!} = \frac{l}{n}
\end{aligned}
$$

According to (5.4), the same probability *l/n* can be obtained regardless of which EV participates in FR. Therefore, the equality of EVs' participation in FR can be ensured in the proposed method.

It is worth noting that the times and duration of different EVs being charged are different. Therefore, the probability of EVs to participate in FR is different. By adopting the proposed method, the probability of charging EVs to participate in FR can be ensured.

5.5 Case Study

5.5.1 Simulation Model and Parameters

Simulations are implemented to validate the proposed control method for dispersed charging EVs in FR on the IEEE 14-bus transmission system, as shown in Fig. 3.3 in Chap. 3. The IEEE 14-bus system data are available in [27, 28]. And the simulations are implemented in MATLAB software by using the Power System Analysis Toolbox. With the increasing integration of renewable energy to power grid, more and more disturbances will occur randomly, resulting in frequency fluctuation in power systems. Thus, different types of disturbances, including step load disturbance, large shock load disturbance and random disturbances, are simulated to verify the effectiveness of the proposed control method.

The rated capacity of EV battery is generally within the range of 16−85 kWh. There are two types of batteries for EVs, DENZA and BYD E6, each accounting for half of the total number of charging EVs participating in FR. DENZA has a

capacity of 47.5 kWh, maximum power 6 kW and charging voltage 220 V; BYD E6 has a capacity of 63.4 kWh, maximum power 40 kW and charging voltage 380 V. The equivalent circuit of the grid-connected EVs adopts the battery model in [29] to simulate its discharging/charging characteristics. EVs are idle in most of time and at least 90 % of them are parked based on previous literature analysis [10]. Therefore, most of EVs can participate in FR if EV owners are willing. In the simulation studies, two thousand EVs are available and allocated on bus 2, 4, 6 with the number of 680, 680, 640 respectively. Considering the battery life and driving demands, SOC_u and SOC_l are set at 90 and 10 %, respectively [20]. The initial SOC values of all these batteries are assumed to follow the normal distribution N (0.5, 0.12), and 30 % of the charging EV users are assumed to have the 50 % minimum SOC demand value (SOC_s). Meanwhile, the battery charging/discharging power (in the normal state) of each EV is supposed to achieve its maximum value within some constraints. Charging EVs can participate in FR by setting the measurement cycle T within several seconds, i.e. 2–8 s. This interval is determined based on the following two reasons. First, the shorter the frequency measurement cycle is, the more EVs there are within the unit time. For a shorter interval, the frequency measurement of charging EVs is almost synchronous, and thus the EVs will respond almost simultaneously. Hence, the implementation of asynchronous response can't be guaranteed. Second, the characteristic of EVs' faster response would not be fully utilized with a longer measurement cycle. Therefore, the measurement cycle is set to be 6 s in this chapter. In addition, a power system with a rated frequency of 50 Hz is considered in the simulations.

Different frequency deviation thresholds and response amplitude should be set in different conditions of power system when charging EVs participate in the FR. And the threshold and amplitude depend on the scale of power system as well as the penetration of fluctuating load. However, considering the users' benefits, charging EVs shouldn't respond frequently. The frequency deviation is allowed within ±0.5 Hz according to the criterion of the Chinese power system, and it is limited to ±0.03 Hz by the State Grid Corporation of China. The total time of frequency deviation of more than 0.03 Hz was less than 100 s in most provinces in China in the whole year of 2013. Consequently, in this case, the response threshold is set to 0.03 Hz, which means charging EVs will not respond within [49.97, 50.03] Hz. Meanwhile, since EVs' participation in FR is treated as an emergency method for power grid, the probabilities for charging EVs to participate in FR are a little lower and the duration is shorter. Thus the proportion of power regulation should be relatively high. In the simulations, the charging EVs will reduce their charging power to 50 % of the current value once negative frequency deviation is detected. In the emergency condition, charging EVs can return their energy back into power grid. Charging EVs will rise to the maximum charging power when positive frequency deviation exceeds the upper threshold. Specific expressions for the response amplitude are given in (5.5), which defines different regulating values ($\Delta P_{t_{EV_j}}$) according to the above descriptions.

$$\Delta P_{t_{EVj}} = \begin{cases} P_{jd\max} + P_{jch} & (\Delta f_{EVj} \leq -0.2\,\text{Hz}) \\ \frac{1}{2} P_{jch} & (-0.2\,\text{Hz} < \Delta f_{\text{EVj}} \leq -0.03\,\text{Hz}) \\ 0 & (-0.03\,\text{Hz} < \Delta f_{\text{EVj}} < 0.03\,\text{Hz}) \\ P_{jch\max} - P_{jch} & (\Delta f_{EVj} \geq 0.03\,\text{Hz}) \end{cases} \tag{5.5}$$

where $\Delta P_{t_{EV_j}}$ is the changed charging power of EV_j at t_j, Δf_{EV_j} is the measured frequency deviation of EV_j, $P_{j\text{ch}}$ is the current charging power, $P_{j\text{chmax}}$ and $P_{j\text{dmax}}$ are the maximum charging and discharging power of EV_j, respectively. And the total regulated power of EVs (ΔP_{EV}) can be formulated as shown in (5.2).

5.5.2 *Validation of Coordination*

Different types of disturbances are simulated to verify the effectiveness of the proposed method in system FR. Coordination of the proposed method is illustrated in detail in simulations.

(1) *Scenario 1*: *Step load disturbance.* In this scenario, the response to a step load disturbance is studied. The step load disturbance is simulated with a sudden increase ΔP_{d} in load demand at t = 120 s. Figure 5.3 describes the results of EVs' participation in FR with proposed method under three different magnitude of disturbances: 30, 45, 60 MW. By observing the simulation results, it can be obtained that the frequency value doesn't exceed the upper threshold no matter how large the disturbance is. And there is no oscillation and over-response caused by charging EVs by adopting the proposed method.

(2) *Scenario 2*: *Large shock load disturbance.* At t = 60 s, a large shock disturbance ΔS_d occurs on bus 3, while at t = 120 s the disturbance is cleared as shown in Fig. 5.4. In general, ΔS_d is supposed to contain not only active power

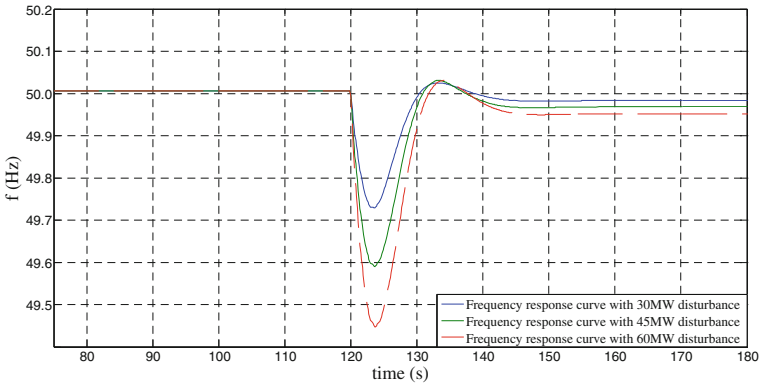

Fig. 5.3 Simulation of FR under different magnitude of step load disturbances at 120 s

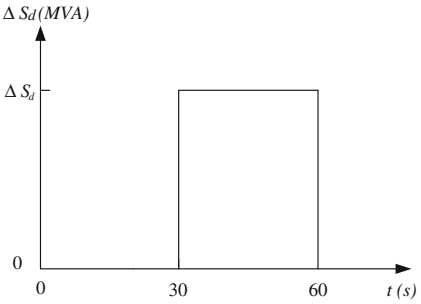

Fig. 5.4 Diagram of the large impact disturbance

but also reactive power. With the assumption that ΔS_d is (40 + j25) MVA, the system frequency response curve is shown in Fig. 5.5. It can be obtained that system frequency can restore to the range of 50 ± 0.03 Hz within 9.5 s in the proposed method while that cannot restore to this range with conventional generators. As the figure shows, the frequency response curve is smooth without oscillation and over-response during the whole process. And the steady-state error is less than 0.0189 Hz by adopting the proposed method.

(3) *Scenario 3*: *Random disturbances.* The time-series data of the random disturbances, including the disturbance magnitude and positions applied to this simulation scenario, are given in Table 5.1. The random positive ΔS_d is to represent rising load demand or the decreasing wind power generation. Conversely, negative ΔS_d represents a reduction in load demand or the increasing wind power generation due to the increase of wind speed. Figure 5.6 describes the results of FR under three conditions, including FR with conventional generators, dispersed EVs' asynchronous control method and EVs' participation in FR without control method, respectively. In addition, it can be observed that the maximum frequency rises to 50.31 Hz in conventional

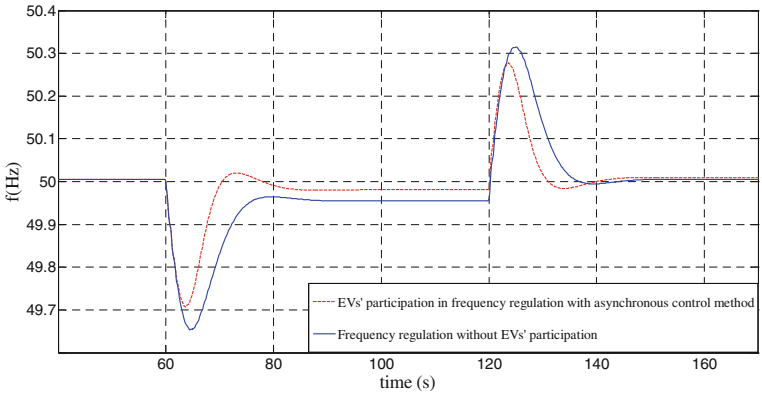

Fig. 5.5 FR under the large shock load disturbance

Table 5.1 Random disturbances

Disturbance time (s)	Magnitude ΔS_d (MVA)	Disturbed bus
30	−(30.00 + j20.00)	5
72	−(5.20 + j5.80)	3
100	32.00 + j26.00	1
140	9.00 + j9.50	9
170	−(4.50 + j2.00)	6

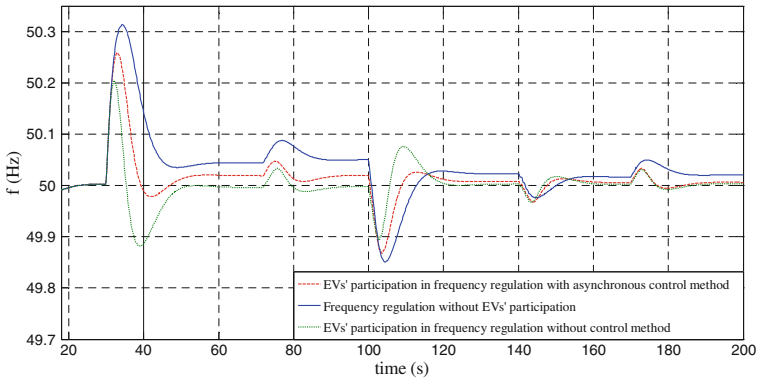

Fig. 5.6 FR under random disturbances

generators method, while it reaches 50.25 Hz in the proposed method, which also presents a smoother response curve. Thus, it is clear that the response of charging EVs would not result in over-response.

5.5.3 Validation of Equality

EVs are set with different response thresholds and delays to verify the equal participation in FR in the proposed method.

The number of disturbances, which are independent of each other, is increased to twenty four, and these disturbances are distributed at different buses and time. Then, statistics, including the times and the probabilities for charging EVs to participate in FR, are used to analyze the simulation results. As shown in Fig. 5.7, there is little difference in the times and the probabilities for each charging EV. Consequently, the responsive probability for each charging EV will tend to be same with the increasing number of disturbances.

Charging EVs' participation in FR with different response thresholds is simulated in scenario 1. And average probability is obtained based on twenty-four simulations. The results of the comparison of the probabilities for charging EVs to

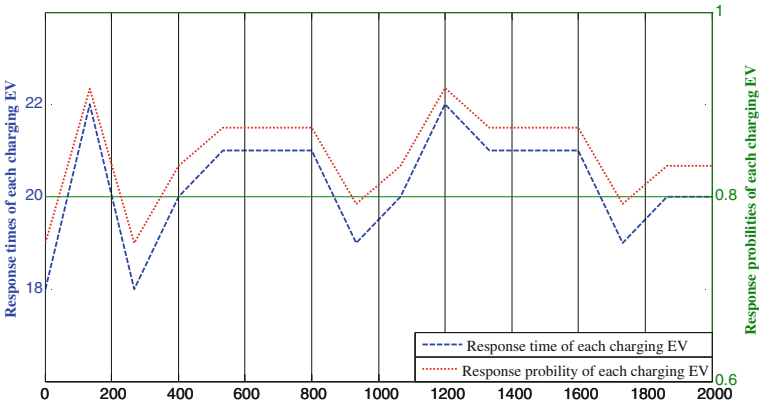

Fig. 5.7 Statistics of the times and the probabilities for each charging EV to participate in FR

Table 5.2 The Probabilities of EVs' participation in FR with different response thresholds and delays

Response threshold (Hz)	0.03	0.05	0.1	0.15	0.20
Response probability (%)	75.12	70.83	58.68	46.53	33.85
Response delays (ms)	0	125	250	375	500
Response probability (%)	75.25	39.89	26.61	19.78	15.69

participate in FR are shown in the Table 5.2. The probabilities are 75.12 and 33.85 % with the response threshold 0.03 and 0.20 Hz, respectively. It is obvious that the smaller the frequency deviation threshold is, the larger the probability for EVs to participate in the FR is.

Charging EVs' participation in FR with different response delays is simulated in scenario 3. The results of the comparison of the probabilities for charging EVs to participate in FR are shown in the Table 5.2. On condition that the frequency deviation threshold is set to 0.03 Hz the probabilities are 75.25 and 15.69 % with the zero delay and 500 ms delay, respectively. It is obvious that the smaller the frequency response delay is, the larger the probability for EVs to participate in the FR is.

According to the comparative analysis based on simulation results, the probabilities of participation in FR are various for EVs with different response thresholds and delays while that are the same for each EV in the proposed method.

5.6 Conclusions

Charging EVs' participation in FR can effectively alleviate the frequency deviations and contribute to the integration of intermittent renewable sources to the grid, such as wind and solar energy. In this chapter, an asynchronous control method is

proposed for dispersed charging EVs to participate in FR without central control entity and communication network. Under the proposed method, the same FR parameters are set for each charging EV. Therefore, the gradual participation of EVs in FR can be ensured if the frequency deviation is over the allowable range. By adopting the proposed method, the coordination and the equal probability for each charging EV to participate in FR can be guaranteed. Finally, the simulation results under different disturbance conditions prove the effectiveness of this method.

References

1. Peter S, Henrik L, Anders NA. Future power market and sustainable energy solutions—the treatment of uncertainties in the daily operation of combined heat and power plants. Appl Energy. 2015;144:129–38.
2. Purvins A, Zubaryeva A, Llorente M, et al. Challenges and options for a large wind power uptake by the European electricity system. Appl Energy. 2011;88(5):1461–9.
3. Inman RH, Pedro HTC, Coimbra CFM. Solar forecasting methods for renewable energy integration. Prog Energy Combust Sci. 2013;39(6):535–76.
4. Jonghe CD, Hobbs BF, Belmans R. Optimal generation mix with short-term demand response and wind penetration. IEEE Trans Power Syst. 2012;27(2):830–9.
5. Georgilakis PS. Technical challenges associated with the integration of wind power into power systems. Renew Sustain Energy Rev. 2008;12(3):852–63.
6. Broeer T, Fuller J, Tuffner F, et al. Modeling framework and validation of a smart grid and demand response system for wind power integration. Appl Energy. 2014;113:199–207.
7. Mohammadreza M, Alireza Z, Shahram J, Pierluigi S. Integrated scheduling of renewable generation and demand response programs in a microgrid. Energy Convers Manage. 2014;86:453–75.
8. Tian WQ, He JH, Niu LY, et al. Simulation of vehicle-to-grid (V2G) on power system frequency control. IEEE Innovative Smart Grid Technologies-Asia, Conference, Tianjin; 2012;1–3.
9. Jonathan D, Marija I. Stochastic Co-optimization of charging and frequency regulation by electric vehicles. North American Power Symposium (NAPS), Conference, Champaign, IL; 2012;9–11.
10. Zhong J, He LN, Li CB, et al. Coordinated control for large-scale EV charging facilities and energy storage devices participating in frequency regulation. Appl Energy. 2014;123:253–62.
11. Mu Y, Wu J, Ekanayake J, et al. Primary frequency response from electric vehicles in the Great Britain power system. IEEE Trans Smart Grid. 2013;4(2):1142–50.
12. Pillai JR, Bac-Jensen B. Vehicle-to-grid system for frequency regulation in an Islanded Danish distribution network. IEEE Vehicle Power Propulsion Conference, Lille; 2010:1–6.
13. Liu H, Hu Z, Song Y, et al. Vehicle-to-Grid control for supplementary frequency regulation considering charging demands. IEEE Trans Smart Grid. 2015;30(6):3110–8.
14. Lin JH, Leung KC, Li VOK. Optimal scheduling with vehicle-to-grid regulation service. IEEE Trans Power Syst. 2014;1(6):556–69.
15. Sakuma H, Hashimoto R, Yano H, et al. Novel demand response scheme for frequency regulation using consumers' distributed energy storages. Innovative Smart Grid Technologies Conference (ISGT), 2014 IEEE PES. IEEE, 2014;1–5.
16. Ahn CS, Li CT, Peng H. Optimal decentralized charging control algorithm for electrified vehiclesconnected to smart grid. J Power Sources. 2011;196:10369–79.
17. Villalobos JG, Zamora I, Martín JIS, et al. Plug-in electric vehicles in electric distribution networks: A review of smart charging approaches. Renew Sustain Energy Rev. 2014;38:717–31.

18. Gan LW, Ufuk T, Steven HL. Optimal decentralized protocol for electric vehicle charging. IEEE Trans Power Syst. 2013;28(2):940–51.
19. Christophe George G. A conceptual frame work for the vehicle-to-grid (V2G) implementation. Energy Policy. 2009;37:4379–90.
20. Han S, Han S, Sezaki K. Development of an optimal vehicle-to grid aggregator for frequency regulation. IEEE Trans Smart Grid. 2010;1(1):65–72.
21. Li RY, Wu QW, Shmuel SO. Distribution locational marginal pricing for optimal electric vehicle charging management. IEEE Trans Power Syst. 2014;29(1):203–11.
22. Liu H, Hu Z, Song Y, et al. Decentralized vehicle-to-grid control for primary frequency regulation considering charging demands. IEEE Trans Power Syst. 2013;28(3):3480–90.
23. Ota Y, Taniguchi H, Nakajima T, et al. Autonomous distributed V2G (Vehicle-to-Grid) satisfying scheduled charging. IEEE Trans Smart Grid. 2012;3(1):559–64.
24. Luo X, Xia SW, Chan KW. A decentralized charging control strategy for plug-in electric vehicles to mitigate wind farm intermittency and enhance frequency regulation. Power Sources. 2014;248(15):604–14.
25. Molina-Garciá A, Bouffard F, Kirschen DS. Decentralized demand-side contribution to primary frequency control. IEEE Trans Power Syst. 2011;26(1):411–9.
26. Xu Z, Jacob Ø, Mikael T. Demand as frequency controlled reserve. IEEE Trans Power Syst. 2011;26(3):1062–71.
27. Bhaskar MA, Venkatesh A, Dash SS, et al. Voltage stability improvement using "Sen" transformer. India International Conference on Power Electronics (IICPE). New Delhi, India Jan 2011;1–6.
28. Kodsi SKM, Cañizares CA. Modeling and simulation of IEEE 14 bus system with FACTS controllers. University of Waterloo, Waterloo, Canada, Technical Report 2003–3. https://ece.uwaterloo.ca/~ccanizar/papers/IEEEBenchmarkTFreport.pdf. Accessed Dec 2013.
29. Yang HM, Chung CY, Zhao JH. Application of plug-In electric vehicles to frequency regulation based on distributed signal acquisition via limited communication. IEEE Trans Power Syst. 2013;28(2):1017–26.

Chapter 6
Analysis on Typical Schemes of the Integration of EV Charging Facilities into the Grid

6.1 Introduction

EVs can benefit the climate and play an important role in power system. The EV charging facility which provides power supply for EVs running is a necessary and important supporting facility for the development of EVs. Therefore, rational planning and distribution of EV charging facilities is a crucial precondition for large-scale application of EVs [1, 2]. Currently, EV charging facilities mainly include EVCSs and electric vehicle charging piles (EVCPs) [3–5].

It is expected that EVCSs will be an important part of future distribution network. As EVs' charging featuring quick charge and high power has a negative impact on the voltage quality of distribution network, EVCSs should be integrated into a proper access point [6]. Many researches focus on the design of EVCSs' integration. In order to improve the utilization of new clean energy, a new EVCS involving several new renewable energies and energy storage systems is presented in [7], and the station is powered by DC bus rather than AC bus. The feasibility of the application of solar energy and wind power to PHEVs' power supply is explored and a computing method of PHEVs' photovoltaic panel area in EVCSs is presented in [8]. The EVCS including storage batteries is put forward in [9], where the storage batteries charge the EVs during peak-load periods and the grid charges the storage batteries during valley-load periods. Considering EV batteries' life and environmental problems, a mobile EVCS that can both serve as power supply of EVs and charge EV batteries is proposed in [10]. EV batteries as storage devices can be a promising supplement for the power source in distribution network [1, 7–10].

The planning of the integration of EV charging facilities to the grid involves the selection of EVs' access points and capacity, which is within power company's business expansions. Researches in these fields are explored in some literatures, but EV batteries' energy storage characteristic that EV charging facilities based on V2G technology can be used as supplementary power of the grid is not considered [2–5, 7, 8]. EVs integrated into the grid are energy storage devices and can

C. Li et al., *Influences of Electric Vehicles on Power System and Key Technologies of Vehicle-to-Grid*, Power Systems,
DOI 10.1007/978-3-662-49364-9_6

discharge power into the grid based on V2G technology. So it can be used as the uninterruptible power supply (UPS) and emergency power supply. Additionally, the conversion of EVs from charging mode to V2G mode is an electromagnetic process rather than a mechanical one, so the delay is short. Based on this characteristic, EVs can participate in frequency regulation and voltage regulation if the load supplied by EVs does not exceed their reverse discharge capacity.

Therefore, the chapter focuses on the reverse discharge capacity of EVs when studying on planning of the integration of EV charging facilities to the grid, on the basis of which, advantages, disadvantages and adaptive range of several typical schemes are deeply analyzed.

6.2 Main Considerations on the Integration of Charging Facilities into the Grid

Firstly, the planning of the scheme of the integration of charging facilities into the grid, should determine the load level and ensure the reliability of power supply according to relevant guidelines and standards [4, 11]. Secondly, with large investment into charging facility construction, the cost should be taken into consideration [5]. At last, as charging facilities will generate harmonic waves, the power quality should also be considered [3, 4].

EVs can discharge power into the grid in V2G mode [2, 7, 8]. Currently, as the development of Smart Grid is still in early stages in China, and core techniques like bilateral interaction and relevant supporting policies are not yet perfect, it is considered that EVs can only work as a provider of short-term power supply to important loads in V2G mode during power system failure, so as to enhance the reliability and economy of the grid.

6.3 Estimate of the EVCS's Reverse Discharge Capacity

The reverse discharge capacity of a single EV depends on the battery's SOC and capacities of charging devices integrated into the grid. The reverse discharge capacity of EVCSs can be represented by the EVCS's discharge time T_{ES} and maximum discharge power P_{disC}.

Definition 1 T_{ES} is the EVCS's average power supply time for unit load during power system failure.

$$T_{ES} = \varepsilon \sum_{i=1}^{n} \frac{\left(S_i - S_{i,\min}\right) \cdot Q_i}{P_u} \tag{6.1}$$

where S_i, $S_{i,min}$ and Q_i are SOC, minimum SOC and capacity of the ith charging EV, respectively. P_u is unit load and ε is the working ratio of charging carports in the EVCS (usually set as 0.8).

Suppose the average SOC, average minimum SOC and average capacity are $\bar{S}$, $\bar{S}_{\min}$ and $\bar{Q}$, respectively, then the estimate of T_{ES} is

$$T_{ES} \approx n\varepsilon \frac{(\bar{S} - \bar{S}_{min}) \cdot \bar{Q}}{P_u} \tag{6.2}$$

Generally, EVCSs are integrated into a 10 or 20 kV distribution network. Since the distribution transformer capacity of 10 or 20 kV distribution network is usually MVA-level, so P_u set as 1 MW can be taken as a benchmark when measuring the reverse discharge capacity of EVCSs. Hereinafter, P_u is set as 1 MW.

According to the definition of small-scale EVCSs in [4], $\bar{Q}$ of the fully-charged small-scale PHEV, $\bar{S}_{\min}$ and $\bar{S}$ are set as 10 kWh, 20 and 50 %, respectively, then the reverse discharge time of a small-scale EVCSs composed of 8 charging carports is estimated to be 69.12 s [12].

Definition 2 Maximum reverse discharge power of EVCSs, P_{disC}, refers to the maximum power transmitted to the grid.

P_{disC} depends on the active capacity of the EVCS's distribution transformer P_{tran} and the reverse discharge power of EVs integrated into charging facilities, etc. Then P_{disC} can be estimated as follows:

$$P_{disC} \approx min\left(\sum_{i=1}^{n} P_{e,i}\ ,\ P_{tran}\right) \tag{6.3}$$

where $P_{e,i}$ is the maximum reverse discharge power of ith charging facility.

So, based on Eqs. (6.1)–(6.3), appropriate schemes of the integration of charging facilities into the grid can be selected, in which charging facilities can be used as security source, backup or short-term backup power and emergency source of important facilities in the distribution network.

6.4 Typical Schemes of the Integration of Charging Facilities into the Grid

6.4.1 Schemes of the Integration of EVCPs into the Grid

Due to a small size and great convenience for installation of the EVCP, the scheme of the integration of EVCPs into the grid is quite flexible, which is reflected in that EVCPs can be installed either in home or near the office [3–5]. Some literatures

present that EVCPs and distributed energy resources can be integrated into grid, and then solar energy and wind energy can be utilized to provide green energy for PHEVs [7, 8].

6.4.2 EVCSs Directly Integrated into or Adjacent to 110 kV Substations

As shown in Fig. 6.1, some existing EVCSs adopt schemes of the integration of EVCSs either directly integrated into or adjacent to 110 kV substations [13, 14].

Typical emergency load of 110 kV substations is on the level of kW [15]. So, EVs can be used as the backup power supply by proper electrical wiring when there is a power failure. Then EVs can provide energy for emergency load, and reduce the recovery time of power supply and the cost of backup power supply.

The emergency load of the 110 kV substations is set as 6 kW and the time of continuous power supply for the emergency load is at least 1 h [11, 15]. Thus, according to the definition of EVCS's reverse discharge time, the reverse discharge time for EVCSs to serve as 110 kV substation backup power supply should satisfy the following condition:

$$T_{ES} \geq \frac{1 \times 3600 \times 6}{1000} s = 21.6\, s \tag{6.4}$$

Thus, based on Eq. (6.2), $\bar{S}$, $\bar{S}_{\min}$ and stored energy of fully-charged small-scale PHEVs are set as 20, 50 % and 10 kWh respectively [8, 12], then the estimate of minimum number of charging carports of a small-scale EVCS is as follows:

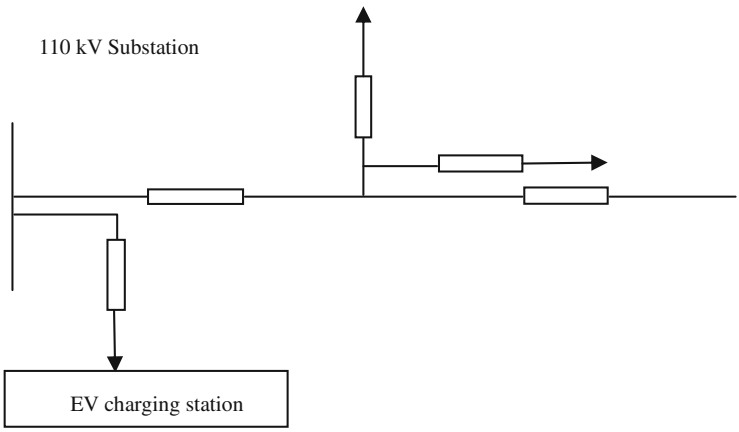

Fig. 6.1 EVCSs integrated into or adjacent to 110 kV substations

$$n = \frac{T_{ES} \cdot P_u}{\varepsilon \cdot (\bar{S} - \bar{S}_{min}) \cdot \bar{Q}} \approx 3 \tag{6.5}$$

The simulation results in [6] present a short electrical distance from EVCSs to the source, a relatively small voltage deviation and a relatively large stored energy when EVCSs are directly integrated into or adjacent to the substation. In medium voltage distribution network with monophyletic wiring mode, EVCSs directly integrated into or adjacent to the substation have a higher reliability of power supply. However, it is of great difficulty for the construction of EVCSs such as electrical wiring due to the complicated environment around 110 kV substations.

6.4.3 *EVCSs Integrated into the Tie Point of Looped Distribution Grid*

In dual-power ring-net medium-voltage distribution grid, the tie points are proper access points for EVCSs. As shown in Fig. 6.2, the charging loads of EVCSs are divided into two parts: P_{EV1} and P_{EV2} which are respectively integrated into source S_1 and S_2. So the reverse discharge capacity of EVCSs is divided into two portions.

As shown in Fig. 6.2, suppose each section of main feeder is equipped with section switches and the repair time is the same. After the EVCS is integrated into the tie point of looped distribution grid, when source S_1 blacks out, the section switches of L_1 will start to work and assign a proper range of emergency power supply for EVCSs without waiting for the switching of tie switch. Then the EVs previously charged by S_1 reversely discharge and work as short-term backup

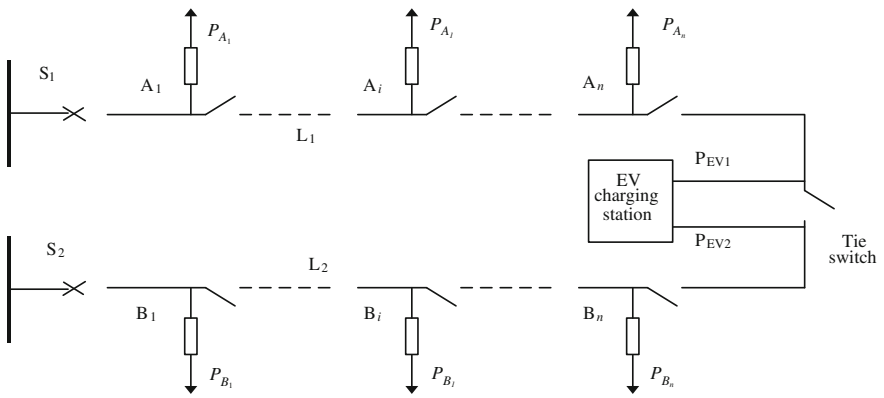

Fig. 6.2 EVCSs integrated into the tie point of looped distribution grid

power. The EV will return to the charging state after switching tie switch and facilities supplied by S_2 remain unchanged for power supply.

The capacity of one 10 kV line is on the level of several MW and the maximum reverse discharge power of each section of EVCSs is limited. Therefore, when lines in the distribution network need to transfer loads to other lines, it is essential to correctly allocate the actions of section switches and assign a proper range of emergency power supply of EVCSs. Based on the above analysis, suppose the EVCSs' EPS load points on feeder L_1 is Φ_A, the kth load point on feeder L_1 is A_k, $A_k \in \Phi_A$. If the EVCS is not integrated into tie points, then the annual blackout time of load point A_k is as follows [16]:

$$U'_{A_k} = \sum_{j=1}^{k-1} \lambda_{A_j} \cdot t_c + \lambda_{A_k} \cdot r + \sum_{j=k+1}^{n} \lambda_{A_j} \cdot t_s + \gamma_{A_k} \cdot t_{A_k} \tag{6.6}$$

If the EVCS is integrated into tie points, the annual blackout time of load point A_k is:

$$U_{A_k} = \sum_{j=1}^{k-1} \lambda_{A_j} \cdot (t_{EV} + t_s) + \lambda_{A_k} \cdot r + \sum_{j=k+1}^{n} \lambda_{A_j} \cdot t_s + \gamma_{A_k} \cdot t_{A_k} \tag{6.7}$$

In (6.6) and(6.7), n is the number of load points on feeder L_1, λ_{A_j} is the failure rate of the A_i section of main feeder, r is the repair time of each main feeder, γ_{A_i} is the failure rate of the A_i load branch, t_{A_i} is the repair time of the A_i load branch, t_s is the operation time of section switches, t_c is the switching time of tie switches, and t_{EV} is the time needed to change from default mode to V2G mode for an EV, $r > t_c > t_s$.

The charge and discharge of EV are electromagnetic transient processes, and they are much faster than mechanical tie switches, namely $t_{EV} << t_c$, so t_{EV} can be neglected compared with t_c. In addition, $t_s < t_c$ and t_s/t_c is relatively small, so $t_s + t_{EV} < t_c$ [16, 17]. The result can be concluded as follows:

$$U_{A_k} < U'_{A_k} \tag{6.8}$$

Therefore, EVCSs integrated into the tie point in looped distribution grid will reduce the annual average blackout time of some load points. No matter which source of the EVCS fails, the facilities supplied by the other source will still work well, so this scheme enhances the power supply reliability of EVCSs.

The scheme of the integration of EVCSs into the tie point of looped distribution grid requires that EVCSs have sufficient reverse discharge capacity to serve as backup power before the switching of tie switch. So, based on Eqs. (6.2) and (6.3), the scheme needs to satisfy the following constraint conditions:

$$\begin{cases} T_{ES1} \cdot P_u \Big/ \sum\limits_{j \in \Phi_A} P_{A_j} \geq \mathrm{t}_c - \mathrm{t}_s \\ P_{disC1} \geq \sum\limits_{j \in \Phi_A} P_{A_j} \end{cases} \tag{6.9}$$

$$\begin{cases} T_{ES2} \cdot P_u \Big/ \sum\limits_{j \in \Phi_B} P_{B_j} \geq \mathrm{t}_c - \mathrm{t}_s \\ P_{disC2} \geq \sum\limits_{j \in \Phi_B} P_{B_j} \end{cases} \tag{6.10}$$

In (6.9) and (6.10), T_{ES1} and T_{ES2} are the reverse discharge time of each section of EVCS; P_{disC} and P_{disC2} are the maximum reverse discharge power of each section of EVCS; Φ_A and Φ_B are emergency power supply ranges of feeder L_1 and feeder L_2, respectively.

Generally, there is relatively far electrical distance between the tie point of looped distribution grid and power supply point, so the charge capacity of EVCSs will be limited if EVCSs are integrated into this kind of tie point [18].

6.4.4 *Parallel Operation of EVCSs with the Special Important Load*

The special important load in the first level load (hereinafter referred to as special load) has a high demanding for power supply reliability and usually needs EPS to reduce the blackout time in island state [11].

As shown in Fig. 6.3, the EVCS is integrated into the load point of the special load, so the EVCS can serve as EPS for the special load. Normally, the switch S is closed and EVCSs are in parallel operation with the special load; when the load point loses all the power supply, the switch S will open, and then EVCSs will serve as EPS to reduce the blackout time of special load.

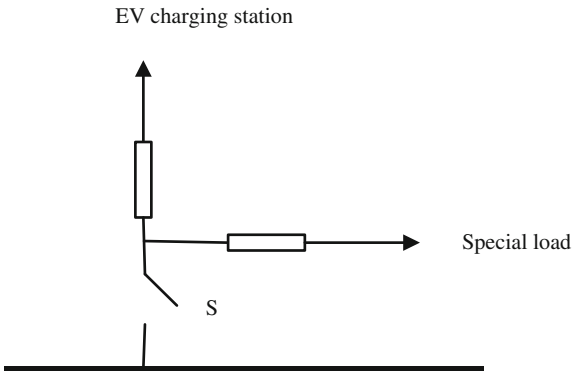

Fig. 6.3 The EVCS and the special load in parallel operation

As the EPS of special load, EVCSs should satisfy the following constraint conditions:

$$\begin{cases} T_{ES} \cdot P_u / P_I \geq T_I \\ P_{disC} \geq P_I \end{cases} \tag{6.11}$$

where T_{ES} and P_{disC} are the reverse discharge time and maximum reverse discharge power respectively, P_I is the size of special load, and T_I is the working hours of EPS required by the special load.

Based on Eqs. (6.2), (6.3) and (6.11), the constraint condition for the number of charging carports can be concluded:

$$n \geq \frac{P_I \cdot T_I}{\varepsilon \cdot (\bar{S} - \bar{S}_{min}) \cdot \bar{Q}} \tag{6.12}$$

The scheme of parallel operation of EVCSs with the special load can reduce the cost of EPS. However, the special load requires high-quality power supply, while the integration of EV charging loads into the distribution network may lead to harmonic pollution. Thus special harmonic suppression devices should be equipped.

6.5 Conclusions

With the support of the national policy and the rapid development of the EV industries, EV charging facilities have been under large-scale planning and construction. The EV is one of the energy storage units in the distribution network, whose reverse discharge capacity should be taken into account when EV charging facilities are integrated into the grid. Therefore, the chapter mainly focuses on the reverse discharge capacity of EVs when studying on the planning of the integration of EV charging facilities into the grid, on the basis of which, advantages, disadvantages and adaptive range of several typical schemes are deeply analyzed. This chapter can serve as a useful reference for the planning of EV charging facilities.

References

1. Zhang W, Wu B, Li W, et al. Discussion on development trend of battery electric vehicles in China and its energy supply mode. Power Syst Technol. 2009;33(4):1–5 (In Chinese).
2. Winkler T, Komarnicki P, Mueller G, et al. Electric vehicle charging stations in Magdeburg. 2009 IEEE Vehicle Power and Propulsion Conference. 2009.
3. State Grid Corp of China. Guidance on the construction of electric vehicle charging facilities in State Grid Corp of China. Beijing: China Electric Power Press; 2010 (In Chinese).

4. Shenzhen Market Supervision and Administration Bureau. Technical specification for electric vehicle charging system. http://www.szaic.gov.cn/xxqk/qt/tzqq/zhl/201005/P020100521341526068713.pdf.
5. Yao J, Wang M, Luo W. Construction and application of charging systems for electric mobiles. East China Electric Power. 2008;36(8):107–10 (In Chinese).
6. Etezadi-Amoli M, Choma K, Stefani J. Rapid-charge electric-vehicle stations. IEEE Trans Power Delivery. 2010;25(3):1883–7.
7. Du Y, Zhou X, Bai S, et al. Review of non-isolated bi-directional DC-DC converters for plug-in hybrid electric vehicle charge station application at municipal parking decks. Applied Power Electronics Conference and Exposition (APEC), 2010 Twenty-Fifth Annual IEEE. IEEE, 2010;1145–1151.
8. Li X, Lopes LAC, Williamson SS. On the suitability of plug-in hybrid electric vehicle (PHEV) charging infrastructures based on wind and solar energy. Power and Energy Society General Meeting, 2009. PES'09. IEEE, 2009;1–8.
9. Zhenpo W, Peng L. Analysis on storage power of electric vehicle charging station. Power and Energy Engineering Conference (APPEEC), 2010 Asia-Pacific. IEEE, 2010;1–4.
10. Yu Z, Zhang Y, Yang J. Design of energy management systems for mobile power station of electric vehicles. 2009 International Conference on Information Management, Innovation Management and Industrial Engineering. IEEE, 2009;4:250–253.
11. China Machinery Industry Association. Code for distribution system design. Beijing: China Planning Press; 2009 (In Chinese).
12. Clement-Nyns K, Haesen E, Driesen J. The impact of charging plug-in hybrid electric vehicles on a residential distribution grid. IEEE Trans Power Syst. 2010;25(1):371–80.
13. Lin Z, Shi Y. The first installment of electric car charging pile in Quanzhou. http://fj.qq.com/a/20101112/000032.htm.
14. Xiang L. The country's largest and most advanced Charging equipment. http://www.morning.sc.cn/new/html/tfzb/20100531/tfzb369963.html.
15. Xia H. Capacity calculation of storage battery in 10 kV integrated automation substation. Relay. 2004;32(18):64–6 (In Chinese).
16. Wan G, Ren Z, Jing Y, et al. Deployment of disconnect switches on main feeder. Proceedings of the CSEE. 2003;23(4):l24–127 (In Chinese).
17. Allan RN, Billinton R, Breipohl AM, et al. Bibliography on the application of probability methods in power system reliability evaluation. IEEE Trans Power Syst. 1999;14(1):51–7.
18. Cao Y, Tan Y, Li C, et al. Typical schemes of electric vehicle charging infrastructure connected to grid. Autom Electric Power Syst. 2011;35(14):48–52 (In Chinese).

Chapter 7
EV Charging Facility Planning

7.1 Introduction

EV charging facility provides power supply for EVs running and it is a necessary and important supporting facility for the development of EVs. Therefore, the EV charging facility planning has been studied in many literatures. The basic principles of EV charging mode and EV charging facility are explored in [1, 2]. As the EV technology is not yet fully mature, charging demand with a lot of uncertainties can result in various charging modes [3]. In the initial stage, the planning and construction of EV charging facility should not take profits as the purpose. The planning and location of EV charging facility is different from that of the substation, gas station and other mature service terminals [4–6]. The influence of EVs on the regional power supply is explored in [7], presenting that the EV charging facility planning should combine with the regional distribution network planning. And the construction of EV charging facility can also promote the development of the smart grid [8, 9].

In this chapter, the EV charging facility planning is divided into three stages based on popularity of EVs, namely demonstration stage, public service stage and commercial operation stage. In addition, characteristics of each stage are analyzed and an optimized model of charging modes is put forward. Based on the proposed model, charging demand of each charging mode is predicted.

7.2 Stages of EV Charging Facility Planning

Due to different stages of EVs' development, different technology levels of EVs and their batteries, and different EVs' ownership, user types and driving range, charging demand has diverse characteristics and corresponding EV charging facility planning is at different stages. Battery performances, such as mass specific energy, volume

C. Li et al., *Influences of Electric Vehicles on Power System and Key Technologies of Vehicle-to-Grid*, Power Systems,
DOI 10.1007/978-3-662-49364-9_7

specific energy and charging ratio, have a great influence on the development of EV charging facility planning. Specific energy determines EVs' driving range (distance per charge) and charging ratio determines charging time. Based on the popularity of EVs, the EV charging facility planning is divided into three stages: the demonstration stage, public services stage and commercial operation stage. Each stage has its own feature.

1. Demonstration stage

The features of this stage are as follows: the EV technology is not mature and the market mechanism that can steadily and effectively promote development of EVs is not formed; the ratio of EVs to all vehicles is extremely low and EVs mainly involve special vehicles supported by the government, such as electric engineering vehicles and garbage collecting trucks; and the driving range is usually referred to certain small areas or certain routes.

Planning in demonstration stage is a kind of short-term planning.

2. Public services stage

The features of this stage are as follows: the EV technology is still at a low level in spite of its rapid development and implicit bottleneck constraints like safety factor also exist; the ratio of EVs to all vehicles is relatively low; the development of EVs relies on subsidies and propaganda of the government; there are more types of EVs, such as electric buses, large official vehicles and public vehicles.

Planning in public promotional stage is a kind of medium-term planning.

3. Commercial operation stage

The features of this stage are as follows: the EV technology is basically mature; there is a certain amount of EVs with high charging demand and various types, including taxis and private EVs besides EVs mentioned in public services stage; the economy of EVs equals or even surpasses that of vehicles powered by fuel and the development of EVs basically relies on market promotion.

Planning in commercial operation stage is a kind of long-term planning.

7.3 Charging Modes Selection and Demand Forecasting

7.3.1 Charging Modes Selection

Based on differences in driving routes or tasks, EVs are usually divided into fixed-route vehicles (special purpose) like buses, engineering vehicles and

municipal vehicles; and random-route vehicles like taxis and some private cars. Different types of vehicles have different charging modes; currently, charging modes of EVs include battery replacing and vehicle charging.

1. Battery replacing

This charging mode features one-time large investment but low costs in the long run, thus it is suitable for fixed-route vehicles.

2. Vehicle charging

This charging mode is suitable for random-route vehicles. Currently, it includes fast charging in EVCSs, slow charging in EVCSs and slow charging in EVCPs, etc.

Suppose there are k kinds of charging modes and EV users base on the charging cost to choose charging modes. For an EV, the charging cost contains empty-run energy cost (caused by unintended distance for charging) and equipment wear cost (caused by indirect depreciation of equipment) which are set as c, besides charging fee and reduced cost of battery loss. If charging time has an influence on the economic interest of users, then indirect cost of charging time should also be considered. Suppose electricity price is x_i, actual charging capacity is q_i, value of travel time in this city is u [10], average charging power is e_i, battery price is b_i, rechargeable times during the battery life is t_i. Thus cost of each charging n_i and cost of unit electricity m_i are:

$$n_i = c + x_i q_i + \mu \frac{q_i}{e_i} + \frac{b_i}{t_i} \tag{7.1}$$

$$m_i = \frac{n_i}{q_i} = \frac{c}{q_i} + x_i + \frac{\mu}{e_i} + \frac{b_i}{t_i q_i} \tag{7.2}$$

In (7.1), i represents one kind of charging modes, $i = 1, 2, \ldots, k$.

When choosing different charging modes, charging power and electricity can be different, so cost of each charging and cost of unit electricity will vary. When cost of each charging is the lowest, cost of unit electricity is not necessarily the lowest, so both of them should be taken into account. The comprehensive charging cost z_i is:

$$z_i = \sqrt{m_i n_i s_0} h_{ii} \, \mathrm{J} = \min\{z_i\} \sqrt{m_i n_i s_0} h_{ii} \neq 0 \tag{7.3}$$

where s_0 = 1 kWh; h_{ii} is a decision variable, which equals 1 if charging mode i satisfies EV charging demand, otherwise h_{ii} equals 0.

Equation (7.3) indicates that based on users' interests, the comprehensive charging cost is proportional to square root of the product of cost of unit electricity

and cost of each charging. Thus, the comprehensive charging cost J of the charging mode the user finally chooses is:

$$\mathrm{J} = \min\{z_i\}\sqrt{m_i n_i s_0 h_{ii}} \neq 0 \tag{7.4}$$

Equation (7.4) indicates that based on users' interests, the charging mode with lowest cost will be the final choice.

7.3.2 Charging Demand Forecasting

Suppose in the planning year of planning areas, EV ownership is L, the number of EVs which can select the charging mode i is L_i', the actual number of EVs which select the charging mode i is L_i, the average daily charging times for each EV is a_i, then charging capacity demand for different charging modes P_i and daily electricity demand Q_i are:

$$P_i = \sum_{l=1}^{L_i} e_{il} \tag{7.5}$$

$$Q_i = a_i \sum_{l=1}^{L_i} q_{il} \tag{7.6}$$

Cooperation of charging capacity demand for various charging modes can be shown in Fig. 7.1 (take charging capacity as an example).

In Fig. 7.1, an elliptical area enclosed by dashed line and solid line represents charging capacity demand of this charging mode, and area P_1, P_2, …, P_k enclosed by solid line represent the actual charging capacity demand after choosing the charging mode.

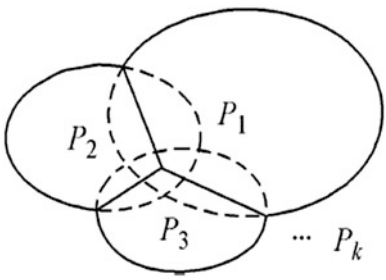

Fig. 7.1 Cooperation of charging capacity demand

7.4 Charging Facility Planning

7.4.1 Planning Principles and Process

Charging facility planning should fully consider the layout and planning of current grid, reduce the cost, achieve coordinated development and have the potential for update. Besides, charging facility planning should comply with urban master planning and transportation planning.

A major difference between EV charging facility planning and normal power supply facility planning lies in that several charging modes can work together to satisfy the charging demand. The planning process for charging facilities is shown in Fig. 7.2 [11].

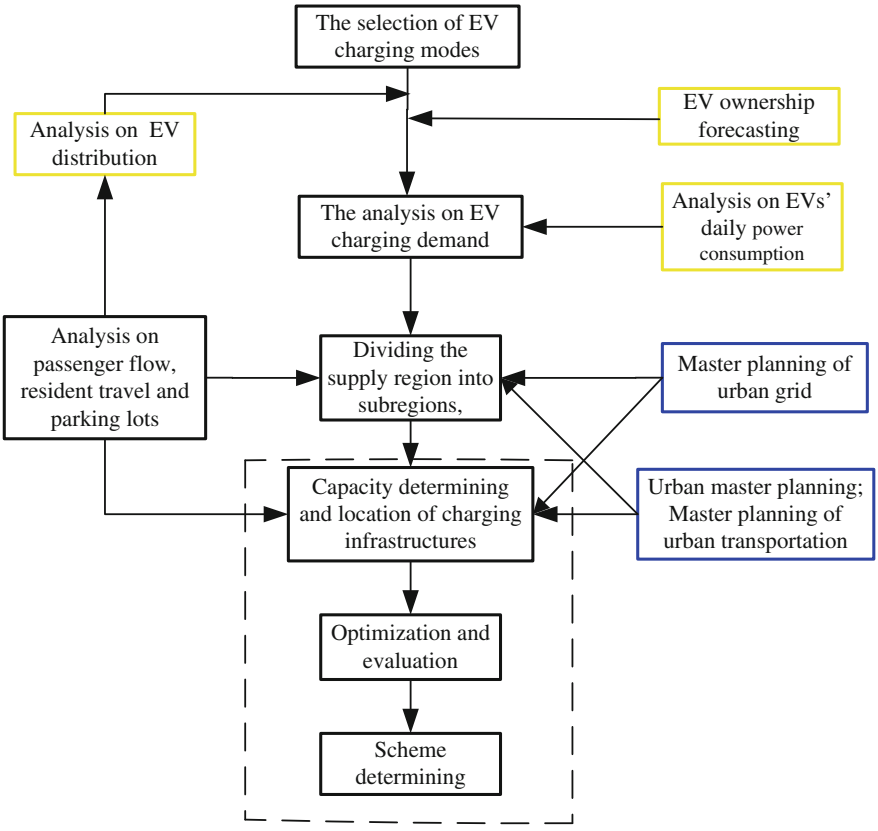

Fig. 7.2 The planning process of charging facilities

7.4.2 Planning Model

Based on the charging demand, this chapter divides the supply region into irregular subregions, represented by the geometric center of each subregion. Based on this, the optimization of location and capacity of charging facilities in the planning year can be described by the following model with the aim of lowest total cost:

$$\min C = \min(C_a + C_b) \tag{7.7}$$

where C is the total cost of a subregion and C_a is the investment cost,

$$C_a = \sum_{i-1}^{k} \sum_{j-1}^{N_i} \left\{ F\left(P_{ij}\right)_{ij} \left[\frac{r_0(1+r_0)^{y_{ij}}}{(1+r_0)^{y_{ij}}-1} \right] \right\} \tag{7.8}$$

C_b is the operation and maintenance cost,

$$C_b = \sum_{i}^{k} \sum_{j}^{N_i} W\left(p_{ij}\right)_{ij} \tag{7.9}$$

$F(p_{ij})_{ij}$ is the investment cost of jth charging facility with ith charging mode, and is a function of construction capacity p_{ij}, where investment cost of existing charging facilities is 0; r_0 is the discount rate; y_{ij} is the depreciation life of jth charging facility with ith charging mode; N_i is the number of charging facilities with ith charging mode; $W(p_{ij})_{ij}$ is the operation and maintenance cost of jth charging facility with ith charging mode.

Constraints of EV charging facility planning are as follows:

$$R_1 = \frac{\eta_{ij} p_{ij}}{n_{ij} e_i} \geq \rho \tag{7.10}$$

$$R_2 = \frac{\eta_{ij} p_{ij} T_{ij}}{\tau n_{ij} q_i} \geq \sigma \tag{7.11}$$

where R_1 is charging capacity redundancy; R_2 is charging power redundancy; $n_{ij}, \eta_{ij}, T_{ij}$ are the number of charging ports, overall load rate, comprehensive load time (determined by daily working time), respectively; τ is the average charging times; $i = 1, 2, \ldots, k$; $j = 1, 2, \ldots, N_i$.

Equations (7.10) and (7.11) indicate that capacity and power of charging facilities should satisfy the charging demand and reserve some margin. Thus the actual construction capacity P_i' and daily power reserve Q_i' can be obtained:

$$P_i' = \sum_{j=1}^{N_i} p_{ij} = R_1 P_i \tag{7.12}$$

$$Q_i' = \sum_{j=1}^{N_i} q_{ij} = R_2 Q_i \tag{7.13}$$

Besides, when choosing the location of charging facilities, the number of charging facilities an EV can come across within its driving range should be taken into account, which is described by spacing ratio r (the ratio of driving range to maximum distance between charging facilities). Suppose the average power consumption is q_0, the distance between neighboring charging facilities is d, and then constraint of spacing ratio r is as follows:

$$\mathrm{r} = \frac{\frac{q_i}{q_0}}{max\{d\}} \geq \omega \tag{7.14}$$

In different stages of EV development, the constraints may vary, i.e. take different values. Each stage should make corresponding adjustments to improve the utilization and economy of charging facilities.

7.5 Case Study

7.5.1 Analysis on Charging Mode Selection

Suppose a random-route EV in city Z gives an alarm and needs charging because of low electricity. Based on relevant parameters of existing EVCSs in China, it is supposed that the charging power of different charging modes q_i and other parameters are shown in Table 7.1.

Suppose the maximum charge power demand of this EV is 60 kWh, only 30 kWh is needed for the time being and the value of travel time is 15 yuan/h, then the comprehensive cost of slow charging in the EVCS is the lowest from Table 7.1, so slow charging in the EVCS is selected. Also it is seen that for different charging modes, the weight of depreciation cost is different and much bigger in fast charging mode compared with other two modes. Under emergency conditions, the value of travel time is much larger. Suppose the value is 200 yuan/h, and then the comprehensive costs of three modes are 231.87, 115.39 and 126.46 yuan, respectively. Obviously fast charging in the EVCS should be selected.

7.5.2 Analysis on Charging Facility Planning

Take city Z as an example. Demonstration stage and public service stage are skipped here and it is supposed that in the planning year the development of EVs is in the commercial operation stage where the EV ownership is 100 thousand and other parameters are shown in Table 7.2. Based on Eqs. (7.1)–(7.6), the charging mode is selected and the charging demand (specially the capacity demand of EVCSs and power demand of converter station) is forecasted; then based on Eqs. (7.7)–(7.10), the construction capacity of EVCSs and power reserve of converter station are determined, as is shown in Table 7.2.

From Table 7.2, the overall construction capacity of EVCSs and overall power reserve of converter station in the planning year for different charging modes can be obtained. Based on the actual conditions of road network in city Z, the supply

Table 7.1 Charging mode selection

Charging mode	q_i/kWh	e_i/kW	b_i/yuan	t_i/time	x_i/yuan $(\text{kWh})^{-1}$
Slow charging in charging piles at parking lots	30	5	40,000	800	0.6
Quick charging in charging stations	30	30	40,000	100	1.0
Slow charging in charging stations	30	10	40,000	600	0.8
Charging mode	c/yuan	u/yuan h^{-1}	n_i/yuan	m_i/yuan $(\text{kWh})^{-1}$	z_i/yuan
Slow charging in charging piles at parking lots	2	15	160.00	5.33	29.21
Quick charging in charging stations	2	15	447.00	14.90	81.61
Slow charging in charging stations	2	15	137.67	4.59	25.13

Table 7.2 Charging demand forecasting and charging facility planning

Charging mode	L_i'/thousand	L_i/thousand	e_i/kW	P_i/MW	R_i/thousand	P_i'/MW
Replacing battery	60	30				
Quick charging in charging stations	80	10	30	300	1.5	450.0
Slow charging in charging stations	90	25	10	250	1.3	325.0
Slow charging in charging piles at parking lots	95	30	5	175	1.1	192.5
Charging mode	a_i/time	q_i/kWh	Q_i/MWh	R_i	Q_i'/MWh	
Replacing battery	3	40	3600	1.3	4680	

region can be divided into different subregions and the location and capacity of charging facility can be determined, where the location is constrained by Eq. (7.12). The specific configurations of each charging facility are skipped for concision here.

7.6 Conclusions

The EV charging facility planning is explored in this chapter. Based on popularity of EVs, the planning is divided into three stages: demonstration stage, public service stage and commercial operation stage. Characteristics of each stage are analyzed and based on the optimized model of charging mode put forward in this chapter, the charging demand of each charging mode is forecasted. This chapter also puts forward concepts such as spacing ratio, charging capacity redundancy and charging power redundancy, and principles, process and models of EV charging facility planning. Results of the case studies demonstrate the applicability of this planning method. This chapter can serve as a useful reference for EV charging facility planning.

References

1. Kang J, Wei Z, Cheng D, et al. Research on electric vehicle charging mode and charging stations construction. Power Demand Side Manag. 2009;11(5):64–6 (In Chinese).
2. Xu F, Yu G, Gu L, et al. Tentative analysis of layout of electrical vehicle charging stations. East China Electric Power. 2009;37(10):1678–82 (In Chinese).
3. Nansai K, Tohnob S, Konoc M, et al. Life-cycle analysis of charging infrastructure for electric vehicles. Appl Energy. 2010;70(3):251–65.
4. Wang C, Wei H, Xiao J, et al. Two- phase optimization planning approach to substation location and sizing. Autom Electric Power Syst. 2005;29(4):62–6 (In Chinese).
5. Ge S, Li H, Liu H, et al. Substation optimization planning based on the weighted diagram. Autom Electric Power Syst. 2007;31(3):29–33 (In Chinese).
6. Lin J, Li H, Luo P, et al. Integrated planning for the distribution system with the unified optimization of substation and network frame. Autom Electric Power Syst. 2006;30(19):42–6 (In Chinese).
7. Hadley SW. Evaluating the impact of plug-in hybrid electric vehicles on regional electricity supplies. Proceedings of 2007 IREP Symposium: Bulk Power System Dynamics and Control VII: Revitalizing Operational Reliability, 19–24 Aug 2007, Charleston, SC, USA.
8. Yao J, Lei Y. The essential cause and technical requirements of the smart grid. Autom Electric Power Syst. 2010;34(2):1–4 (In Chinese).
9. Li W, Ding J, Yao J. Views on smart evolution. Autom Electric Power Syst. 2010;34(2):24–8 (In Chinese).
10. Qie Z. Highway transportation economics. Beijing: People's Communications Press; 1998 (In Chinese).
11. Wu C, Li C, Du L, Cao Y. A method for electric vehicle charging infrastructure planning. Autom Electric Power Syst. 2010;34(24):36–9 (In Chinese).